Nondestructive Evaluation (NDE) Methods and Capabilities Handbook

Volume II Appendices —Appendix E Volume 3

Patricia A. Howell, Editor
Langley Research Center, Hampton, Virginia

APPROVED FOR PUBLIC RELEASE

February 2020

NASA STI Program . . . in Profile

Since its founding, NASA has been dedicated to the advancement of aeronautics and space science. The NASA scientific and technical information (STI) program plays a key part in helping NASA maintain this important role.

The NASA STI program operates under the auspices of the Agency Chief Information Officer. It collects, organizes, provides for archiving, and disseminates NASA's STI. The NASA STI program provides access to the NTRS Registered and its public interface, the NASA Technical Reports Server, thus providing one of the largest collections of aeronautical and space science STI in the world. Results are published in both non-NASA channels and by NASA in the NASA STI Report Series, which includes the following report types:

- TECHNICAL PUBLICATION. Reports of completed research or a major significant phase of research that present the results of NASA Programs and include extensive data or theoretical analysis. Includes compilations of significant scientific and technical data and information deemed to be of continuing reference value. NASA counter-part of peer-reviewed formal professional papers but has less stringent limitations on manuscript length and extent of graphic presentations.

- TECHNICAL MEMORANDUM. Scientific and technical findings that are preliminary or of specialized interest, e.g., quick release reports, working papers, and bibliographies that contain minimal annotation. Does not contain extensive analysis.

- CONTRACTOR REPORT. Scientific and technical findings by NASA-sponsored contractors and grantees.

- CONFERENCE PUBLICATION. Collected papers from scientific and technical conferences, symposia, seminars, or other meetings sponsored or co-sponsored by NASA.

- SPECIAL PUBLICATION. Scientific, technical, or historical information from NASA programs, projects, and missions, often concerned with subjects having substantial public interest.

- TECHNICAL TRANSLATION. English-language translations of foreign scientific and technical material pertinent to NASA's mission.
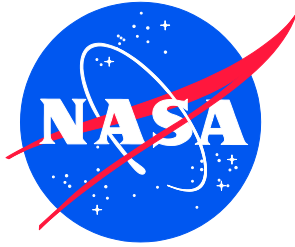
Specialized services also include organizing and publishing research results, distributing specialized research announcements and feeds, providing information desk and personal search support, and enabling data exchange services.

For more information about the NASA STI program, see the following:

- Access the NASA STI program home page at *http://www.sti.nasa.gov*

- E-mail your question to help@sti.nasa.gov

- Phone the NASA STI Information Desk at 757-864-9658

- Write to:
NASA STI Information Desk
Mail Stop 148
NASA Langley Research Center
Hampton, VA 23681-2199

Nondestructive Evaluation (NDE) Methods and Capabilities Handbook

Volume II Appendices —Appendix E Volume 3

Patricia A. Howell, Editor
Langley Research Center, Hampton, Virginia

APPROVED FOR PUBLIC RELEASE

Table of Contents

List of Figures

List of Tables

Nomenclature

µA	Microampere
µm	Micrometer/Micron
µs	Microseconds
1D	One-Dimensional
2D	Two-Dimensional
3D	Three-Dimensional
ABS	Acrylonitrile Butadiene Styrene
ACAD	Air Coupled Acoustic Drive
ACC	Advanced Composites Consortium
ACP	Advanced Composites Project
ACT	Air Coupled Transducer
ADR	Assisted Defect Recognition
AFP	Automated fiber placement
AISI	American Iron and Steel Institution
AMT	Active Microwave Thermography
ANSI	American National Standards Institute
APF	Automated Fiber Placement
ARC	Ames Research Center
ASME	American Society of Mechanical Engineers
ASNT	American Society of Nondestructive Testing
ASTM	American Society for Testing and Materials
ATL	Automated Tape Lay-Up
AWG	Arbitrary Waveform Generator
AWS	American Welding Society
BMS	Boeing Material Specification
BSI	British Standards Institution
BVID	Barely Visible Impact Damage
BW	Back Wall
C	Celsius
CAD	Computer-Aided Design
CAFA	Combined Analytical Finite Element Approach
CCD	Charge-coupled Device
CDRH	Center for Devices and Radiological Health
CFRP	Carbon Fiber Reinforced Polymer
CMOS	complementary metal oxide semiconductor
CNN	Convolutional Neural Network
CO_2	Carbon Dioxide
COPV	Composite Over-Wrap Pressure Vessel
CPV	Composite Pressure Vessel
CR	Computed Radiography
CST	Charge Simulation Technique
CT	Computed Tomography
CTE	Coefficient of Thermal Expansion
DAQ	Data Acquisition
dB	Decibel
dB/in	Decibels Per Inch
DDA	Digital Detector Array
DOF	Degree of Freedom
DR	Digital Radiography
DRC	Digital Radiography Center
ECT	Eddy Current Thermography
EFIT	Elastodynamic Finite Integration Technique

FBH	Flat-bottom holes
FD	Finite Difference
FDA	Food and Drug Administration
FEA	Finite Element Analysis
FEM	Finite Element Method
FEP	Fluorinated Ethylene Propylene
FLIR	Forward-looking Infrared
FMC	Full Matrix Capture
FOD	Foreign Object Debris
FOV	Field of View
ft-lbs	Foot Pounds
GE	General Electric
GHz	Gigahertz
GN_2	Gaseous Nitrogen
gsm	Grams per square meter
GWUT	Guided Wave Ultrasound
Hz	Hertz
ID	Inner Diameter
IDIQ	Indefinite Delivery/Indefinite Quantity
IEC	International Electrotechnical Commission
IML	Inner Mold Line
in	Inch
in/min	Inches per Minute
InSb	Indium Antimonide
ipm	Images per Minute
IR	Infrared
IRT	Infrared Thermography
ISTIS	*In Situ* Thermal Inspection System
J/cm^2	Joules Per Square Centimeter
K	Kelvin
KeV	Kiloelectron Volt
kg	Kilograms
kg/cm^2	kilogram per square centimeter
kHz	Kilohertz
kV	Kilovolts
kW	kilowatt
LaRC	Langley Research Center
LBI	Laser Bond Inspection
LMCO	Lockheed-Martin Company
LPS	Local Positioning System
LST	Line Scanning Thermography
LT	Lock-In Thermography
m^2	Square Meter
m^2/hr	Meters Square per Hour
mA	Miliampere
MECAD	Mechanically Coupled Acoustic Drive
MGBM	Multi-Gaussian Beam Model
MHz	Megahertz
mHz	Millihertz
mK	Millikelvin
mm	Millimeter
MPa	Megapascals
ms	Meter per Second
MS/s	Megasamples/second

msec	Millisecond
MSFC	Marshall Space Flight Center
NAS	National Aerospace Standard
NASA	National Aeronautics and Space Administration
Nd:Glass	Neodymium Glass Laser
NDE	Nondestructive Evaluation
NDI	Nondestructive Inspection
NDT	Nondestructive Test
NEDT	Noise Equivalent Differential Temperature
NGIS	Northrop Grumman Innovation Systems
nm	Nanometer
ns	Nanosecond
OEM	Original Equipment Manufacturer
OML	Outer Mold Line
ONR	Office of Naval Research
OSHA	Occupational Safety and Health Administration
PA	Phased Array
PCA	Principal Component Analysis
PEUT	Pulse Echo Ultrasound
PMC	Polymer Matrix Composite
PML	Perfectly Matched Layer
POC	Point of Contact
PoD	Probability of Detection
PPT	Pulsed-Phase Thermography
psi	Pounds Per Square Inch
PT	Pressure-Sensitive Tape
PTFE	Polytetraflouroethylene (Teflon™)
PVDF	polyvinylidene fluoride
PWI	Plane Wave Imaging
PW-UTC	Pratt Whitney – United Technology Corporation
PZT	Piezoelectric Sensors/Transducer
R&D	Research and Development
RAH	Refresh After Heat
RBH	Refresh Before Heat
RGB	Red, Green, and Blue
RMS	Root Mean Squared
ROI	Region of Interest
RPF	Release Ply Fabric
RSG	Rotated-Staggered Grid
RVE	Representative Volume Element
s	Seconds
SAE	Society of Automotive Engineers
SAFE	Semi-Analytical Finite Element
SAR	Synthetic Aperture Radar
sec	Seconds
SHM	Structural Health Monitoring
SLDV	Scanning Laser Doppler Vibrometer
SMAAART	Structures, Materials, Aerodynamics, Aerothermodynamics, and Acoustics Research and Technology
SME	Subject Matter Expert
SNR	Signal to Noise Ratio
SOFI	Spray on Foam Insulation
SoP	State-of-Practice
sq. ft/hr	square foot per hour

SSFT	Single-Side Flash Thermography
SSIR	Single-Sided Infrared Thermography
SVD	Singular Value Decomposition
TC2	Technical Challenge 2
TDRS	Time Domain Reflectometry Systems
TFM	Total Focus Method
Tg	Glass Transition Temperature
THz	Terahertz
TPS	Thermal Protection System
TSR	Thermographic Signal Reconstruction
TT	Through Transmission
TTIR	Through-Transmission Infrared Thermography
TTUT	Through-Transmission Ultrasound
TWI	Thermal Wave Imaging System
USC	University of South Carolina
UT	Ultrasound
VaRTM	Variation Resin Transfer Molding
VSHM	Visualized Structural Health Monitoring
XCT	X-ray Computed Tomography

Appendix E   Individual Test Reports by Specimen (Sections 41-60)

★☆☆	Not Suitable for this Specimen
★★☆	Marginally suitable for this Specimen, or only provides qualitative information
★★★	Highly successful for this Specimen, including quantifiable information

E.41   Specimen #41: Boeing-8276-200-58-26B – Not Tested

Structure	Material	Details	Dimensions (inches)	Partner Methods
Laminates	8276 Tape	S curve (__/⌐) 58° slant with two 0.2 inch radii. Multiple types of delamination simulators.	20 × 6 × 2.4	Not Tested

E.42   Specimen #42: Boeing-8276-200-58-48B – Not Tested

Structure	Material	Details	Dimensions (inches)	Partner Methods
Laminates	8276 Tape	S curve (__/⌐) 58° slant with two 0.2 inch radii. Multiple types of delamination simulators.	20 × 6 × 2.4	Not Tested

E.43   Specimen #43: Boeing-8276-200-56-48B

Structure	Material	Details	Dimensions (inches)	Partner Methods	
Laminates	8276 Tape	S curve (__/⌐) 56° slant with two 0.2 inch radii. Multiple types of delamination simulators.	20 × 6 × 2.4	NASA	E.43.1 XCT

Figure E.43-1. Photograph of Specimen #43: Boeing-8276-200-56-48B.

E.43.1   Method: X-ray Computed Tomography (XCT)

E.43.1.1   Partner: NASA

E.43.1.2   Technique Applicability: ★★★

XCT is capable of imaging the delaminations at the flat and curved regions in this specimen.

E.43.1.3   Laboratory Setup

The microfocus XCT system at NASA Langley Research Center (LaRC) is a commercially available Avonix (Nikon C2) Metrology System designed for high-resolution Nondestructive

Evaluation (NDE) inspections. The system is an advanced microfocus X-ray system, capable of resolving details down to 5 μm, and with magnifications up to 60X. Supplied as complete, the system is a large-dimension radiation enclosure with X-ray source, specimen manipulator, and an amorphous silica detector, as shown in Figure E.43-2. The imaging controls are housed in a separate control console. The detector is a Perkin-Elmer, 16-bit, amorphous-silicon digital detector with a 2000 × 2000-pixel array.

A consistent Cartesian coordinate system is used to define slice direction as illustrated in Figure E.43-2 and Figure E.43-3. Slices normal to the X-, Y-, and Z-directions are shown in Figures E.43-3a, b, and c, respectively.
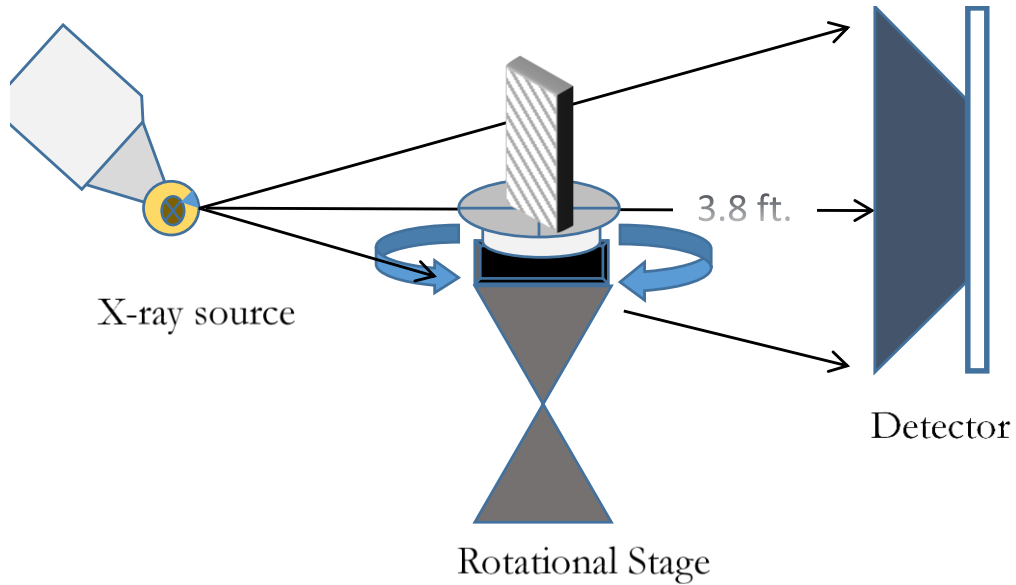
Figure E.43-2. XCT system components.

2
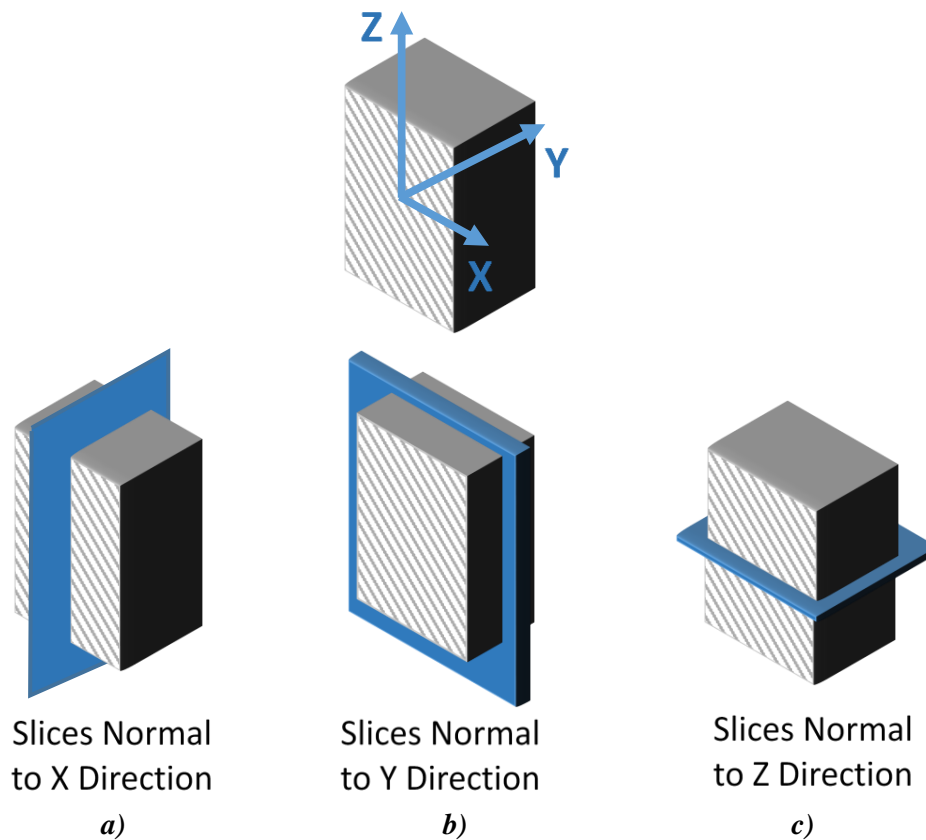
Figure E.43-3. Slice direction nomenclature.
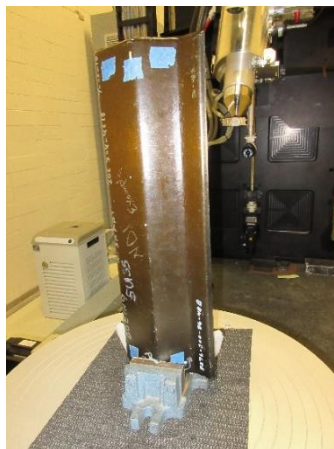
Figure E.43-4. Microfocus XCT system showing orientation of Specimen #34: Boeing-Wrinkles A4.

E.43.1.4   Equipment List and Specifications:

- Avonix 225 Computed Tomography (CT) System
- 225 kV microfocus X-ray source with 5-µm focal spot size
- 15 or 30 kg Capacity, 5-axis, fully programmable manipulator
- Detector: Perkin Elmer XRD 1621 – 2000 × 2000 pixels with 200 µm pitch
- 10 µm spatial resolution for specimens 1.5 cm wide
- Thin panels 10 × 10 inches – full volume 200 µm spatial resolution

E.43.1.5 Settings

Table E.43-1. Data collection settings.

Source Energy	120 kV
Current	90 µA
Magnification	1.65 X
Filter	NF
# Rotational angles	3142
Exposure time / frame	1.0 sec
Max Histogram Grey Level	22 K
# Averages	8
Resolution (µm)	114.894 µm
Array Dimensions (pixels)	2K × 2K

The specimen is placed vertically (rotated about the smallest dimension) on the rotational stage located between the radiation source and the detector. The rotational stage is computer-controlled and correlated to the position of the sample. As the sample is rotated the full 360° (~0.11° increments), the detector collects radiographs at each rotated angle as the X-ray path intersects the sample. 3D reconstruction of the collection of radiographs produces a volume of data that is observed along any plane in the volume. The closer the sample is placed to the X-ray source, the higher the spatial resolution that can be obtained.

E.43.1.6 Inspection Results

Section A

Specimen #43 is an S-curve 56° slant with two 0.2-inch radii. There are multiple types of delamination simulators within the sample. XCT was performed on this specimen in NASA LaRC's large CT system with the settings defined in Section E.43.1.5. The scan was done using a large viewing window encompassing the whole specimen (Figure E.43-5 and Figure E.43-6) and a small window covering a smaller area to increase the resolution of the scan (Figure E.43-7). This cannot always been done on larger specimens.

Figure E.43-5. 3D X-ray generated view of specimen #43: Boeing-8276-200-56-48B using a small viewing window showing the y direction.

4
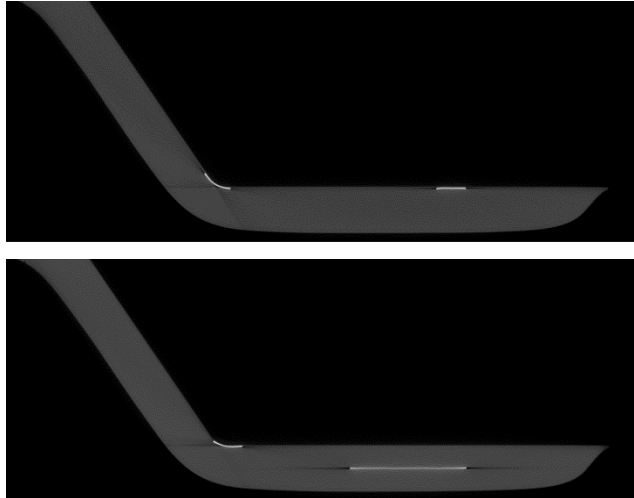
Figure E.43-6. 3D X-ray generated view of specimen #43: Boeing-8276-200-56-48B using a small viewing window showing the z direction.

The delaminations are seen from all viewing directions as seen in Figure E.43-5 and Figure E.43-6. The white regions represent inserts of higher density than the bulk within the specimen to simulate delaminations. The specimen is fabricated in such a way that the delaminations are present in the curved radius and the flat regions at varying depths. No matter the depth or region of the specimen, all simulated delaminations are easily viewed. The dark regions next to the inserts are air gaps much like delaminations seen in practice.
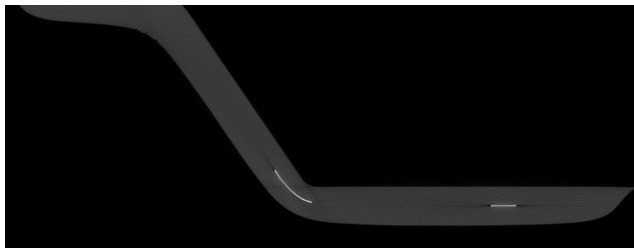
Figure E.43-7. 3D X-ray generated view of specimen #43: Boeing-8276-200-56-48B using a larger viewing window showing the z direction.

Section B

Semantic CT Image Segmentation Technique:

The developed semantic CT image segmentation technique, originally designed at NASA LaRC, applies the Convolutional Neural Network (CNN) to identify and segment cracks and delamination in carbon fiber due to impact. The segmentation is done on the specimens' CT scan grayscale images. This method was first developed by D. T. Delelegn [1] as his master's thesis and then improved as a NASA white paper.

There are two implemented CNN models, each identifying the two damage types separately (i.e., crack and delamination). The first model easily identifies delamination, whereas the second is optimized to detect cracks and 'linear-type' damage. Each model prediction outputs are floating numbers between (0,1) indicating how likely an area is damaged. Class label one representing a highest damage prediction certainty while zero for a no-damage area. To seek the most damaged area in the material, this probabilistic prediction value of an area-damage indication is used.

5

The prediction is done on the CT images with a 4×4 window (patch) size. Then, the predicted class labels for each patch from the two models are combined as the Red (crack) and the Green (delamination) channels of the Red, Green, and Blue (RGB) color model representing the two damage types in different colors. For further reading, refer D. T. Delelegn [1].

This segmentation technique is able to easily point out cracks or linear damage that are collocated with a delamination. This is because the prediction of the two models are represented in the different channels of the RGB color model.

While originally developed to detect impact damage, the method was applied to ACP Handbook standards (porosity, delamination, AFP defects, etc.) with varying degrees of success. Here, the method is applied to handbook specimen #43, is a $20 \times 6 \times 2.4$-inch S-curve laminate panel with multiple delaminations that are easily identified.

Segmentation Output:
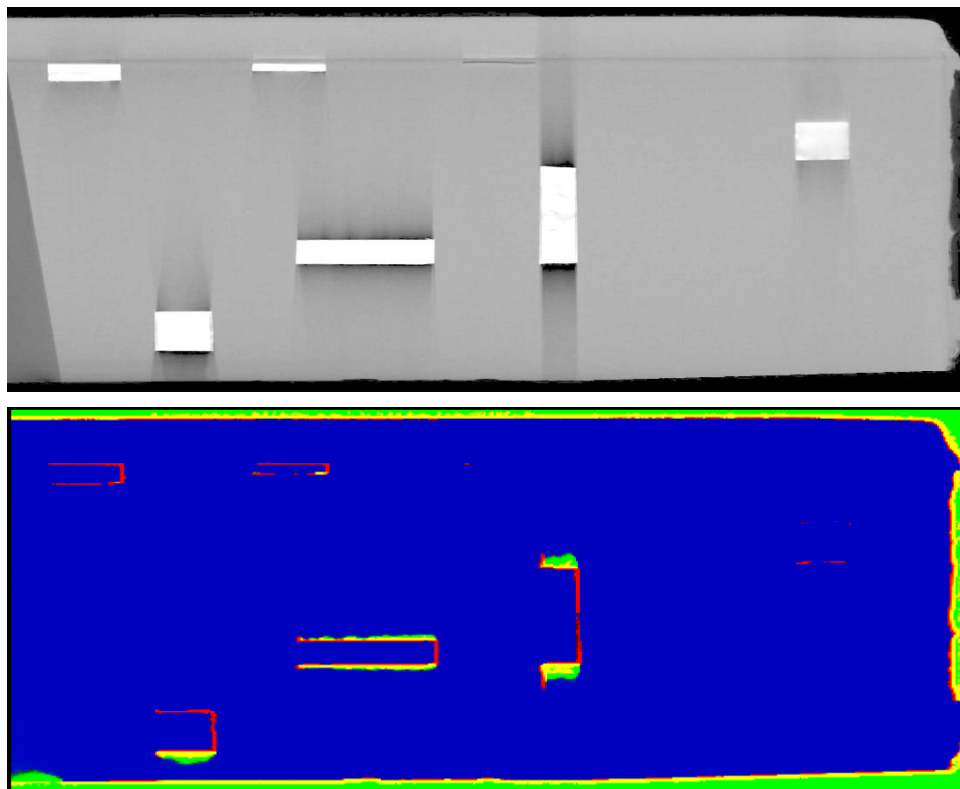
Figure E.43-8. XCT slice greyscale (top) and CNN segmentation RBG color model (bottom).

E.43.1.7   References

[1]   Delelegn, Desalegn Temesgen: "Non-destructive Evaluation for Composite Material," Master of Science Thesis, Old Dominion University, August 2018.

E.44   Specimen #44: Boeing-8276-200-59-48B

Structure	Material	Details	Dimensions (inches)	Partner Methods	
Laminates	8276 Tape	S curve (__⌐) 56° slant with two 0.2-inch radii. Multiple types of delamination simulators.	$20 \times 6 \times 2.4$	NASA	E.44.1 XCT

Figure E.44-1. Photograph of Specimen #44: Boeing-8276-200-59-48B.

E.44.1   Method: X-ray Computed Tomography (XCT)

E.44.1.1   Partner: NASA

E.44.1.2   Technique Applicability: ★★★

XCT is capable of imaging the delaminations at the flat and curved regions in this specimen.

E.44.1.3   Laboratory Setup

The microfocus XCT system at NASA LaRC is a commercially available Avonix (Nikon C2) Metrology System designed for high-resolution NDE inspections. The system is an advanced microfocus X-ray system, capable of resolving details down to 5 microns (µm), and with magnifications up to 60X. Supplied as complete, the system is a large-dimension radiation enclosure with X-ray source, specimen manipulator, and an amorphous silica detector, as shown in Figure E.44-2. The imaging controls are housed in a separate control console. The detector is a Perkin-Elmer, 16-bit, amorphous-silicon digital detector with a 2000×2000-pixel array.

A consistent Cartesian coordinate system is used to define slice direction as illustrated in Figure E.44-2 and Figure E.44-3. Slices normal to the X-, Y-, and Z-directions are shown in Figures E.44-3a, b, and c, respectively.

Figure E.44-2. XCT system components.

7

Figure E.44-3. Slice direction nomenclature.

Slices Normal to X Direction

Slices Normal to Y Direction

Slices Normal to Z Direction

a)   *b)*   *c)*
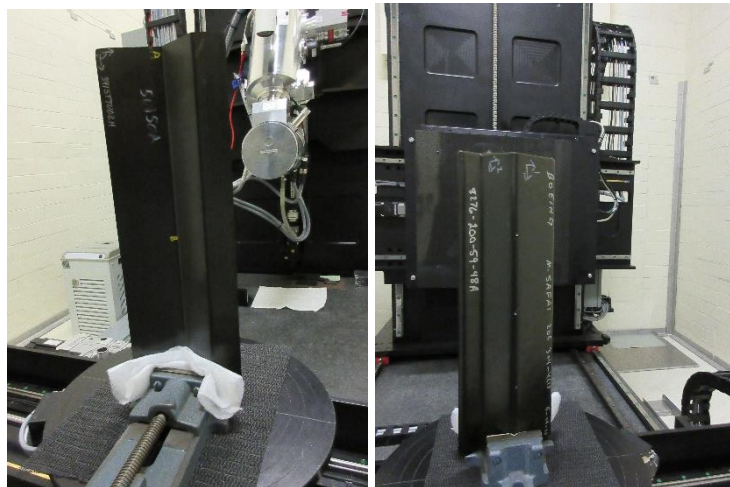
Figure E.44-4. Microfocus XCT system showing orientation of Specimen #44: Boeing-Wrinkles A4.

E.44.1.4   Equipment List and Specifications:

- Avonix 225 CT System
- 225 kV microfocus X-ray source with 5-µm focal spot size
- 15 or 30 kg Capacity, 5-axis, fully programmable manipulator
- Detector: Perkin Elmer XRD 1621 – 2000 × 2000 pixels with 200 µm pitch

- 10 µm spatial resolution for specimens 1.5 cm wide
- Thin panels 10×10 inches – full volume 200 µm spatial resolution

E.44.1.5 Settings

Table E.44-1. Data collection settings.

| Source Energy	120 kV
Current	90 µA
Magnification	1.65 X
Filter	NF
# Rotational angles	3142
Exposure time / frame	1.0 sec
Max Histogram Grey Level	22 K
# Averages	8
Resolution (µm)	114.894 µm
Array Dimensions (pixels)	Set 1: $1999 \times 362 \times 1998$ Set 2: $1998 \times 686 \times 1997$

The specimen is placed vertically (rotated about the smallest dimension) on the rotational stage located between the radiation source and the detector. The rotational stage is computer-controlled and correlated to the position of the sample. As the sample is rotated the full 360° (~0.11° increments), the detector collects radiographs at each rotated angle as the X-ray path intersects the sample. 3D reconstruction of the collection of radiographs produces a volume of data observed along any plane in the volume. The closer the sample is placed to the X-ray source, the higher the spatial resolution that can be obtained.

E.44.1.6 Inspection Results

Section A

Specimen #44 is an S-curve 59° slant with two 0.2-inch radii. There are multiple types of delamination simulators within the sample. XCT was performed on this specimen in NASA LaRC's large CT system with the settings defined in E.44-5. The scan was done in segments to ensure high resolution. The segments are stitched together using post processing.

The delaminations are seen from all viewing directions as seen in Figure E.44-5 and Figure E.44-6. The white regions represent inserts of higher density than the bulk within the specimen to simulate delaminations. The specimen is fabricated in such a way that the delaminations are present in the curved radius and the flat regions at varying depths. In Figure E.44-5, the defects are located on the bend leading into the flat section of the y view. No matter the depth or region of the specimen, all simulated defects are easily viewed. The dark regions next to the inserts are air gaps much like delaminations seen in practice.
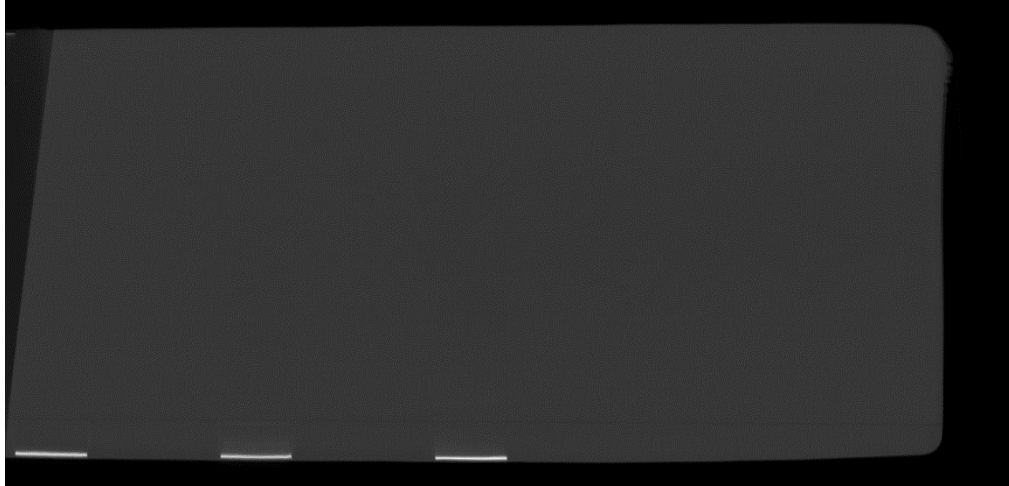
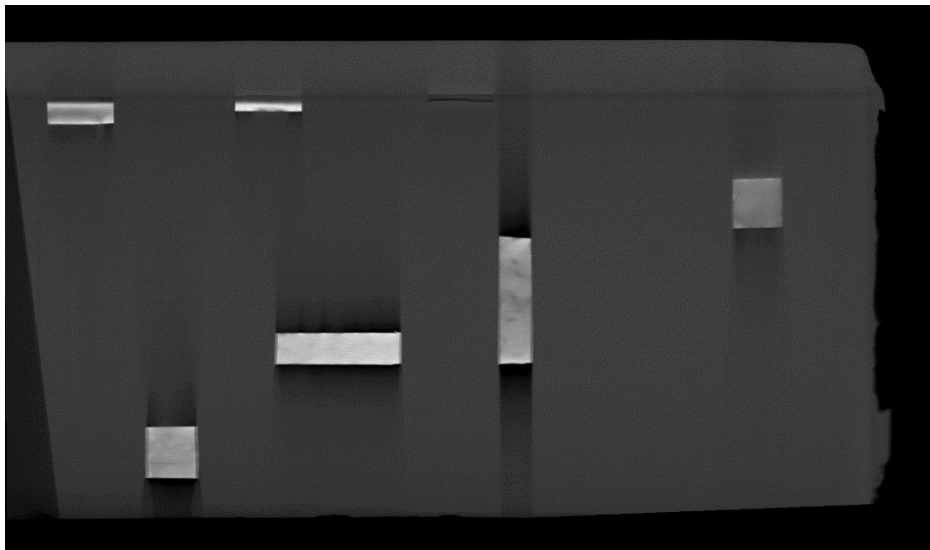*Figure E.44-5. 3D X-ray generated view of specimen #44: Boeing-8276-200-59-48B showing the y direction.*
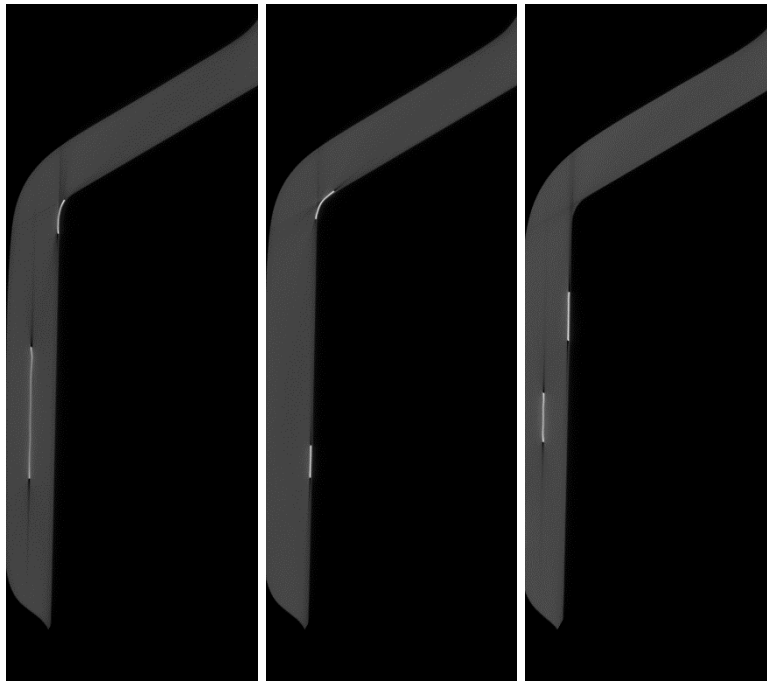
Figure E.44-6. 3D X-ray generated views of specimen #44: Boeing-8276-200-59-48B showing the z direction.

Section B

Semantic CT Image Segmentation Technique:

The developed semantic CT image segmentation technique, originally designed at NASA LaRC, applies a CNN to identify and segment cracks and delamination in carbon fiber due to impact. The segmentation is done on the specimens' CT scan grayscale images. This method was first developed by D. T. Delelegn [1] as his master's thesis, and then improved as a NASA white paper.

There are two implemented CNN models each identifying the two damage types, i.e. crack and delamination, separately. The first model easily identifies delamination whereas the second is optimized to detect cracks and 'linear-type' damage. Each model prediction outputs are floating

numbers between [0,1] indicating how likely an area is damaged. Class label one ("1") representing a highest damage prediction certainty while zero ("0") for a no-damage area. This probabilistic prediction value of an area damage indication can be used to seek the most damaged area in the material.

The prediction is done on the CT images with a 4×4 window (patch) size. Then, the predicted class labels for each patch from the two models are combined as the Red (crack) and the Green (delamination) channels of the RGB color model representing the two damage types in different colors. For further reading, refer D. T. Delelegn [1].

This segmentation technique is able to easily point out cracks or linear damage that are collocated with a delamination. This is because the prediction of the two models are represented in the different channels of the RGB color model.

While originally developed to detect impact damage, the method was applied to ACP Handbook standards (porosity, delamination, AFP defects, etc.) with varying degrees of success. Here, the method is applied to handbook specimen #44, is a $20 \times 6 \times 2.4$-inch S-curve laminate panel with multiple delaminations that are easily identified.

Segmentation Output:

The Teflon-inserts do not depict delamination in a carbon fiber well as they have a brighter pixel intensity values than the material itself. However, the CNN model, which is optimized to detect linear-type damage, was able to pick up the edges, as shown in Figure E.44-7a.

As in Figure E.44-7b, by altering the Teflon-inserts pixel values somewhat represent a delamination, the models were able to predict a better representation of the delamination in the CT images.
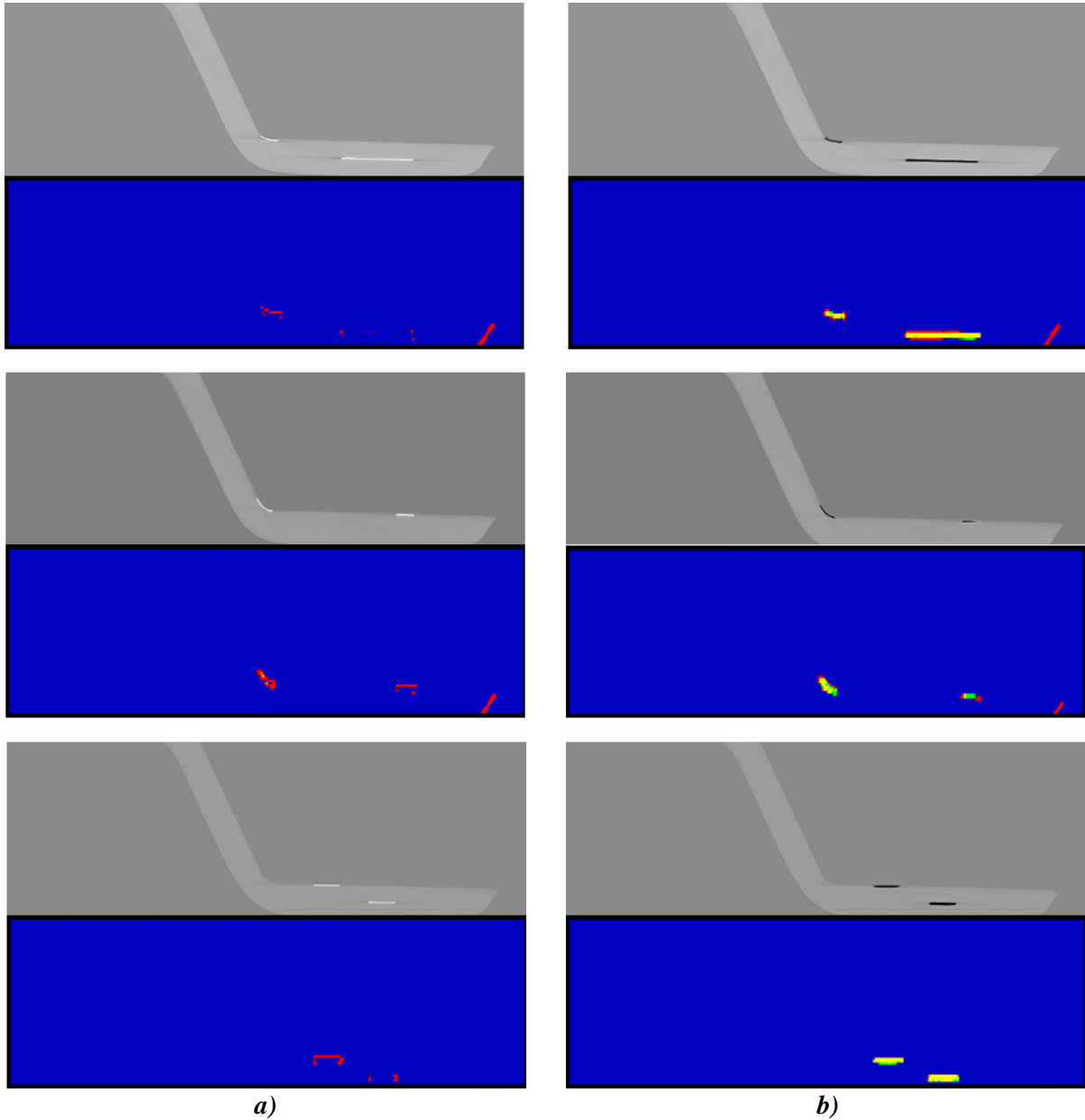
Figure E.44-7. Segmentation of specimen #44: Boeing-8276-200-59-48B.
(a) Prediction on contrast enhanced images of E.44-5 showing the z direction. (b) Predictions after
setting the Teflon-inserts representing pixel intensity values to zero in (a) to their corresponding image
on the left.

E.44.1.7   References

[1]   Delelegn, Desalegn Temesgen: "Non-destructive Evaluation for Composite Material,"
        Master of Science Thesis, Old Dominion University, August 2018.

12

E.45   Specimen #45: UTC-3-FBH

Structure	Material	Details	Dimensions (inches)	Partner Methods	
Uni-ply (0/90/45)	8552/IM7	Delaminations in woven composites simulated with FBH	$16 \times 10 \times 0.75$	NASA	E.45.1 XCT
				USC	E.45.2 GWUT
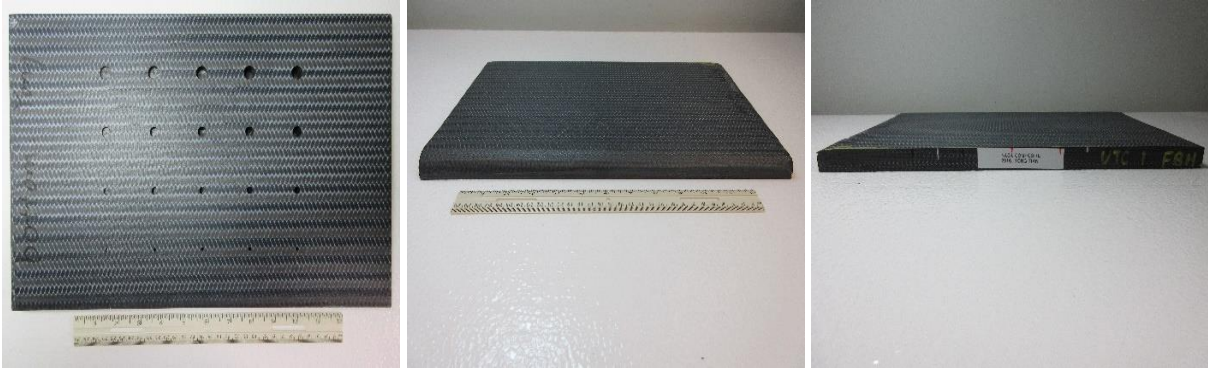
Figure E.45-1. Photograph of Specimen #45: UTC-3-FBH.

E.45.1   Method: X-ray Computed Tomography (XCT)

E.45.1.1   Partner: NASA

E.45.1.2   Technique Applicability: ★★★

XCT is capable of imaging the simulated delaminations in this sample.

E.45.1.3   Laboratory Setup

The microfocus XCT system at NASA LaRC is a commercially available Avonix (Nikon C2) Metrology System designed for high-resolution NDE inspections. The system is an advanced microfocus X-ray system, capable of resolving details down to 5 μm, and with magnifications up to 60X. Supplied as complete, the system is a large-dimension radiation enclosure with X-ray source, specimen manipulator, and an amorphous silica detector, as shown in Figure E.45-2. The imaging controls are housed in a separate control console. The detector is a Perkin-Elmer, 16-bit, amorphous-silicon digital detector with a 2000×2000-pixel array.

A consistent Cartesian coordinate system is used to define slice direction as illustrated in Figure E.45-2 and Figure E.45-3. Slices normal to the X-, Y-, and Z-directions are shown in Figures E.44-3a, b, and c, respectively.
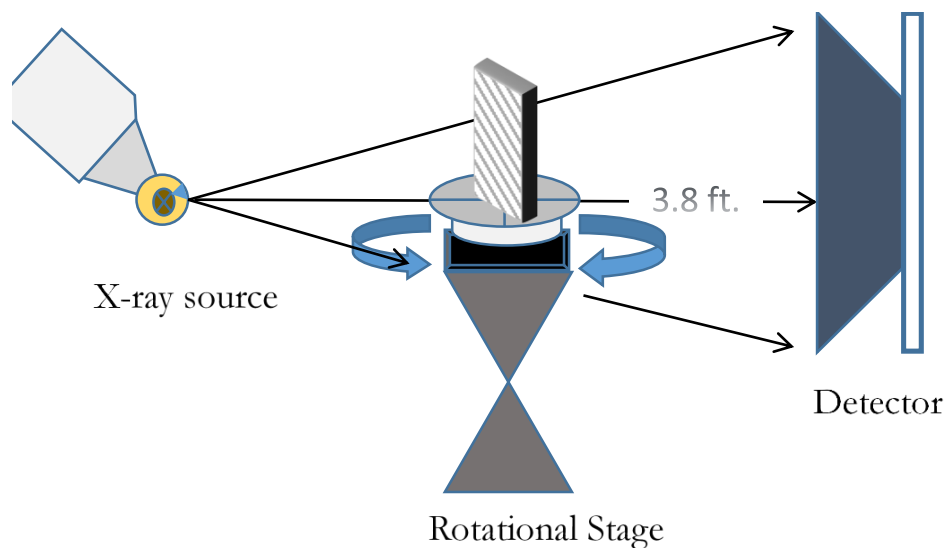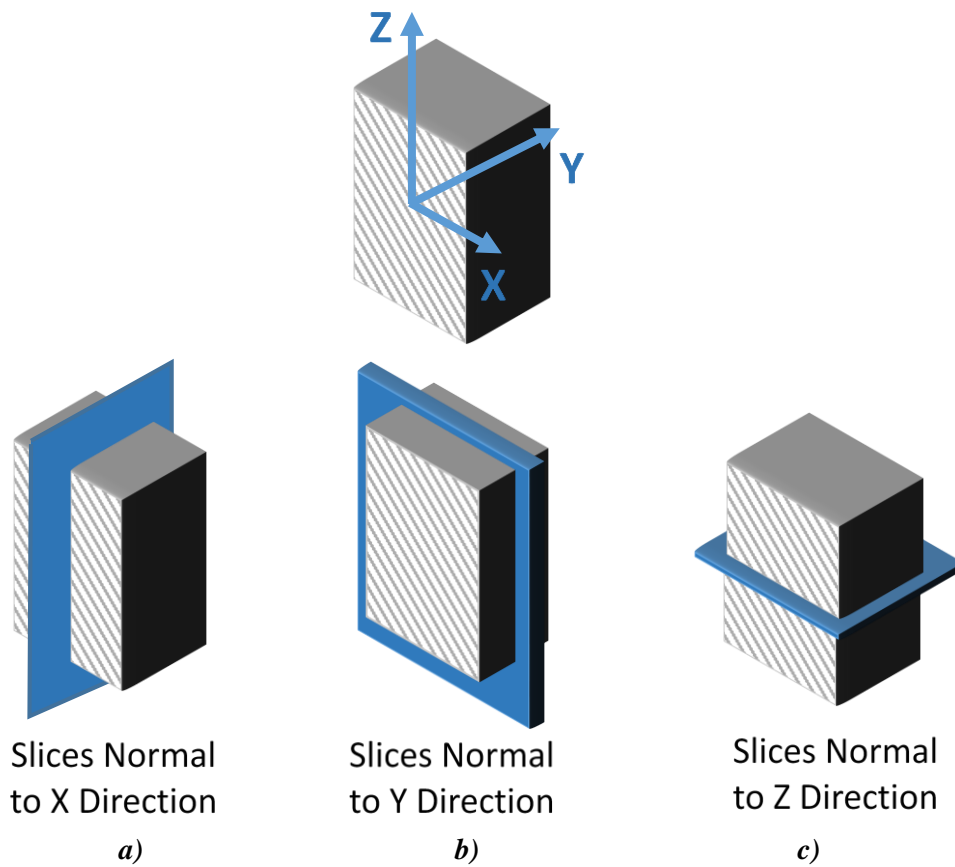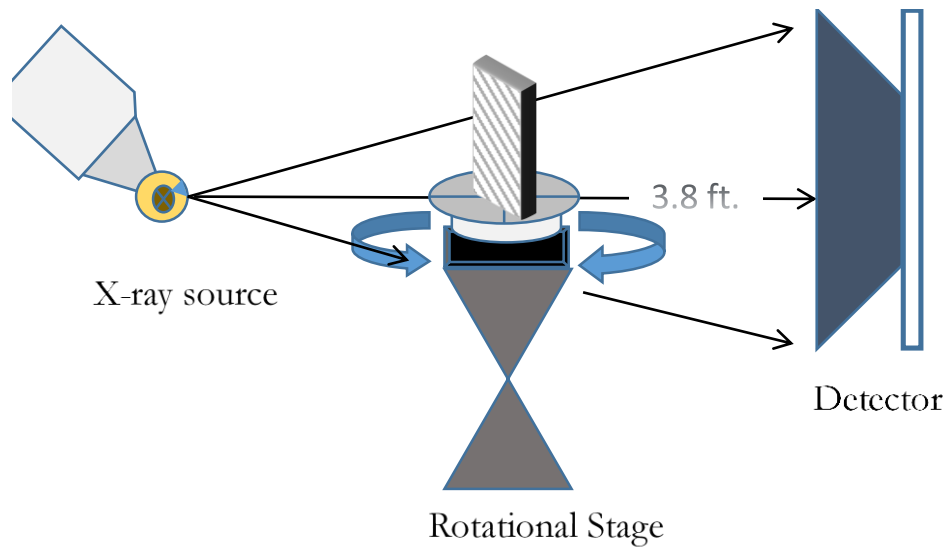
Figure E.45-2. XCT system components.

| Slices Normal to X Direction	Slices Normal to Y Direction	Slices Normal to Z Direction
a)	*b)*	*c)*
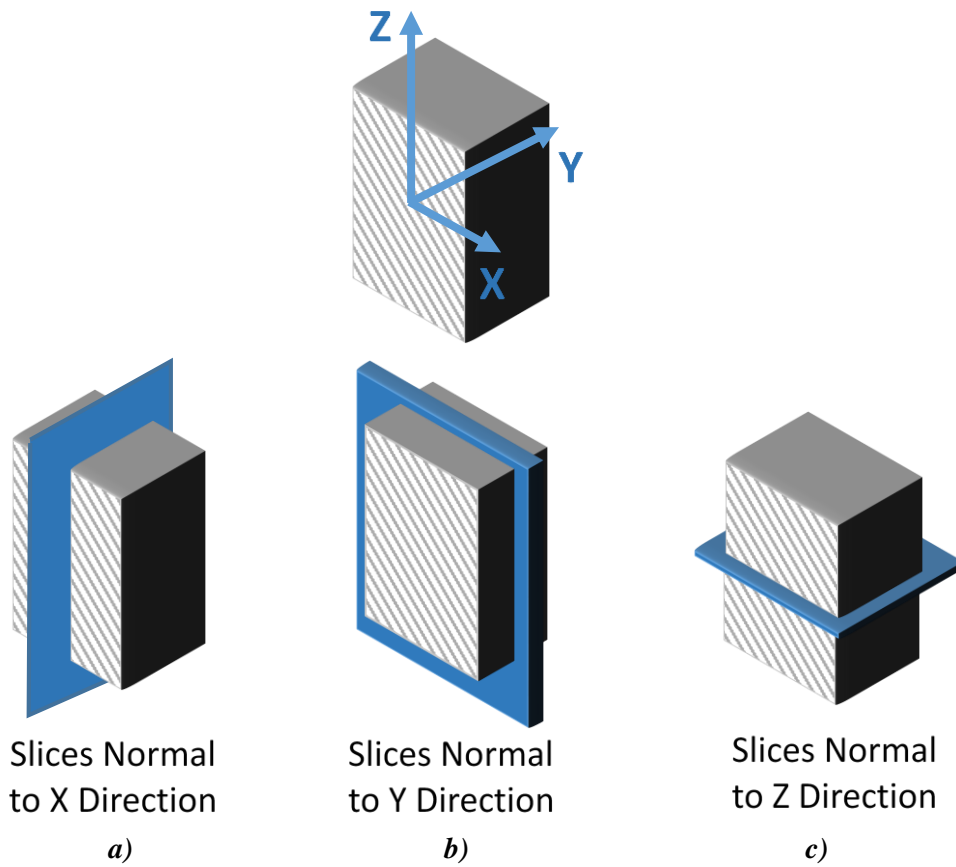
Figure E.45-3. Slice direction nomenclature.
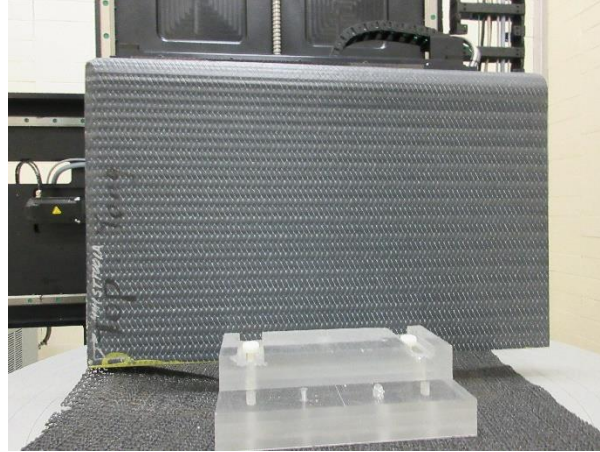
Figure E.45-4. Microfocus XCT system showing orientation of Specimen #45: UTC-3-FBH.

E.45.1.4   Equipment List and Specifications:

- Avonix 225 CT System
- 225 kV microfocus X-ray source with 5-µm focal spot size
- 15 or 30 kg Capacity, 5-axis, fully programmable manipulator
- Detector: Perkin Elmer XRD 1621 – 2000 × 2000 pixels with 200 µm pitch
- 10 µm spatial resolution for specimens 1.5 cm wide
- Thin panels 10 × 10 inches – full volume 200 µm spatial resolution

E.45.1.5   Settings

Table E.45-1. Data collection settings.

Source Energy	120 kV
Current	90 µA
Magnification	1.65 X
Filter	NF
# Rotational angles	3142
Exposure time / frame	1.0 sec
Max Histogram Grey Level	22 K
# Averages	8
Resolution (µm)	114.894 µm
Array Dimensions (pixels)	Set 1: 1999 × 362 × 1998
	Set 2: 1998 × 686 × 1997

The specimen is placed vertically (rotated about the smallest dimension) on the rotational stage located between the radiation source and the detector. The rotational stage is computer-controlled and correlated to the position of the sample. As the sample is rotated the full 360° (~0.11° increments), the detector collects radiographs at each rotated angle as the X-ray path intersects the sample. 3D reconstruction of the collection of radiographs produces a volume of data observed along any plane in the volume. The closer the sample is placed to the X-ray source, the higher the spatial resolution that can be obtained.

E.45.1.6 Inspection Results

Section A

Specimen #45, UTC-3-FBH, is a panel with flat bottom holes intended to simulate delaminations throughout the material. The holes are drilled in varying size and depth within the sample as seen in Figure E.45-5. XCT was performed on this specimen in NASA LaRC's large CT system with the settings defined in Section E.45.1.5.

The holes simulating delaminations caused are clearly seen from all viewing directions as shown in Figure E.45-5. There is excellent contrast indicating where the defects begin compared to the solid grey bulk material. Upon further review of the sample there are little to no other defects present other than the occasional foreign object debris (FOD), indicated by brighter spots due to a typically greater density than the bulk material.
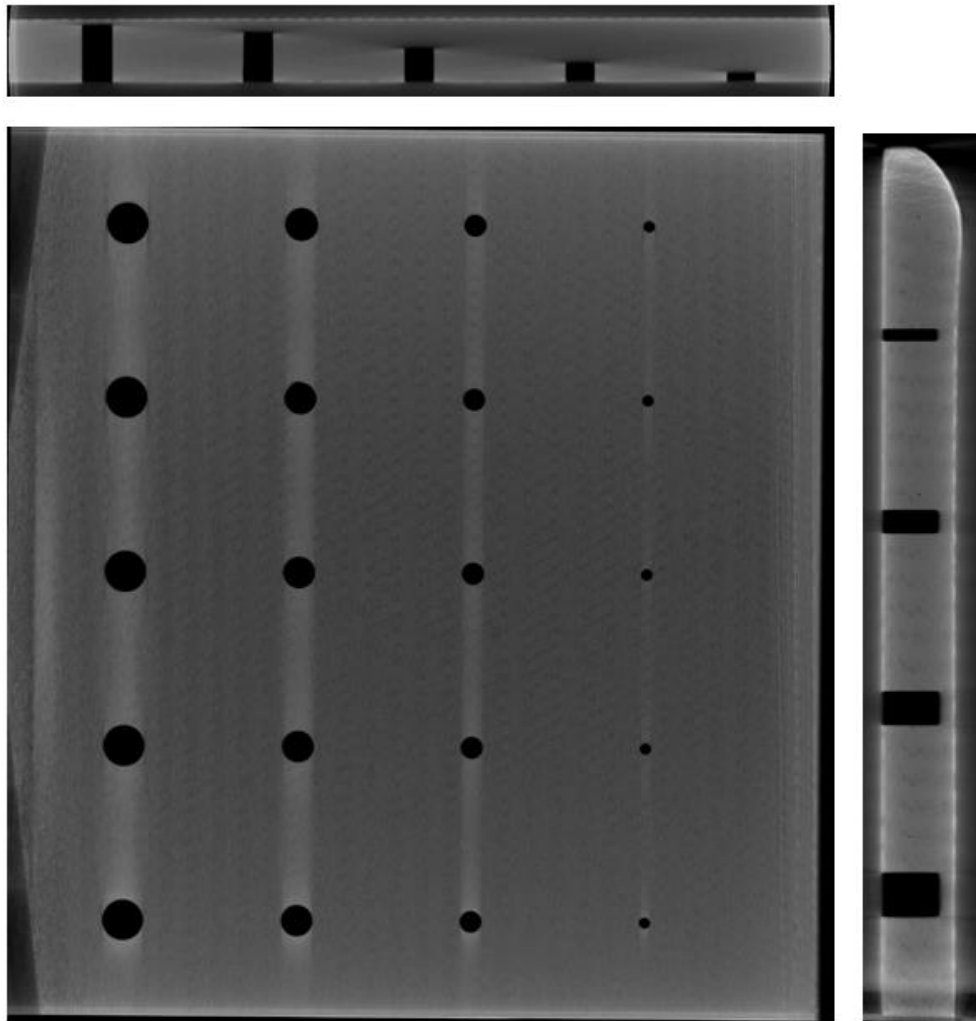
Figure E.45-5. 3D X-ray generated view of Specimen #45: UTC-3-FBH showing the y direction (center), z direction (top) and x direction (right).

Section B

Semantic CT Image Segmentation Technique:

The developed semantic CT image segmentation technique, originally designed at NASA LaRC, applies the CNN to identify and segment cracks and delamination in carbon fiber due to impact. The segmentation is done on the specimens' CT scan grayscale images. This method was first developed by D. T. Delelegn [1] as his master's thesis and then improved as a NASA white paper.

There are two implemented CNN models, each identifying the two damage types separately (i.e., crack and delamination). The first model easily identifies delamination, whereas the second is optimized to detect cracks and 'linear-type' damage. Each model prediction outputs are floating numbers between (0,1) indicating how likely an area is damaged. Class label one representing a highest damage prediction certainty while zero for a no-damage area. To seek the most damaged area in the material, this probabilistic prediction value of an area-damage indication is used.

The prediction is done on the CT images with a 4×4 window (patch) size. Then, the predicted class labels for each patch from the two models are combined as the Red (crack) and the Green (delamination) channels of the RGB color model representing the two damage types in different colors. For further reading, refer D. T. Delelegn [1].

This segmentation technique is able to easily point out cracks or linear damage that are collocated with a delamination. This is due to the fact that the prediction of the two models are represented in the different channels of the RGB color model.

While originally developed to detect impact damage, the method was applied to ACP Handbook standards (porosity, delamination, AFP defects, etc.) with varying degrees of success. Here, the method is applied to handbook specimen #45, is a $20 \times 6 \times 2.4$-inch S-curve laminate panel with multiple delaminations that are easily identified.

Segmentation Output:
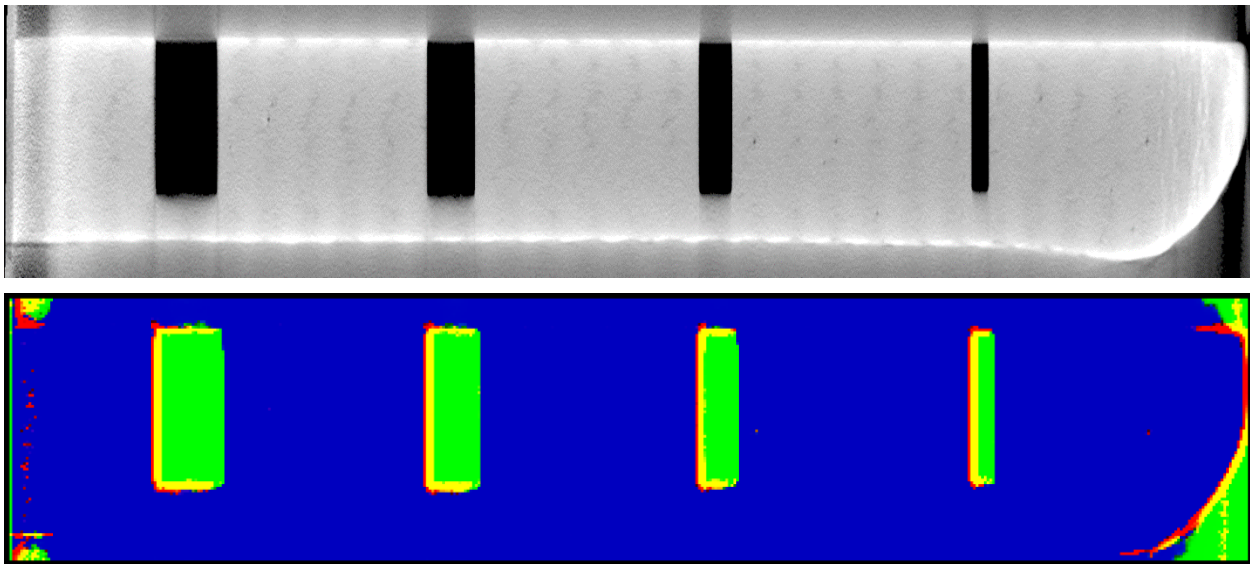
Figure E.45-6. XCT slice of Specimen #45 shown normal to the x-direction (top), and CNN segmentation results of the same slice (bottom).
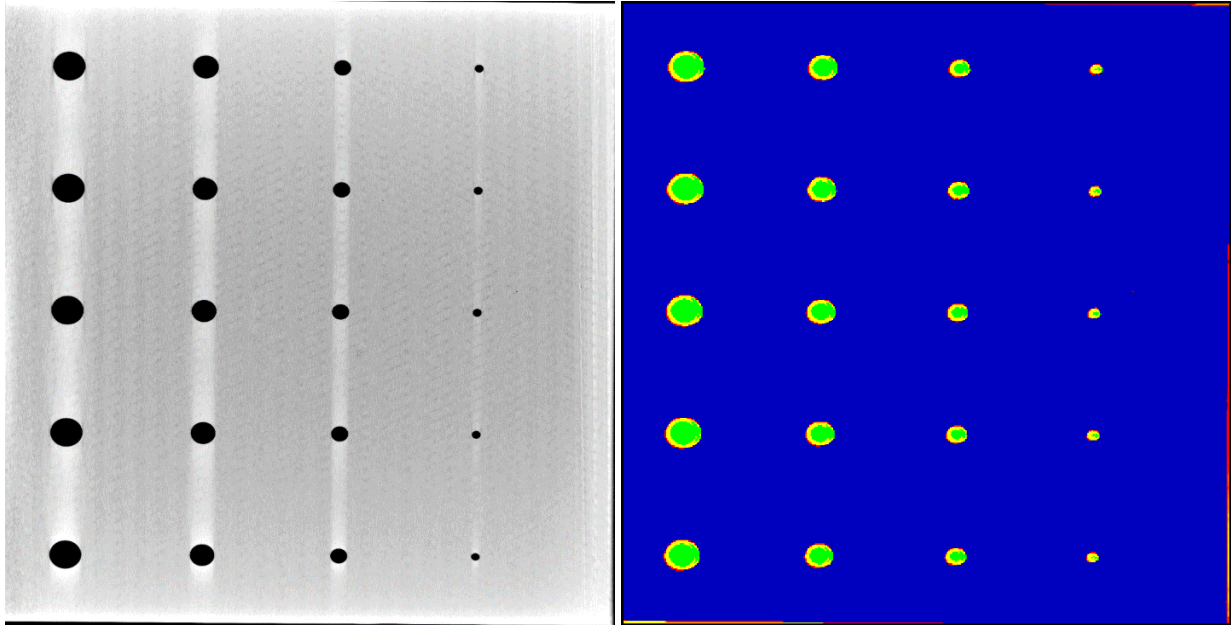
Figure E.45-7. XCT slice of Specimen #45 shown normal to the y-direction (left), and CNN Segmentation results of the same slice (right).

E.45.1.7   References

[1]   Delelegn, Desalegn Temesgen: "Non-destructive Evaluation for Composite Material," Master of Science Thesis, Old Dominion University, August 2018.

E.45.2   Method: Guided Wave Ultrasonic Testing (GWUT)

E.45.2.1   Partner: USC

E.45.2.2   Technique Applicability: ★☆☆

Guided wave ultrasonic testing (GWUT) employs ultrasonic waves that propagate along waveguides by its boundaries, e.g. pipes, rods and plate-like structures, which allows waves propagate a long distance with little energy loss. GWUT shows advantage in many types of defect inspection, e.g. crack in metallic structures [2], and delamination in composite structures [3].

The UTC-1 is inspected using hybrid piezoelectric transducers (PZT)-scanning laser Doppler vibrometer (SLDV) GWUT method in this report. General information of UTC-1 is illustrated in the paragraph below. The relative inspection, results and system rating are illustrated in the inspection results.

The top, bottom, and side view of specimen UTC-1 are shown in Figure E.45-8. The size of the specimen is 406.4 mm by 254 mm, and the thickness is around 20.6 mm. There are 20 holes on the top side of the specimen within four rows by five columns as shown in Figure E.45-8a. Each hole is named as H_{ij} with *i* as the row number and *j* as the column number. The hole diameters are 12.7 mm, 9.525 mm, 6.35 mm and 3.175 mm from row-1 to row-4. The depths are around 18 mm, 15 mm, 10 mm, 6 mm, and 3 mm from column-1 to column 5. No other information about UTC-1 is available to the inspectors.

18
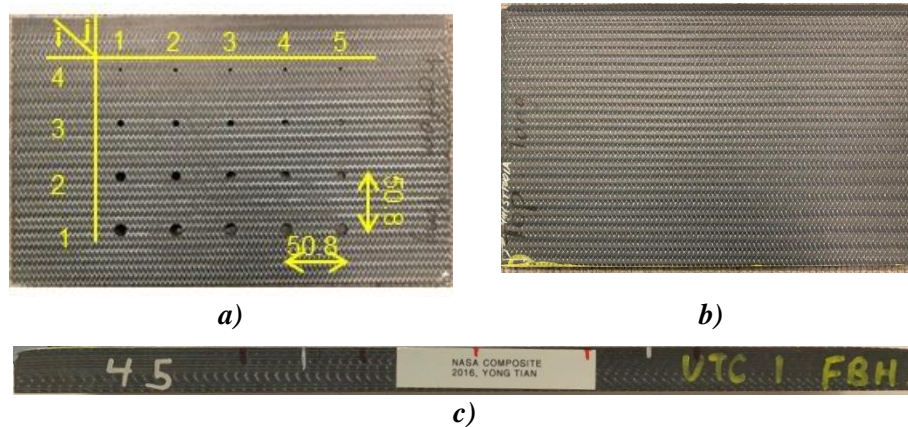
Figure E.45-8. Picture of specimen UTC-1. (a) top view, (b) bottom view, and (c) side view.

E.45.2.3   Laboratory Set Up

The same hybrid PZT-SLDV system is employed for UTC-1 inspection, where contact type PZT is used as actuator and SLDV as sensor to excite and receive guided waves in the testing plate (Lamb waves) [2]. The overall setup also remains the same as reported previously shown in Figure E.45-9 and Figure E.45-10a [4].
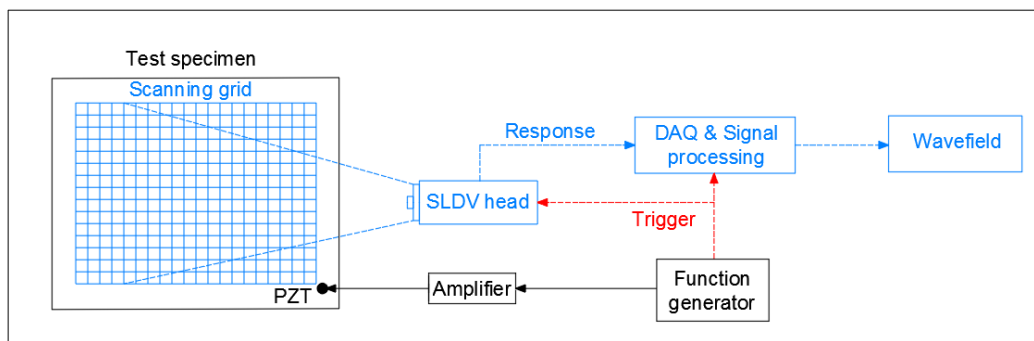
Figure E.45-9. Schematic design of the PZT-SLDV system.
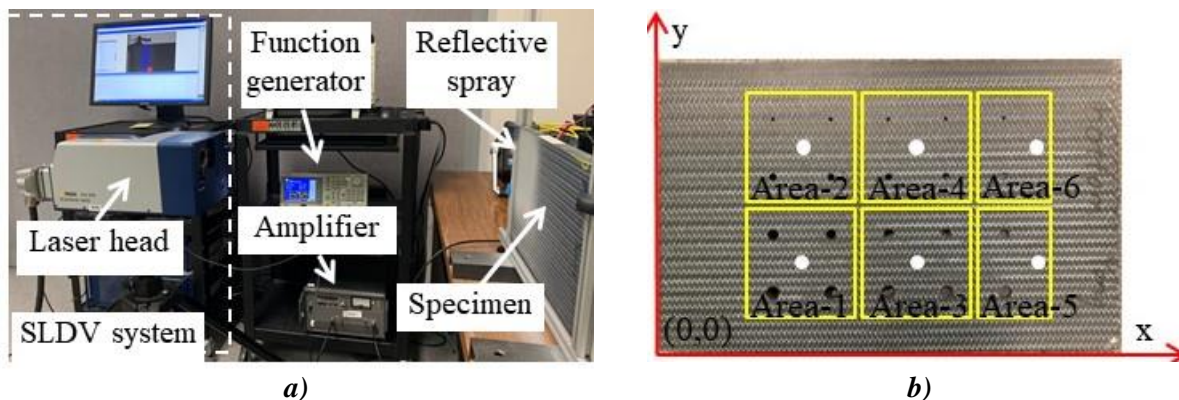
Figure E.45-10. Experimental setup: (a) PZT-SLDV system, and (b) actuation and sensing schematic.

E.45.2.4 Equipment List and Specifications

The detailed specifications of the equipment and devices used for the hybrid PZT-SLDV system at University of South Carolina (USC) Visualized Structural Health Monitoring (VSHM) laboratory are given in Table E.45-2. Data acquisition (DAQ) settings are shown in Table E.45-3.

Table E.45-2. Equipment/device specifications.

Equipment/device	Specifications
Polytec PSV-400-M2	2D scanning laser Doppler vibrometer with a frequency range up to 1 MHz with specific velocity decoders
PZT	Steminc 7-mm circular 0.5-mm thick piezoelectric transducers
Tektronix AFG3022C	2-channel arbitrary function generator with 1µHz to 25MHz
HSA 4014	High speed bipolar amplifier up to 1 MHz and 200 VA
Target Simply Balanced^{TM} organic honey	Natural and organic honey blend performed as couplant
Albedo 100 Reflective Spray	a non-permanent, clear spray with light-reflective properties

E.45.2.5 Settings

Table E.45-3. Data collection settings.

Sampling frequency (MHz)	12.56 MHz
Spatial sampling interval (mm)	1 mm
Average	100
Velocity decoder	VD-07 10mm/s/V
Spray coating	20 layers

A three-count toneburst at 180 kHz amplified to 100 V_{pp} is used as excitation. Since the plate is thick, the excited Lamb wave energy cannot propagate a long distance. In order to cover the whole plate, the inspection is performed through six area scans with six different excitation locations as shown in Figure E.45-10b. Cartesian coordinates are employed (unit: mm), and the coordinates of the six actuation locations for Area-1 to Area-6 are (127,76.2), (127,177.8), (228.6,76.2), (228.6, 177.8), (330.2,76.2), and (330.2, 177.8). The scanning area for Area-1 to Area-4 is around 90 mm by 90 mm. For Area-5 and Area-6, the scanning area is around 90 mm by 45 mm. The area scan spatial resolution is 1 mm.

Wavefield data are acquired for each scanning area. Each area is partitioned to four or two quadrants in order to reduce analysis complexity, aka. one hole for each quadrant. In order to distinguish incident waves and scattered waves, a filter process [5] is applied to remove the incident waves in the wavenumber domain. Inverse Fourier transform is then applied to transfer the remained spectrum to time and space domain. The accumulated energy map without incident waves is then obtained to highlight the damage location.

E.45.2.6 Inspection Results

The time-space wavefield of the third quadrant in Area-1 at 20 µs is plotted in Figure E.45-11a. The wave interaction with H_{11} is obviously observed. Through 3D Fourier transform, the wavenumber spectrum at excitation frequency is obtained and plotted in Figure E.45-11b. Strong incident waves and weak scatter waves are observed. Since H_{11} is the largest and deepest hole in the specimen, it is easy to be observed in the wavefield. For other holes with smaller diameter and depth, a filtering process to remove the strong incident waves is applied to reconstruct the scatter wave energy map.
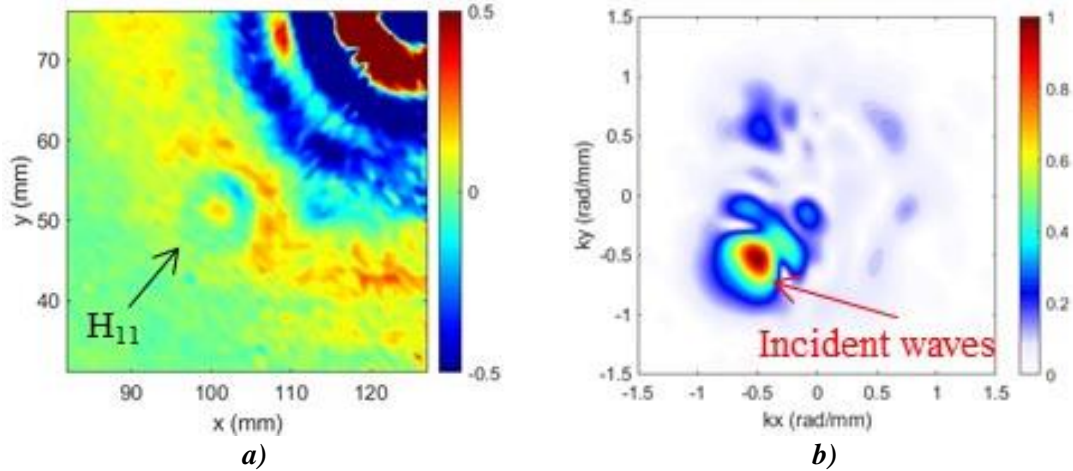
Figure E.45-11. Wavefield analysis: (a) wavefield at 20 µs of the fourth quadrant in Area-1, and (b) frequency-wavenumber spectrum.

The filter process is illustrated through the wavefield data of the third quadrant in Area-1. A filer to remove the strong incident waves is applied on the original *f-k* spectrum (Figure E.45-11b) by multiplication to retain only the scatter waves. The filter is plotted in Figure E.45-12a. After filtering, the retained *f-k* spectrum is obtained and illustrated in Figure E.45-12b. 3D inverse Fourier transform is then applied to transfer the data to time-space domain. The accumulated energy map corresponding to scatter waves is obtained and shown in Figure E.45-12c. The location of the high intensity part of the image matches H_{11} well.
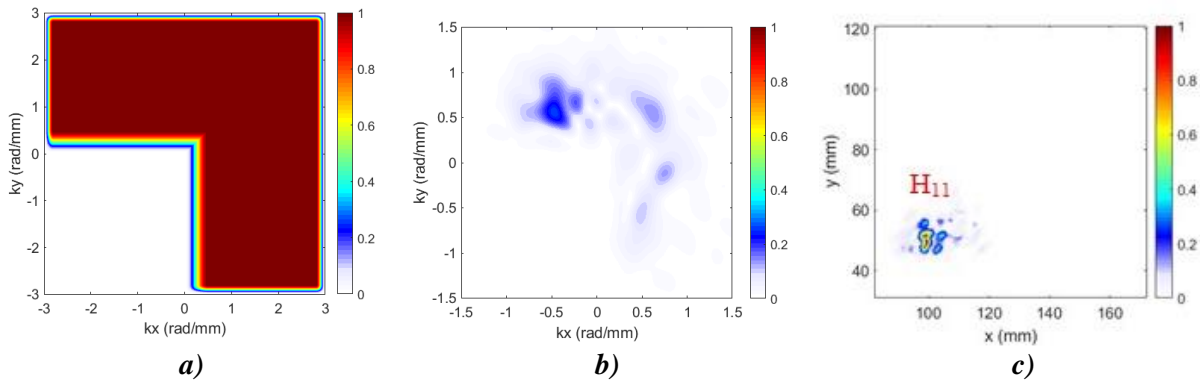
Figure E.45-12. Filtering process: (a) incident wave removal filter, (b) filtered f-k spectrum, and (c) reconstructed energy imaging showing H_{11} location.

Repeating the same process as in Section 3.3.1, the wavefield showing the wave interaction with holes are obtained and plotted in Figure E.45-13, while the filtering reconstructed image is shown in Figure E.45-14. As shown in Figure E.45-13, only the holes in Area-1 area has strong interaction with the waves and is observed in the wavefield image obviously. Other than Area-1, no obvious interactions between the holes and excited Lamb waves. While through filtering reconstruction imaging method, the hole locations are obtained. The hole layout in the imaging results (Figure E.45-14b) have a good agreement with that in the specimen shown in Figure E.45-14a.

21
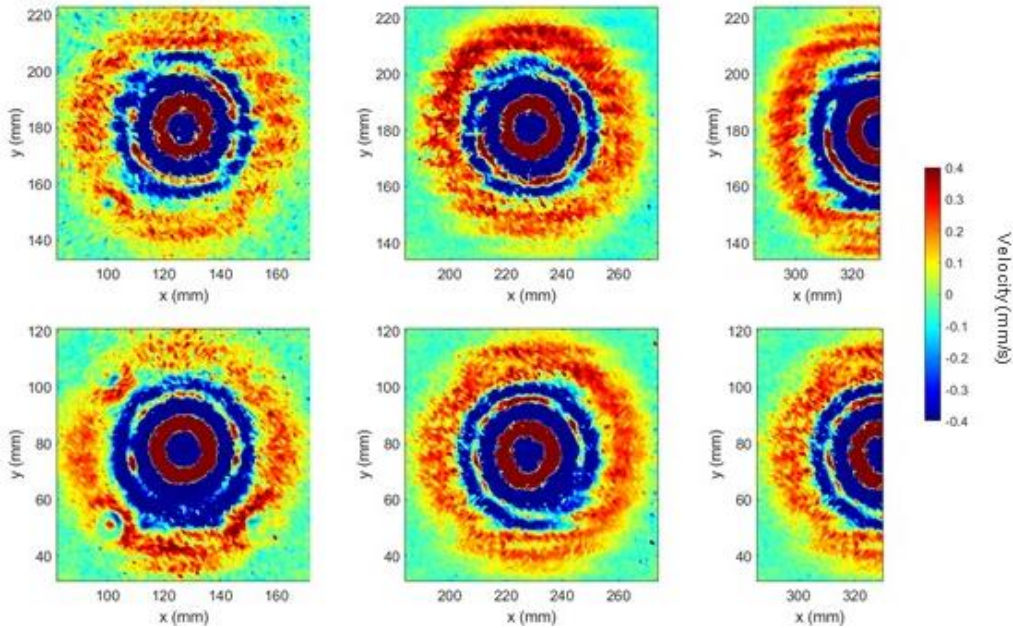
Figure E.45-13. Wave interaction with holes showing that only the holes in Area-1 area has visible interaction with waves.

a)   b)
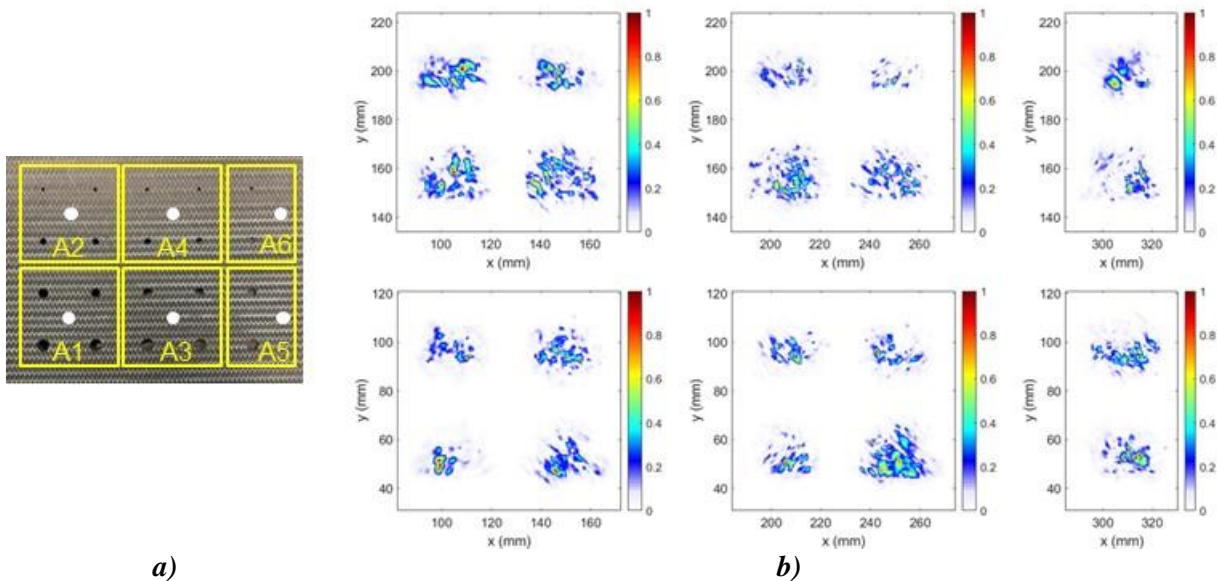
Figure E.45-14. Overall detection results based on filtering reconstruction imaging method. (a) Specimen hole layout, and (b) imaging results showing the highlighted area matches the hole layout well.

In conclusion, the holes on specimen UTC-1 using the hybrid PZT-SLDV system is detected even without material properties. The detailed rating of the system is shown in Table E.45-4. The hole locations are successfully detected through filter reconstruction imaging method. Thus, five stars are rated for this part. For defect visualization, no obvious defect size and shape is identified, so that part gets two of five stars. For inspection time, the inspection time for one 2D scanning is around 30 minutes for areas illustrated in this test, which is fast. Thus, the inspection time gets five stars overall. Last, the actuator PZT is $3.60 per piece, which is cost effective. However, the SLDV

22

is an expensive equipment, which costs $300,000 when purchasing. Thus, this part gets two stars. In the future, expensive SLDV can be replaced by customized fixed LDV and gantry system to reduce the system cost. Overall, this hybrid PZT-SLDV guided wave inspection in general gets three out of five stars.

Table E.45-4. Hybrid PZT-SLDV guided wave inspection rating.

Hybrid PZT-SLDV guided wave inspection		
Sample A2 Defect: wrinkles	Rating	
	Detection:	★★★★★
	Defect visualization	★★☆☆☆
	Inspection time:	★★★★★
	Equipment cost:	★★☆☆☆
	Overall Performance:	★★★☆☆

E.45.2.7 References

[1]   Yu, L.; Leckey, C. A.; and Tian, Z.: "Study on crack scattering in aluminum plates with Lamb wave frequency–wavenumber analysis," *Smart Materials and Structures*, Vol. 22, No. 6, pp065019, 2013.

[2]   Tian, Z.; Yu, L.; and Leckey, C.: "Delamination detection and quantification on laminated composite structures with Lamb waves and wavenumber analysis," *Journal of Intelligent Material Systems and Structures*, Vol.26, No. 13, 2015, pp. 1723-1738, 2015.

[3]   Guided wave inspection on specimen A1 (A1 report, submitted).

[4]   Tian, Z.; Yu, L.; Leckey, C.; and Seebo, J.: "Guided wave imaging for detection and evaluation of impact-induced delamination in composites," *Smart Materials and Structures*, Vol. 24, No. 10, p.105019, 2015.

E.46   Specimen #46: UTC-Mold Release Specimen

Structure	Material	Details	Dimensions (inches)	Partner	Methods
Triaxial Braid, 0/+60/-60	T-800SC with 3M AMD-825	Flat Panel with mold release induced disbond	13 × 12.5 × 0.5	NASA	E.46.1 XCT
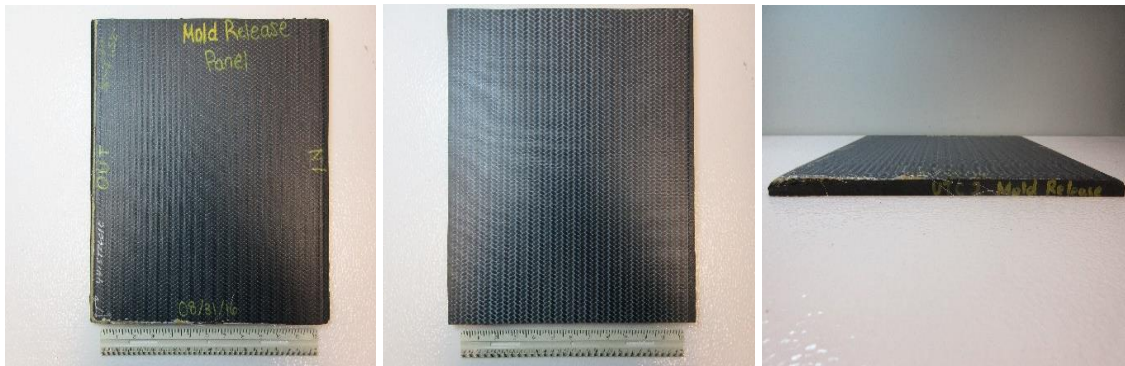
Figure E.46-1. Photographs of Specimen #46: UTC-Mold Release Specimen.

E.46.1   Method: X-ray Computed Tomography (XCT)

E.46.1.1   Partner: NASA

E.46.1.2   Technique Applicability: ☆☆☆

XCT is not capable of imaging the fiber snags in this specimen.

E.46.1.3   Laboratory Setup

The microfocus XCT system at NASA LaRC is a commercially available Avonix (Nikon C2) Metrology System designed for high-resolution NDE inspections. The system is an advanced microfocus X-ray system, capable of resolving details down to 5 μm, and with magnifications up to 60X. Supplied as complete, the system is a large-dimension radiation enclosure with X-ray source, specimen manipulator, and an amorphous silica detector, as shown in Figure E.46-2. The imaging controls are housed in a separate control console. The detector is a Perkin-Elmer, 16-bit, amorphous-silicon digital detector with a 2000 × 2000-pixel array.

A consistent Cartesian coordinate system is used to define slice direction as illustrated in Figure E.46-3. Slices normal to the X-, Y-, and Z-directions are shown in Figures E.46-3a, b, and c, respectively.

X-ray source

3.8 ft.

Detector

Rotational Stage
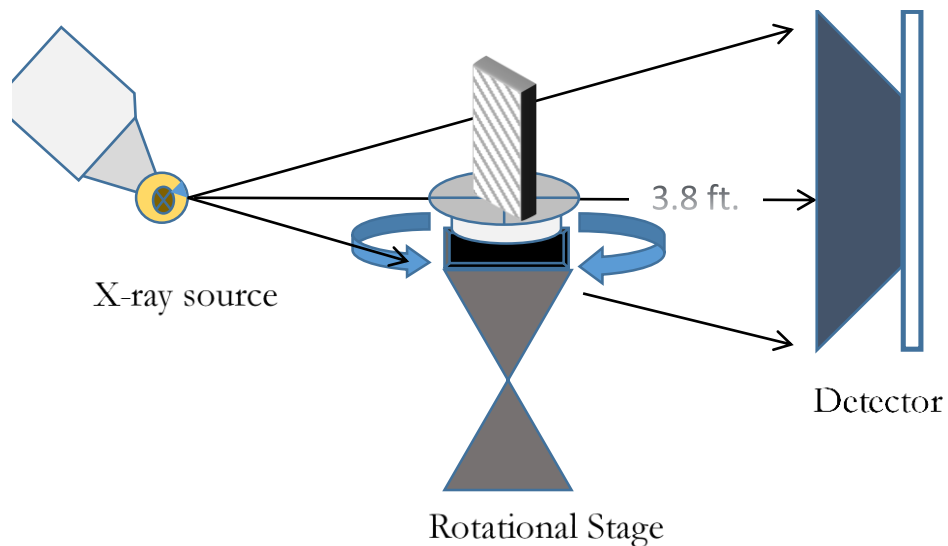
Figure E.46-2. XCT system components.
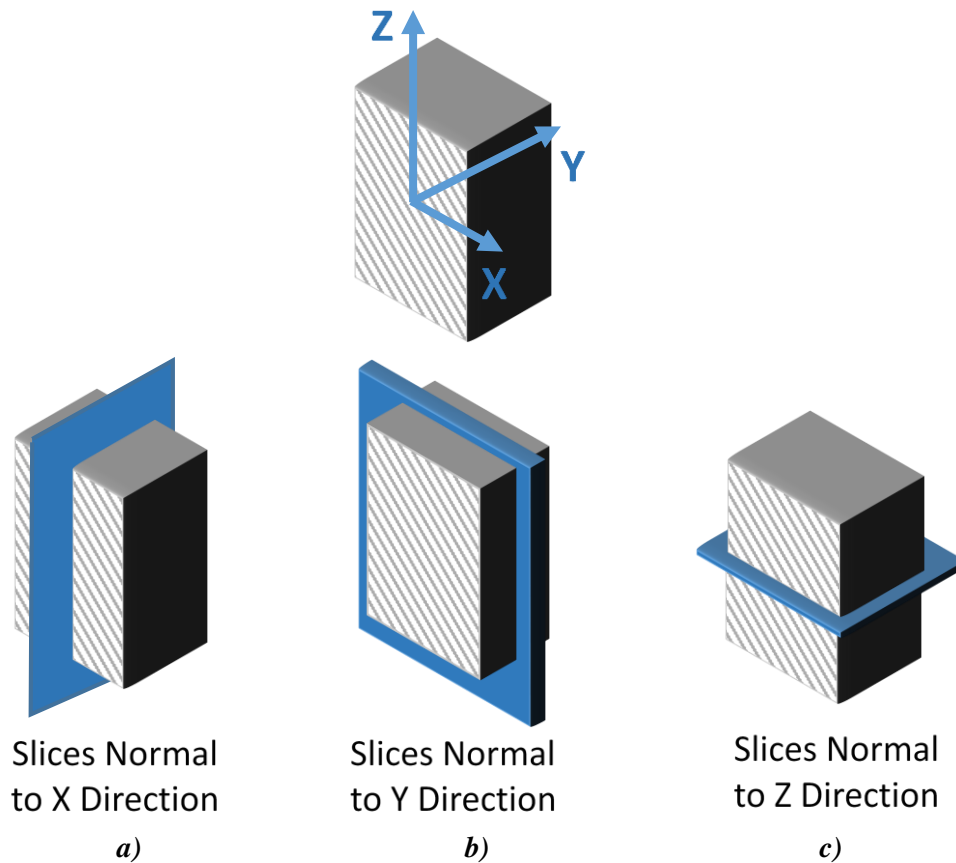
Figure E.46-3. Slice direction nomenclature.
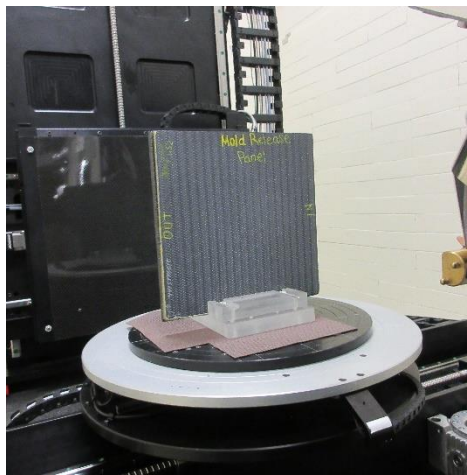
Figure E.46-4. Mold release specimen test stand setup.

E.46.1.4   Equipment List and Specifications:

- Avonix 225 CT System
- 225 kV microfocus X-ray source with 5-µm focal spot size
- 15 or 30 kg Capacity 5-axis fully programmable manipulator.
- Detector: Perkin Elmer XRD 1621 – 2000 × 2000 pixels with 200 µm pitch
- 10-µm spatial resolution for specimens 1.5 cm wide

- Thin panels 10×10 inches – full volume 200 μm spatial resolution

E.46.1.5 Settings

Table E.46-1. Data collection settings.

Source Energy	150 kV
Current	50 μA
Magnification	1.65 X
Filter	NF
# Rotational angles	3142
Exposure time / frame	1.0 sec.
Max Histogram Grey Level	30 K
# Averages	8
Resolution (μm)	120.947 μm
Array Dimensions (pixels)	$2 K \times 2 K$

The specimen is placed vertically (rotated about the smallest dimension) on the rotational stage located between the radiation source and the detector. The rotational stage is computer-controlled and correlated to the position of the sample. As the sample is rotated the full 360° (~0.11° increments), the detector collects radiographs at each rotated angle as the X-ray path intersects the sample. 3D reconstruction of the collection of radiographs produces a volume of data that can then be viewed along any plane in the volume. The closer the sample can be placed to the X-ray source, the higher the spatial resolution that can be obtained.

E.46.1.6 Inspection Results

Specimen #46, UTC-Mold release, is a flat panel fabricated from T-800SC with 3M AMD-825, with an objective of achieving kissing bonds at varying deptsh and sizes in the fabric layup (see Appendix C for defect geometry). XCT was performed on this specimen in NASA LaRC's CT system with the settings defined in Section E.46-5.

From XCT analysis, there were no obvious delaminations seen within the specimen from any viewing direction as seen in Figure E.46-5. This is most likely due to the nature of the defect type. Mold release will cause a kissing bond between plies of the material that will not cause a change in density within the material. Validation testing with ultrasonic methods were unable to confirm the defects (Apppendix D). There are anomolous strands of higher-density material running near the ouside edge as highlighted in Figure E.46-5 and Figure E.46-6. This defect has not been identified though is most likely due to a manufacturing method.

Figure E.46-5. CT slices from the y-direction and z-direction highlighting an anomaly within the sample.
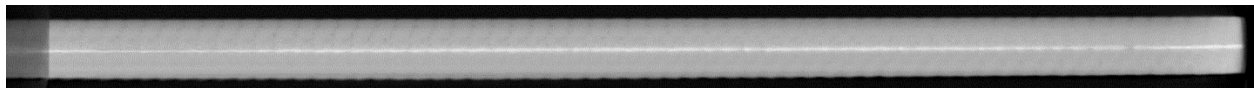
Figure E.46-6. CT slices from the x-direction showing no obvious defects within the bulk of the specimen.

E.47   Specimen #47: UTC-3-Pillow

Structure	Material	Details	Dimensions (inches)	Partner	Methods
Triaxial Braid, 0/+60/-60	T-800SC with 3M AMD-825	Delaminations in woven composites (Air pillow)	13 × 13 × 0.5	NASA	E.47.1 PEUT E.47.2 XCT
				USC	E.47.3 GWUT

a)	*b)*	*c)*
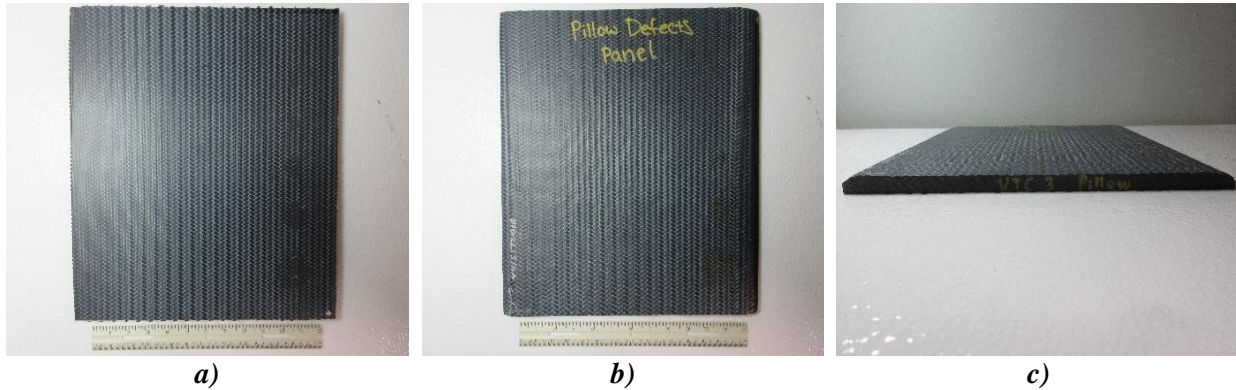
Figure E.47-1. Photographs of Specimen #47: UTC-3-Pillow.

E.47.1 Method: Pulse-Echo Ultrasonic Testing (PEUT)

E.47.1.1 Partner: NASA

E.47.1.2 Technique Applicability: ★ ★ ★

PEUT detected the delaminations in this specimen.

E.47.1.3 Laboratory Setup

Immersion Ultrasonic Testing: NASA LaRC uses a custom-designed single-probe ultrasonic scanning system. The system has an 8-axis motion controller, a multi-axis gantry robot mounted above a medium-size water tank, a dual-channel, 16-bit, high-speed digitizer, and an off-the-shelf ultrasonic pulser receiver. The system can perform through transmission (TT) and PEUT inspections. TT inspection employs two aligned ultrasonic probes, one transmitter and one receiver, placed on either side of a test specimen. Pulse-echo inspection is a single-sided method where a single ultrasonic probe is both transmitter and receiver. In each method, data are acquired while raster scanning the ultrasonic probe(s) in relation to a part. Figure E.47-2 shows a simplified block diagram of a scanning Pulse-echo inspection.
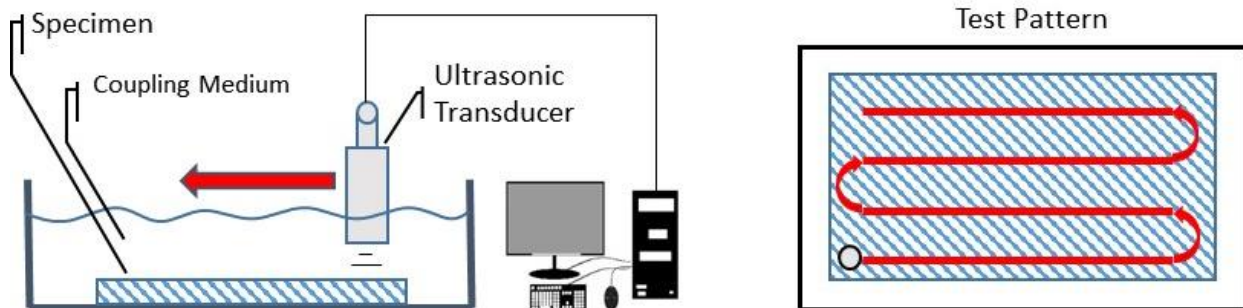
Figure E.47-2. Ultrasonic system components.

E.47.1.4 Equipment List and Specifications:

- Pulser/Receiver: Olympus 5073PR
- Digitizer: AlazarTech ATS9462, dual channel, 16-bit, 180 MS/s
- Sensor: Olympus 2-inch spherical focus immersion ultrasonic transducer
- Motion system: open looped stepper motor based X-YY-Z gantry robot
- Motion Controller: Galil DMC-4183

28

- Acquisition Software: FastScan, custom developed at NASA LaRC
- Signal Processing Software: DataViewer, custom developed at NASA LaRC

E.47.1.5   Settings

Table E.47-1. Data collection settings.

Resolution horizontal [in/pixel]	0.01
Resolution vertical [in/pixel]	0.01
Probe frequency [MHz]	5
Focal Length [in]	2
Array Dimensions [pixels]	536×579

The specimen is placed flat against the zero position of the tank raised above the glass bottom by several metal washers. The test probe is computer-controlled and correlated to the position on the sample. It is also focused to a point 1 mm below the surface of the test material. The specimen remains in place while the transducer follows a preprogrammed test grid across the surface as indicated in Figure E.47-2. At each point, ultrasonic data are collected from individual pulses. Larger step sizes between data collection result in lower image resolution. These data points are reconstructed into a data cube displaying spatial coordinates as time progresses. 2D reconstruction of the collection of ultrasonic responses create flattened slices at varying depths within the material.

E.47.1.6   Inspection Results

Specimen #47 is a flat triaxial braid panel fabricated from T-800SC with 3M AMD-825 with the objective of creating air pillow delaminations throughout the sample. PEUT was performed on this specimen in NASA's immersion tank specified above.

The scan was performed on four different segments to examine defects at a high resolution; as such, the images do not represent the whole of the specimen. In Figure E.47-3a several delamination of various sizes appear just below the surface ply of the specimen at a 0.06-inch depth. Figure E.47-3b shows delaminations at a depth of 0.15-inch depth. The delaminations have a higher reflected signal amplitude due to the acoustic impedance mismatch. Therefore, subsequent data appears darker than the bulk material as there is less remaining energy to propagate through that region. Figure E.47-4 shows several delaminations at 0.24 inch into the specimen.
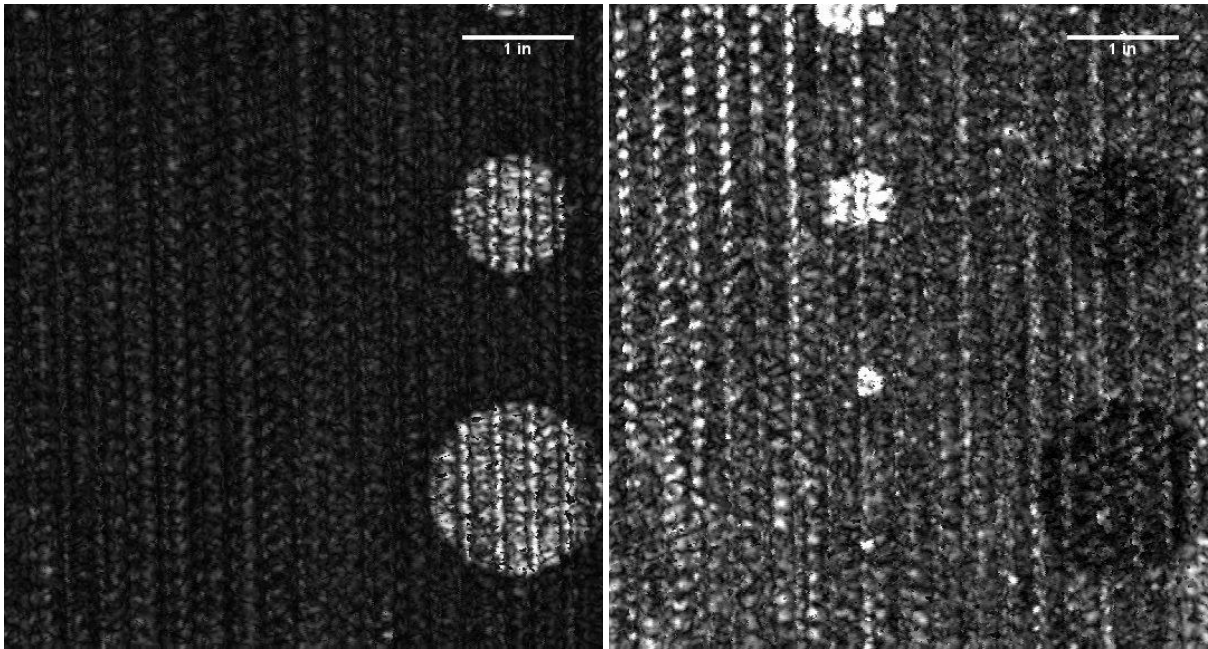
Figure E.47-3. (a) near surface delaminations (b) peak amplitude within the sample.
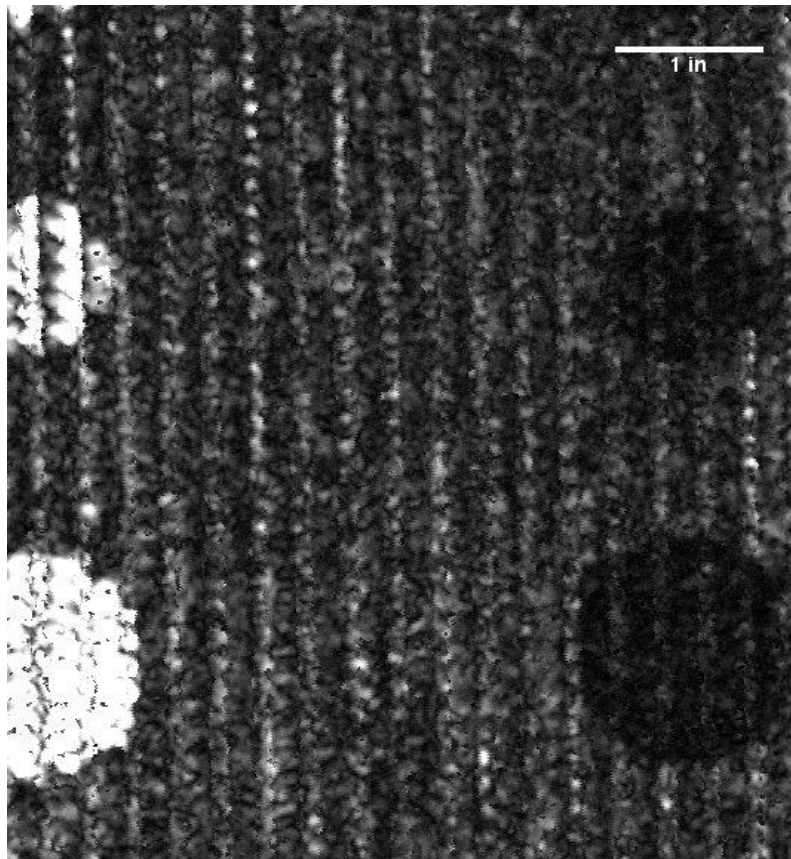
Figure E.47-4. UT image showing delaminations within the bulk of the material.

E.47.2   Method: X-ray Computed Tomography (XCT)

E.47.2.1   Partner: NASA

E.47.2.2   Technique Applicability: ★★★

XCT is capable of imaging the air pillow delaminations in this specimen.

E.47.2.3   Laboratory Setup

The microfocus XCT system at NASA LaRC is a commercially available Avonix (Nikon C2) Metrology System designed for high-resolution NDE inspections. The system is an advanced microfocus X-ray system, capable of resolving details down to 5 μm, and with magnifications up to 60X. The system is supplied as a complete, large-dimension radiation enclosure, with X-ray source, specimen manipulator, and an amorphous silica detector as shown in Figure E.47-5. The imaging controls are housed in a separate control console. The detector is a Perkin-Elmer, 16-bit, amorphous-silicon digital detector with a 2000 × 2000-pixel array.

A consistent Cartesian coordinate system is used to define slice direction as illustrated in Figure E.47-5 and Figure E.47-6. Slices normal to the X-, Y-, and Z-directions are shown in Figures | E.47-6a, b, and c, respectively.
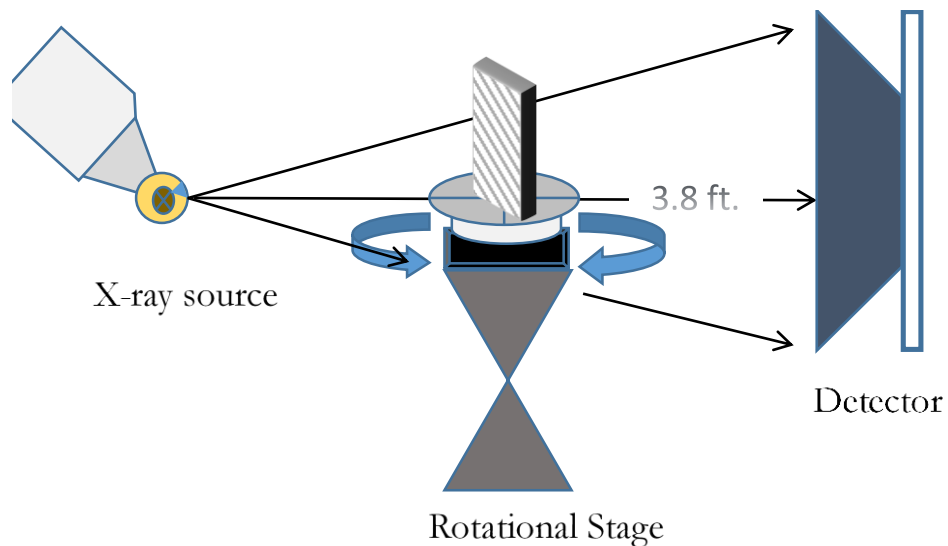
Figure E.47-5. XCT system components.
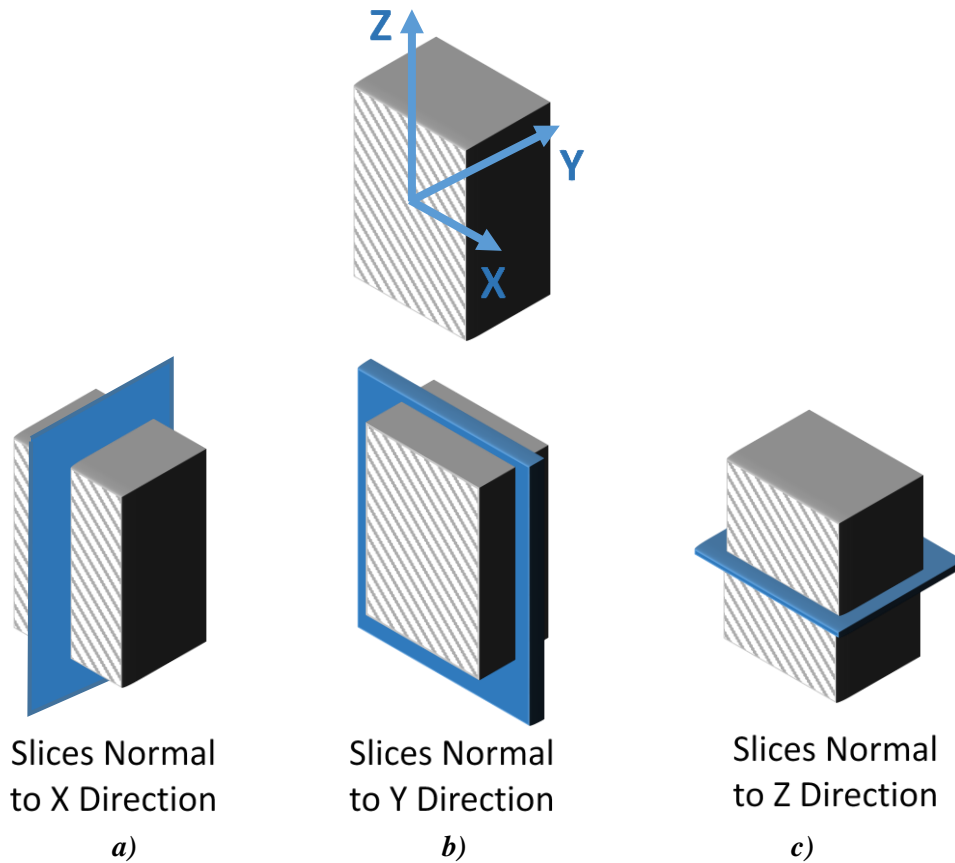
Figure E.47-6. Slice direction nomenclature.

Figure E.47-7. Mold release specimen test stand setup.

E.47.2.4 Equipment List and Specifications:

- Avonix 225 CT System
- 225 kV microfocus X-ray source with 5 µm focal spot size
- 15 or 30 kg Capacity, 5-axis, fully programmable manipulator
- Detector: Perkin Elmer XRD 1621 – 2000 × 2000 pixels with 200 µm pitch
- 10 µm spatial resolution for specimens 1.5 cm wide
- Thin panels 10 × 10 inches – full volume 200 µm spatial resolution

32

E.47.2.5   Settings

Table E.47-2. Data collection settings.

Source Energy	105 kV
Current	59 µA
Magnification	1.65 X
Filter	NF
# Rotational angles	3142
Exposure time / frame	1.0 sec
Max Histogram Grey Level	25 K
# Averages	8
Resolution (µm)	128.430 µm
Array Dimensions (pixels)	2K × 2K

The specimen is placed vertically (rotated about the smallest dimension) on the rotational stage located between the radiation source and the detector. The rotational stage is computer-controlled and correlated to the position of the sample. As the sample is rotated the full 360° (~0.11° increments), the detector collects radiographs at each rotated angle as the X-ray path intersects the sample. 3D reconstruction of the collection of radiographs produces a volume of data that can then be viewed along any plane in the volume. The closer the sample can be placed to the X-ray source, the higher the spatial resolution that can be obtained.

E.47.2.6   Inspection Results

Specimen #47, NASA-S-MP, is a flat panel with the object of achieving several instances of air pillow delaminations. The air pillows are of varying size and depth within the sample as seen in Figure E.47-9. XCT was performed on this specimen in NASA LaRC's large CT system with the settings defined in Section E.47.1.5.

The delaminations caused by air pillows can be clearly seen from all viewing directions as shown in Figure E.47-8. There is excellent contrast indicating where the defects begin compared to the solid grey bulk material. Upon further review of the sample there are little to no other defects present other than the occasional FOD, which is indicated by brighter spots due to a typically greater density than the bulk material. There is also low porosity dispersed evenly throughout the sample, indicated by small dark regions.
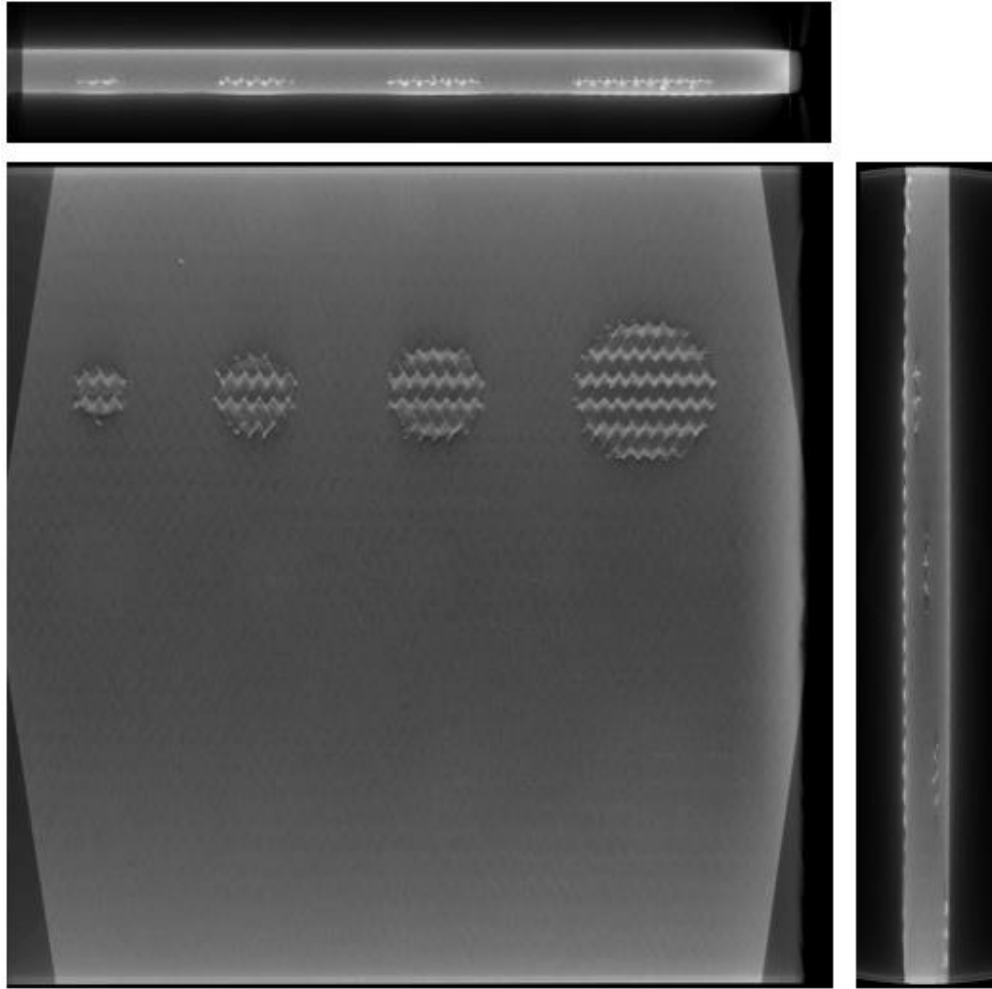
Figure E.47-8. 3D X-ray generated view of specimen #47.
UTC-3-Pillow showing the y direction (center), z direction (top) and x direction (top).

E.47.3   Method: Guided Wave Ultrasonic Testing (GWUT)

E.47.3.1   Partner: USC

E.47.3.2   Technique Applicability: ★★★

GWUT employs ultrasonic waves that propagate along waveguides by its boundaries, e.g. pipes, rods and plate-like structures, which allows waves propagate a long distance with little energy loss. GWUT shows advantage in many types of defect inspection, e.g. crack in metallic structures [2], and delamination in composite structures [3].

The UTC-3 is inspected using hybrid PZT-SLDV GWUT method in this report. General information of UTC-3 is illustrated in the paragraph below. The relative inspection, results and system rating are illustrated in the inspection results.

The top and bottom view of specimen UTC-3 are shown in Figure E.47-9. The size of the specimen is 335 mm by 335 mm, and the thickness is around 13.3 mm. Ten pillow defects are observed with five closer to top surface and five closer to bottom surface as pointed in yellow arrow. The size of the defects increases from up edge to bottom edge of the specimen. No other information about UTC-3 is available to the inspectors.

34

a)   *b)*
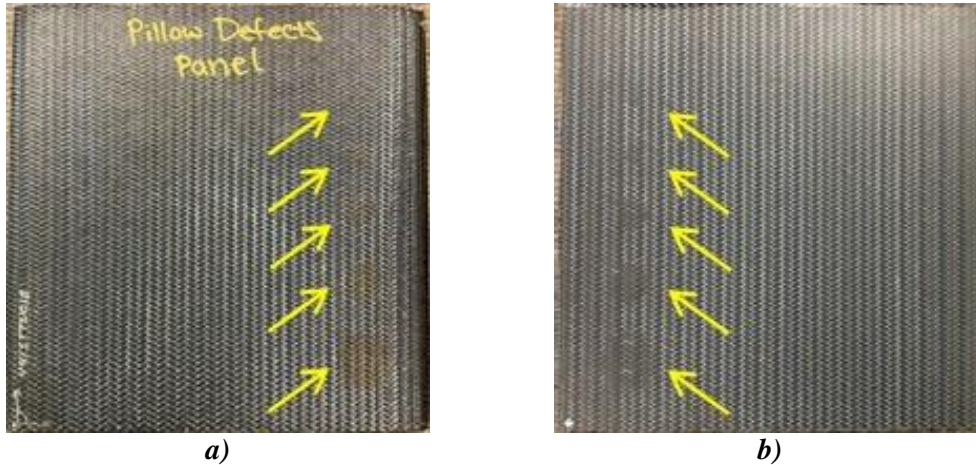
Figure E.47-9. Picture of specimen UTC-3. (a) top view, and (b) bottom view.

E.47.3.3   Laboratory Set Up

The same hybrid PZT-SLDV system is employed for UTC-3 inspection, where contact type PZT is used as actuator and SLDV as sensor to excite and receive guided waves in the testing plate (Lamb waves) [2]. The overall setup also remains the same as reported previously shown in Figure E.47-10 and Figure E.47-11a [4].
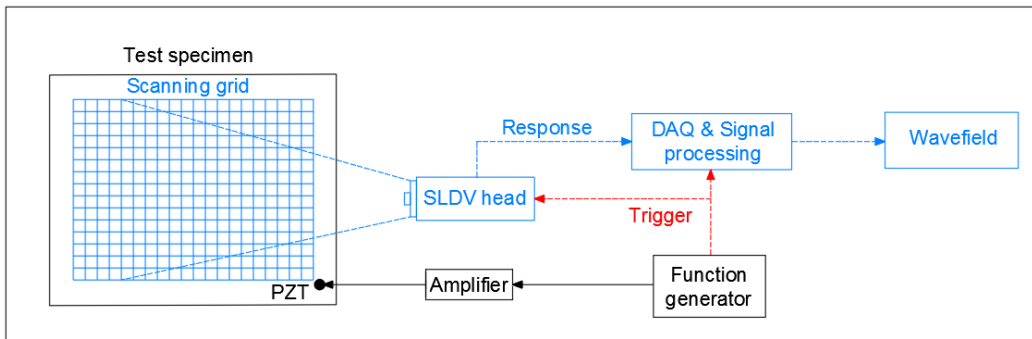
Figure E.47-10. Schematic design of the PZT-SLDV system.

a)   *b)*
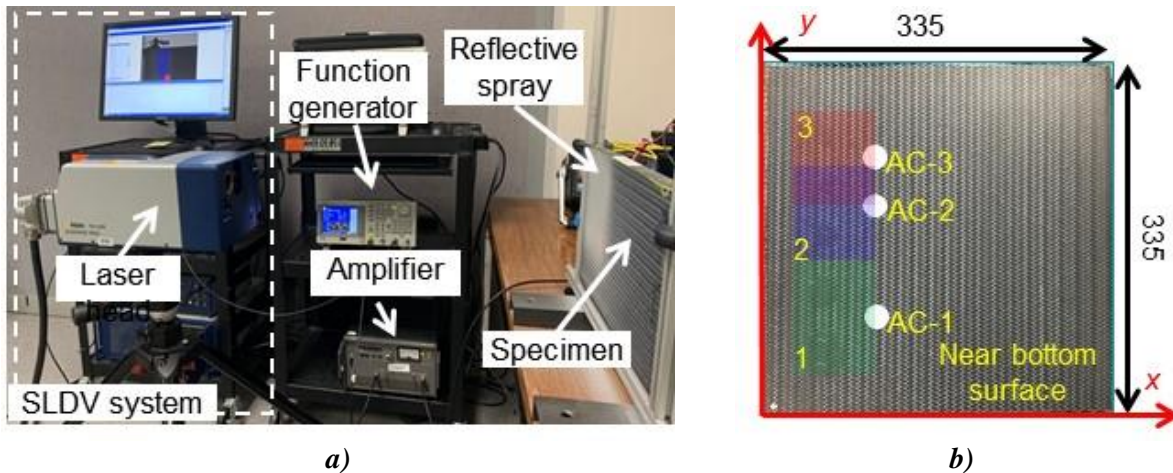
Figure E.47-11. Experimental setup.
(a) PZT-SLDV system, and (b) actuation and sensing schematic.

E.47.3.4 Equipment List and Specifications

The detailed specifications of the equipment and devices used for the hybrid PZT-SLDV system at USC VSHM laboratory are given in Table E.47-3. DAQ settings are shown in Table E.47-4.

Table E.47-3. Equipment/device specifications.

Equipment/device	Specifications
Polytec PSV-400-M2	2D scanning laser Doppler vibrometer with a frequency range up to 1 MHz with specific velocity decoders
PZT	Steminc 7-mm circular 0.5-mm thick piezoelectric transducers
Tektronix AFG3022C	2-channel arbitrary function generator with 1µHz to 25MHz
HSA 4014	High speed bipolar amplifier up to 1 MHz and 200 VA
Target Simply Balanced^{TM} organic honey	Natural and organic honey blend performed as couplant
Albedo 100 Reflective Spray	a non-permanent, clear spray with light-reflective properties

E.47.3.5 Settings

Table E.47-4. Data collection settings.

Sampling frequency (MHz)	12.56 MHz
Spatial sampling interval (mm)	1 mm
Average	100
Velocity decoder	VD-07 10mm/s/V
Spray coating	20 layers

A three-count toneburst at 180 kHz amplified to 100 V_{pp} is used as excitation. The bottom of the specimen is smoother finish compared to the bottom surface, which is better for the reflective spray application. Thus, the five defects closer to the bottom surface are first inspected. In order to cover the whole plate, the inspection is performed through three area scans with three different excitation locations as shown in Figure E.47-11b. Cartesian coordinates are employed (unit: mm), and the coordinates of the three actuation locations for AC-1 to AC-3 are (110,90), (110,200), and (110,245). The area scan spatial resolution is 1 mm. The same setup is adopted for top surface except the excitation locations for AC-1 to AC-3 are (225,90), (225,200), and (225,245), respectively.

Inspection Results

Inspection Results on Bottom Surface

The time-space wavefield of the three scanning area are plotted in Figures E.47-12b through E.47-12d, respectively. One can see that strong wave interactions appeared in the defect area. Waves trapped in the defect area and the trapped waves have shorter wavelength. The defect shape is clearly observed, which is circular. Wavefield images are generated and plotted in Figures E.47-12e through E.47-12-g, respectively, using the methodology in [4]. The defect diameters are estimated from the plots as 38 mm, 25 mm, 19 mm, 13 mm, 6 mm, respectively.
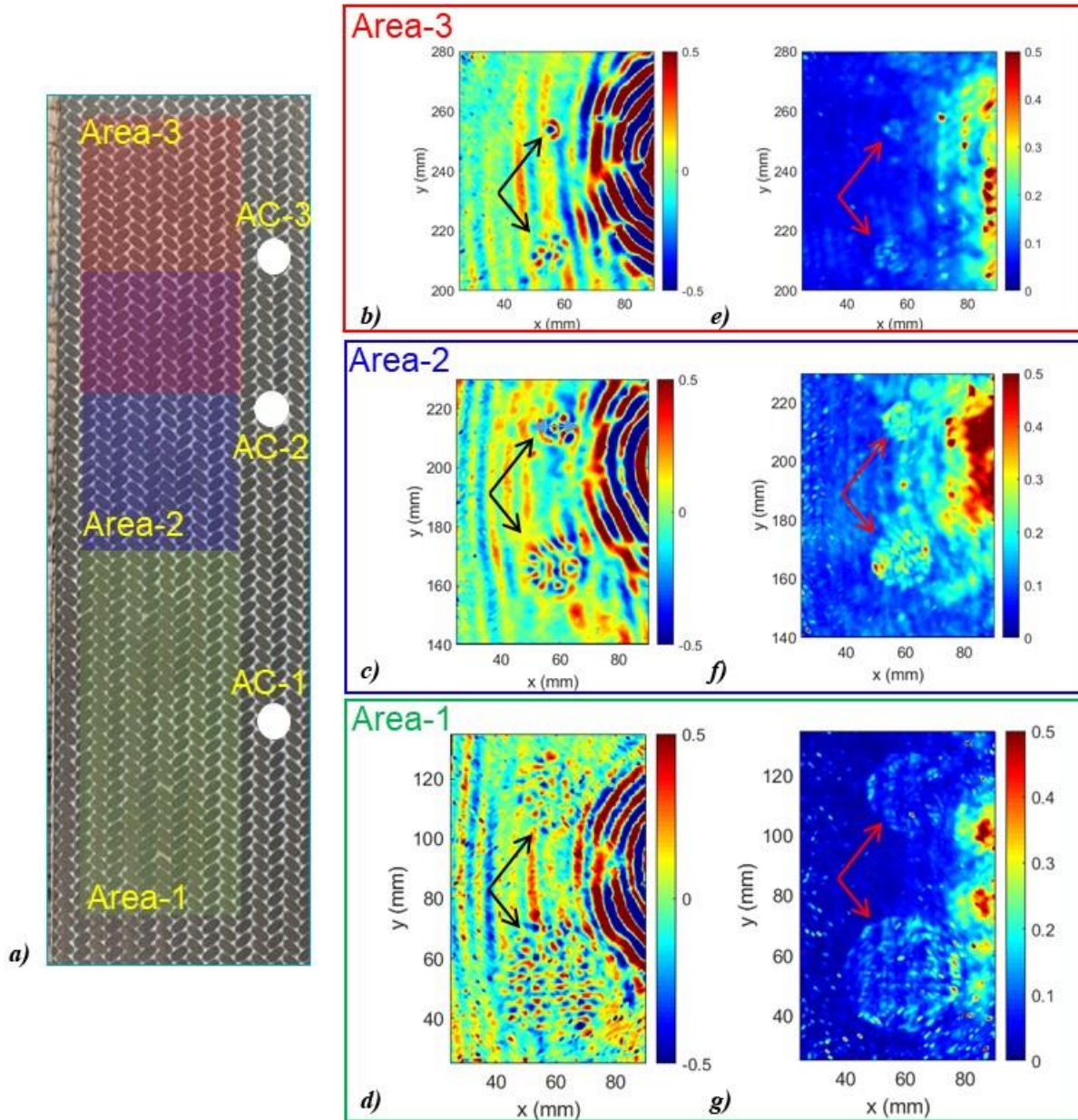
Figure E.47-12. Bottom surface inspection results.
(a) Actuation and sensing setup, (b)⌐(d), wavefield snapshot to show wave interaction with defects, and
(e)⌐(g) wavefield imaging for better visualization of defects.

Inspection Results on Top Surface

The time-space wavefield of the three scanning area are plotted in Figure E.47-13b through E.47-13d, respectively. Strong wave interactions are observed for four defects (larger sizes) in the defect area. Wave interaction was not observed for the smallest defect. Wavefield images are generated and plotted in Figure E.47-13e through E.47-13g, respectively. The smallest defect showed up in the wavefield image as shown in Figure E.47-13e. The defect shape is circular, and their diameters re estimated from the plots as 38 mm, 25 mm, 19 mm, 13 mm, 4 mm, respectively. The top surface condition is not as smooth as the bottom surface, the light reflection strength

decreased with the same reflective spray application. Thus, the inspection results are not as good as bottom surface.
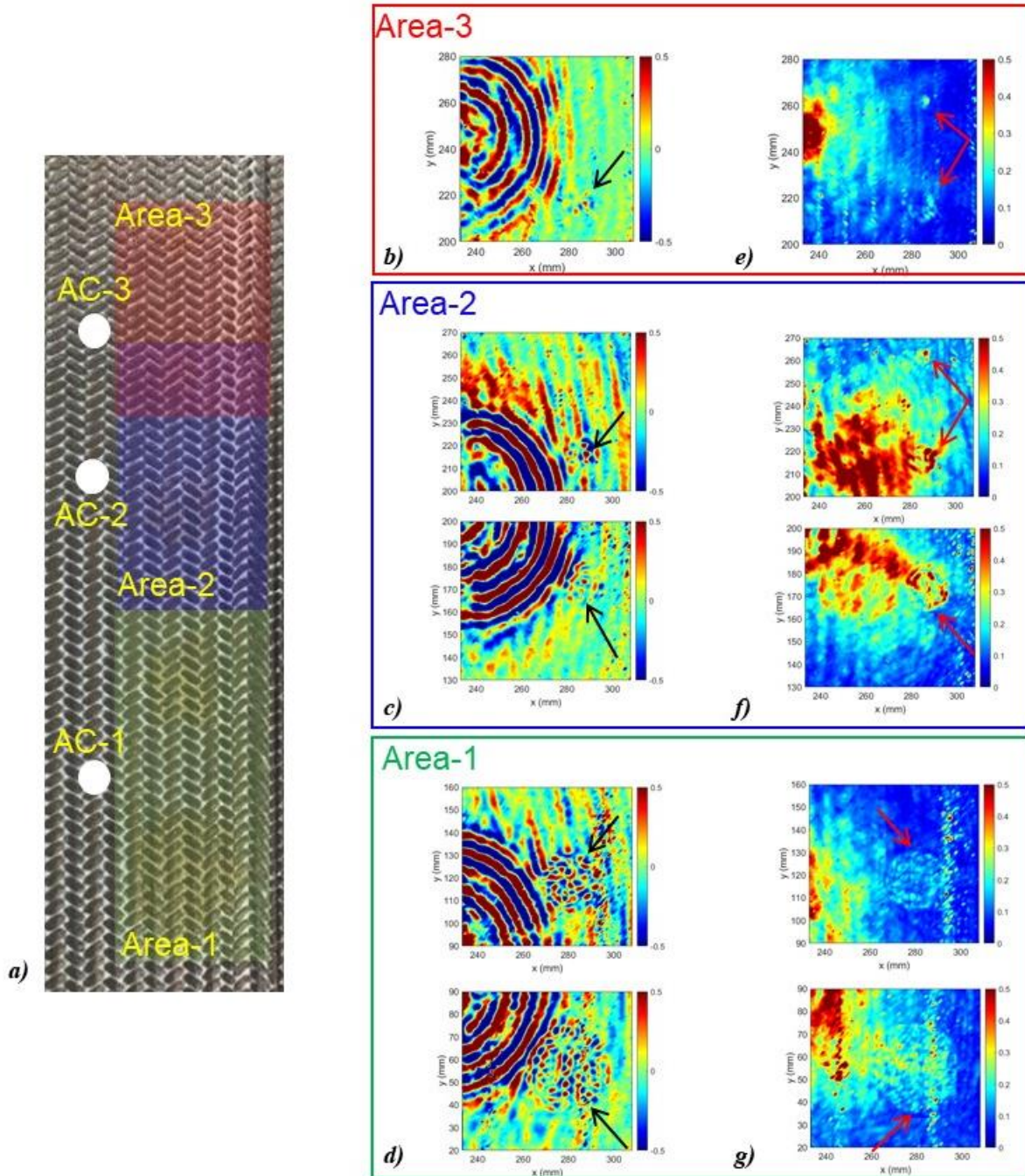
Figure E.47-13. Top surface inspection results.
(a) Actuation and sensing setup, (b)–(d), wavefield snapshot to show wave interaction with defects, and (e)–(g) wavefield imaging results.

In conclusion, the pillow defects in the specimen UTC-3 using the hybrid PZT-SLDV system is detected and quantified even without material properties. The detailed rating of the system is shown in Table E.47.5. The defect locations are successfully detected through wavefield imaging method. Thus, five stars are rated for this part. For defect visualization, both the size and shape are

clearly identified, so that part gets five of five stars. For inspection time, the inspection time for one 2D scanning is around 30 minutes for areas illustrated in this test, which is relatively rapid. Thus, the inspection time gets five stars overall. Last, the actuator PZT is $3.60 per piece, which is cost effective. However, the SLDV is an expensive equipment, which costs $300,000 when purchasing. Thus, this part gets two stars. In the future, expensive SLDV can be replaced by customized fixed LDV and gantry system to reduce the system cost. Overall, this hybrid PZT-SLDV guided wave inspection in general gets four out of five stars.

Table E.47-5. Hybrid PZT-SLDV guided wave inspection rating.

Hybrid PZT-SLDV guided wave inspection		
Sample A2 Defect: wrinkles	Rating	
	Detection:	★ ★ ★ ★ ★
	Defect visualization	★ ★ ★ ★ ★
	Inspection time:	★ ★ ★ ★ ★
	Equipment cost:	★ ★ ☆ ☆ ☆
	Overall Performance:	★ ★ ★ ★ ☆

E.47.3.6   References

[1]   Yu, L.; Leckey, C. A.; and Tian, Z.: "Study on crack scattering in aluminum plates with Lamb wave frequency–wavenumber analysis," *Smart Materials and Structures*, Vol. 22, No. 6, pp065019, 2013.

[2]   Tian, Z.; Yu, L.; and Leckey, C.: "Delamination detection and quantification on laminated composite structures with Lamb waves and wavenumber analysis," *Journal of Intelligent Material Systems and Structures*, Vol.26, No. 13, 2015, pp. 1723-1738, 2015.

[3]   Guided wave inspection on specimen A1 (A1 report, submitted).

[4]   Tian, Z.; Yu, L.; Leckey, C.; and Seebo, J.: "Guided wave imaging for detection and evaluation of impact-induced delamination in composites," *Smart Materials and Structures*, Vol. 24, No. 10, p.105019, 2015.

E.48   Specimen #48: UTC 6 Porosity 2

Structure	Material	Details	Dimensions (inches)	Partner	Methods
Triaxial Braid) [0 +60 -60]	T-800SC Triaxial Braid 0/+60/-60 with 3M AMD-825	Flat panel Triaxial braid with small porosity	13 × 13 × 0.65	NASA	E.48.1 XCT
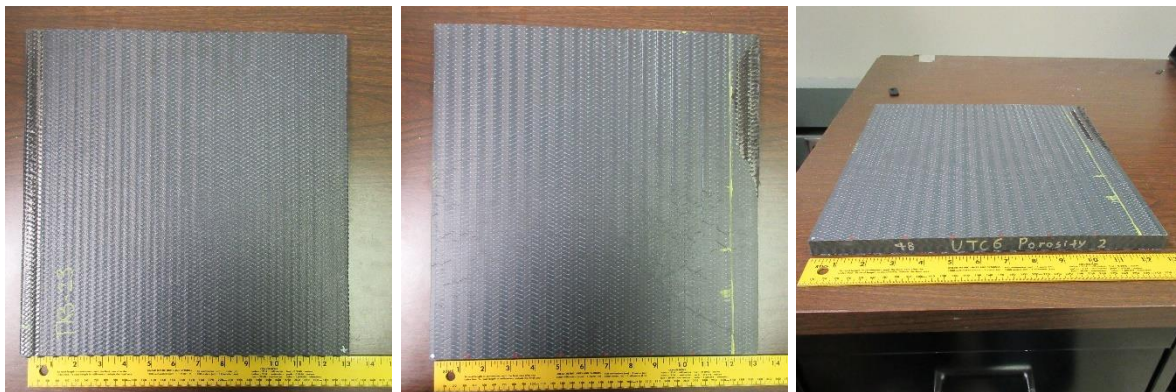
Figure E.48-1. Photographs of Specimen #48: UTC 6 Porosity 2.

E.48.1 Method: X-ray Computed Tomography (XCT)

E.48.1.1 Partner: NASA

E.48.1.2 Technique Applicability: ★★★

XCT is capable of imaging the medium porosity in this specimen.

E.48.1.3 Laboratory Setup

The microfocus XCT system at NASA LaRC is a commercially available Avonix (Nikon C2) Metrology System designed for high-resolution NDE inspections. The system is an advanced microfocus X-ray system, capable of resolving details down to 5 μm, and with magnifications up to 60X. Supplied as complete, the system is a large-dimension radiation enclosure with X-ray source, specimen manipulator, and an amorphous silica detector, as shown in Figure E.48.2. The imaging controls are housed in a separate control console. The detector is a Perkin-Elmer, 16-bit, amorphous-silicon digital detector with a 2000 × 2000-pixel array.
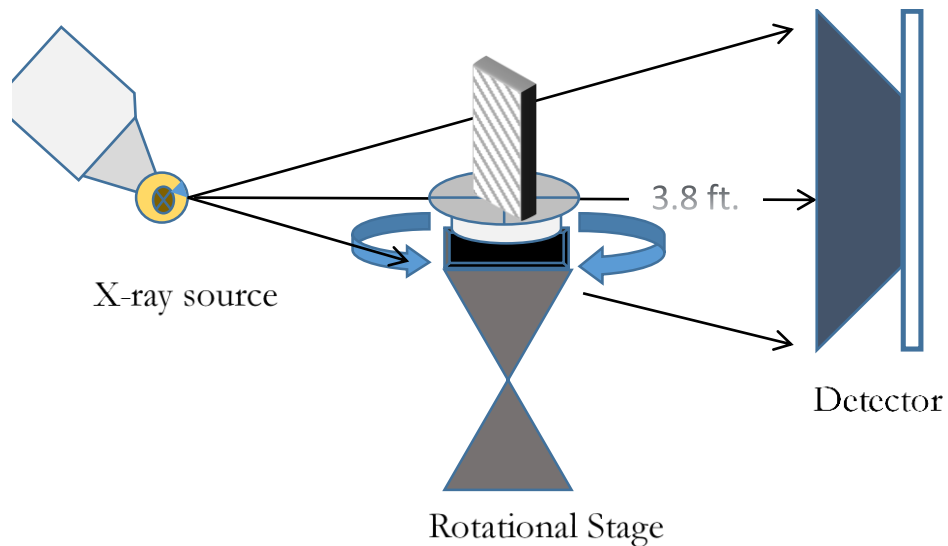
Figure E.48-2. XCT system components.

A consistent Cartesian coordinate system is used to define slice direction as illustrated in Figure E.48-3. Slices normal to the X-, Y-, and Z-directions are shown in Figures E48-3a, b, and c, respectively.
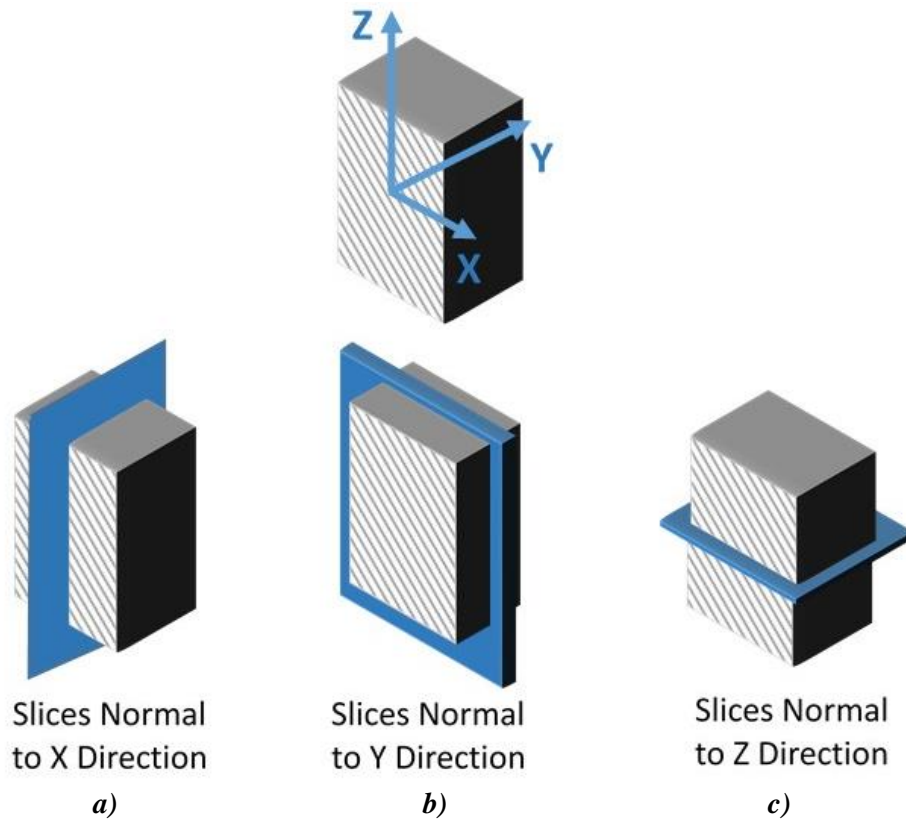
Figure E.48-3. Slice direction nomenclature.
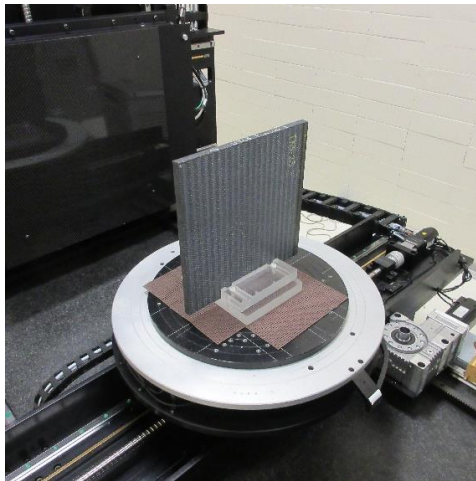
Figure E.48-4. Specimen orientation within apparatus.

E.48.1.4 Equipment List and Specifications:

- Avonix 225 CT System
- 225 kV microfocus X-ray source with 5-µm focal spot size
- 15 or 30 kg Capacity 5-axis fully programmable manipulator.
- Detector: Perkin Elmer XRD 1621 – 2000 × 2000 pixels with 200 µm pitch
- 10-µm spatial resolution for specimens 1.5 cm wide
- Thin panels 10 × 10 inches – full volume 200-µm spatial resolution

E.48.1.5 Settings

Table E.48-1. Data collection settings.

Source Energy	150 kV
Current	50 µA
Magnification	1.65 X
Filter	NF
# Rotational angles	3142
Exposure time / frame	1.0 sec.
Max Histogram Grey Level	30 K
# Averages	8
Resolution (µm)	120.947 µm
Array Dimensions (pixels)	Set 1: 1999 × 362 × 1998 Set 2: 1998 × 686 × 1997

The specimen is placed vertically (rotated about the smallest dimension) on the rotational stage located between the radiation source and the detector. The rotational stage is computer-controlled and correlated to the position of the sample. As the sample is rotated the full 360° (~0.11° increments), the detector collects radiographs at each rotated angle as the X-ray path intersects the sample. 3D reconstruction of the collection of radiographs produces a volume of data that can then be viewed along any plane in the volume. The closer the sample can be placed to the X-ray source, the higher the spatial resolution that can be obtained.

E.48.1.6 Inspection Results

Specimen #48, UTC 6 Porosity 2, is a flat panel fabricated from T-800SC Triaxial Braid 0/+60/-60 with 3M AMD-825, with an objective of achieving medium porosity. XCT was performed on this specimen in NASA LaRC's large walk-in CT system with the settings defined in Section E.48.1.6. Several surface defects are visible in the panel and are easily viewed in the CT slice corresponding to the front surface of the panel, as highlighted in Figure E.48-5.
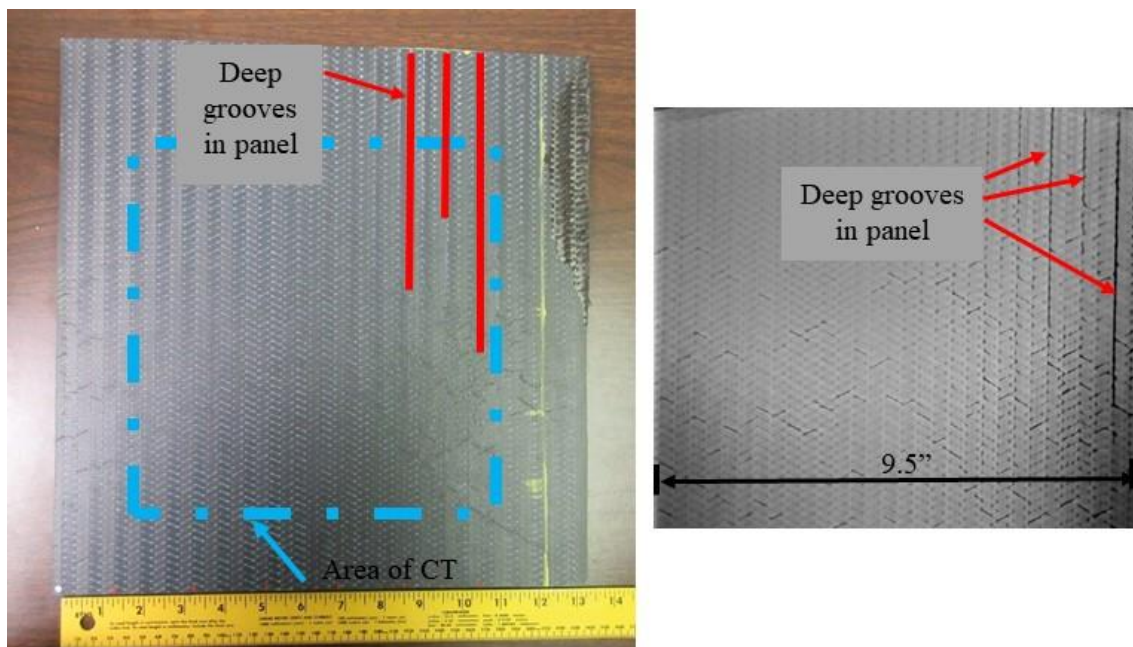
Figure E.48-5. CT slice at the front surface of the panel showing surface scratches.

From XCT analysis, there are a limited, small number of separately identifiable particles of porosity in the specimen as seen distinctly from the weave pattern, mainly located near the back edge of the panel (closest to the detector), with one cluster of porosity near the left edge and a second cluster located approximately centered in the specimen as seen from the 'front view,' as shown in Figure E.48-6. Figure E.48-7 is a closeup view of the cluster near the left edge.
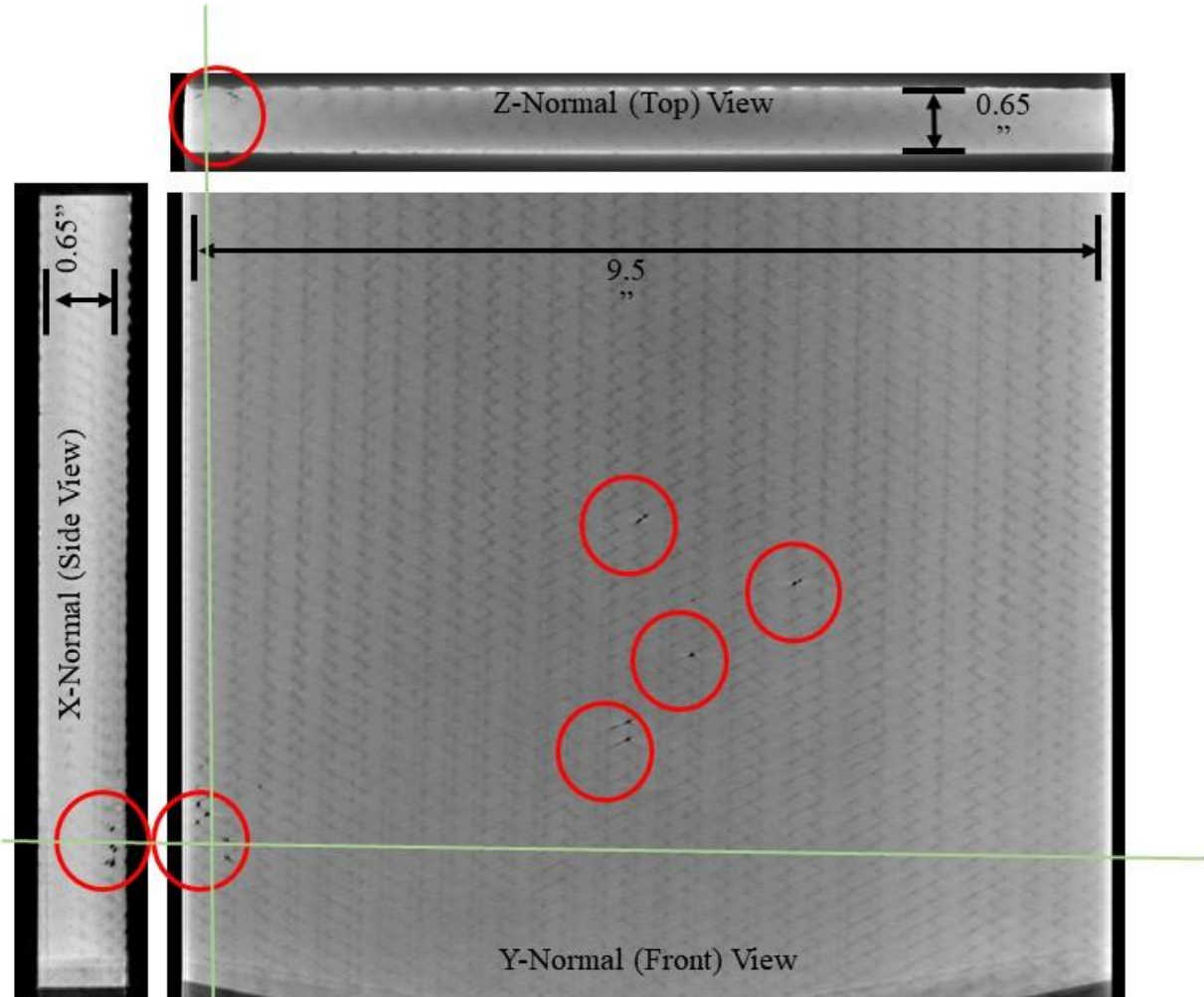
Figure E.48-6. Views of porosity near the back surface of Specimen #48.
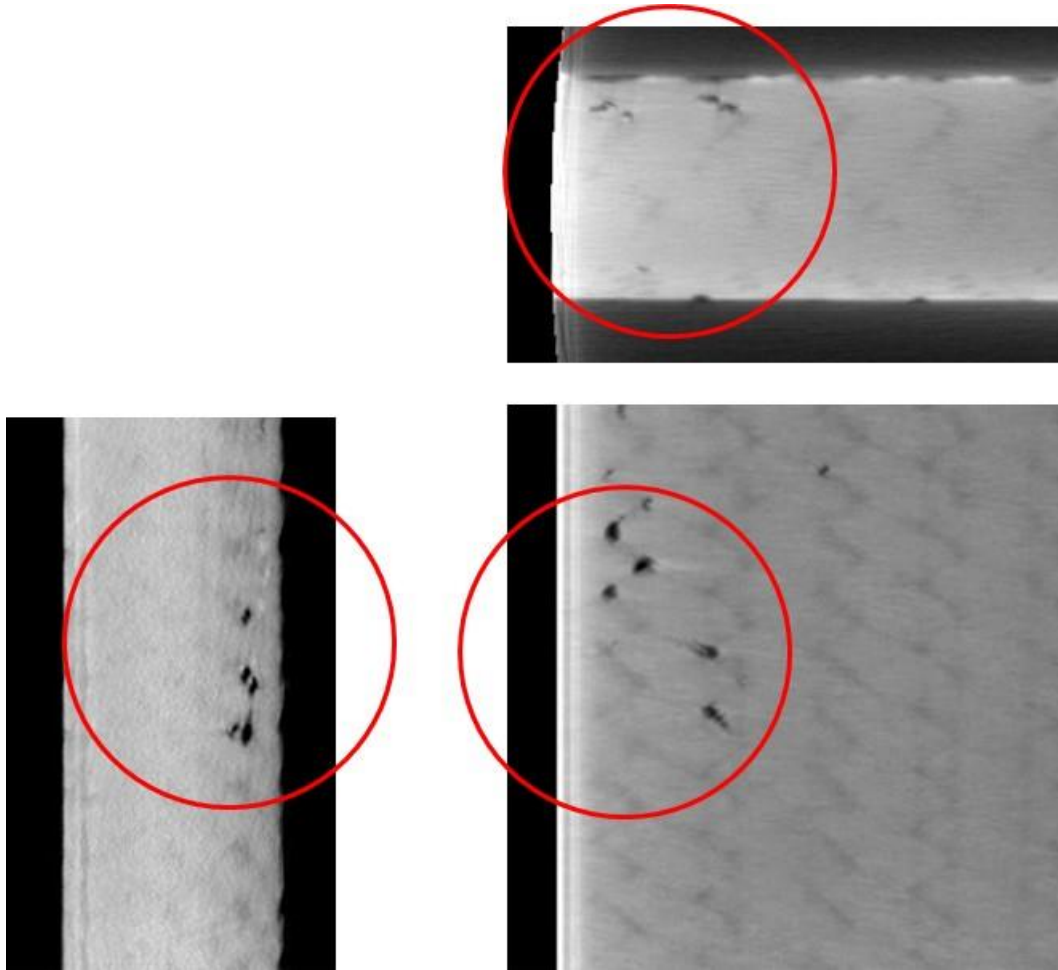
Figure E.48-7. Close-up views of porosity near the left side and back surface of Specimen #48.

E.49 Specimen #49: UTC 8 Porosity 1 – Not Tested

Structure	Material	Details	Dimensions (inches)	Partner Methods
Triaxial Braid 0/+60/-60	T-800SC braid with 3M AMD-825	Flat panel with porosity	$13 \times 13 \times 0.65$	Not Tested

E.50 Specimen #50: UTC 11 Baseline 2 – Not Tested

Structure	Material	Details	Dimensions (inches)	Partner Methods
Triaxial Braid 0/+60/-60	T-800SC braid with 3M AMD-825	Flat panel no defects	$12 \times 11 \times 0.5$	Not Tested

E.51 Specimen #51: UTC NASA-TAB-SNAG13-FLAT – Not tested

Structure	Material	Details	Dimensions (inches)	Partner Methods
Triaxial Braid 0/+60/-60	T-800SC braid with 3M AMD-825	Flat panel with fabric snag	$12 \times 13 \times 0.5$	Not Tested

E.52   Specimen #52: NASA-TAB-BASE1-FLANGE – Not tested

Structure	Material	Details	Dimensions (inches)	Partner Methods
Triaxial Braid 0/+60/-60	T-800SC braid with 3M AMD-825	Flange no defects	11 × 4.5 × 2.25	Not Tested

E.53   Specimen #53: NASA-TAB-BASE2-FLANGE – Not Tested

Structure	Material	Details	Dimensions (inches)	Partner Methods
Triaxial Braid 0/+60/-60	T-800SC braid with 3M AMD-825	Flange no defects	13 × 13 × 0.65	Not Tested

E.54   Specimen #54 NASA-TAB-05P-FLANGE1 – Not Tested

Structure	Material	Details	Dimensions (inches)	Partner Methods
Triaxial Braid 0/+60/-60	T-800SC braid with 3M AMD-825	Flange with air pillow delaminations	12 × 4.5 × 2.5	Not Tested

E.55   Specimen #55: UTC 0.5-inch Pillow Defect Flange 2

Structure	Material	Details	Dimensions (inches)	Partner Methods	
Triaxial Braid (0/60/-60)	T-800SC Triaxial Braid (0/60/-60) with 3M AMD-825	Flange	20 × 6 × 2.4	NASA	E.55.1 SSIR
					E.55.2 TTIR
				TWI	E.55.3
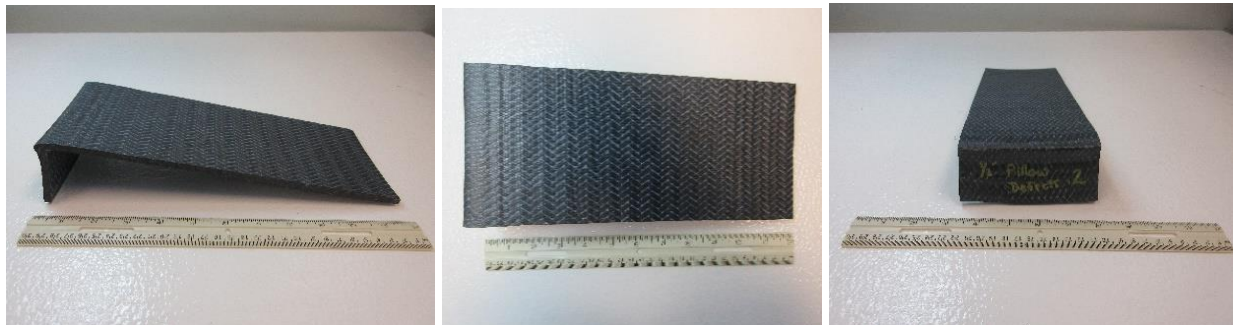
Figure E.55-1. Photographs of Specimen #55: UTC-0.5-inch pillow defect Flange 2.

E.55.1   Method: Single-Sided Infrared Thermography (SSIR)

E.55.1.1   Partner: NASA

E.55.1.2   Technique Applicability: ★☆☆

SS Thermography is capable of imaging the corner defect.

E.55.1.3   Laboratory Setup

A commercially available flash thermography system was used for the inspection. The flash thermography system consisted of two linear flash tubes mounted within a hood. An infrared (IR) camera was mounted at the back of the hood viewing through a circular hole between the flash tubes and were positioned to view the hood opening. In this configuration, the flash lamps heated an area equal to the hood opening and the IR camera captured the thermal response. The IR camera

operates in the mid-wave IR band (3 to 5 μm) and is configured with a 25-mm germanium lens. The focal plane array size for the camera is 640×512 with a detector pitch size of 14×14 μm.
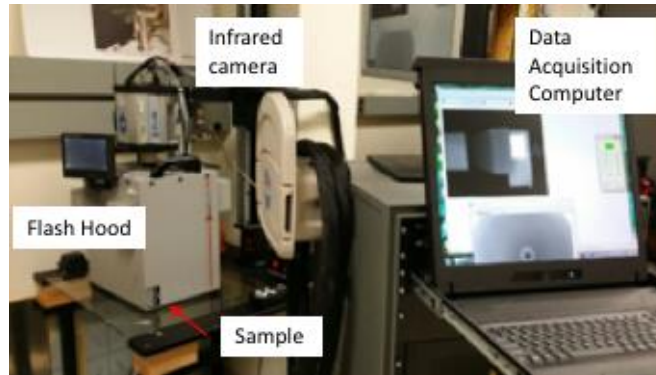
Figure E.55-2. SSIR setup.

E.55.1.4 Equipment List and Specifications:

- Thermal Wave Imaging (TWI) System
- TWI System flash heat source using Speedotron power supplies.
- SC6000 FLIR camera, 640×512 Indium Antimonide (InSb) array, Noise Equivalent Differential Temperature (NEDT) < 20 mK
- 25 mm and 50 mm Germanium Optics

E.55.1.5 Settings:

- 60Hz Frame Rate
- Flash on frame #10
- Total number of Frames 3000
- Total data acquisition time of 50 sec
- The camera/hood was positioned to view the entire sample

E.55.1.6 Principal Component Analysis

Principal component analysis (PCA) is common for processing of thermal data [1−3]. This algorithm is based on decomposition of the thermal data into its principal components or eigenvectors. Singular value decomposition is a routine used to find the singular values and corresponding eigenvectors of a matrix. Since thermal NDE signals are slowly decaying waveforms, the predominant variations of the entire data set are usually contained in the first or second eigenvectors, and thus account for most of the data variance of interest. The principle components are computed by defining a data matrix A, for each data set, where the time variations are along the columns and the spatial image pixel points are row-wise. The matrix A is adjusted by dividing the maximum value (normalization) and subtracting the mean along the time dimension. The covariance matrix is defined as the $A^{T}*A$. The covariance matrix is now a square matrix of number of images used for processing. The covariance matrix can then be decomposed using singular value decomposition as:

$$covariance\ matrix = \ A^{T}A = V * S * V^{T}$$

Where S is a diagonal matrix containing the square of the singular values and V is an orthogonal matrix, which contains the basis functions or eigenvectors describing the time variations. The eigenvectors can be obtained from the columns of V. The PCA inspection image is calculated by

46

dot product multiplication of the selected eigenvector times the temperature response (data matrix A), pixel by pixel.

E.55.1.7 Inspection Results

The 3000 frames of data (50 sec) were processed using iterations of different time windows. The processing of frames 100 to 3000 corresponding to a time window of 1.67–50 sec yielded the best results. Only one possible flaw situated at the corner was detected. This flaw, named A, is shown in Figure E.55-3 and E.55-4. There exists a contrast between the outer edges and middle of the top section of the specimen. Using a longer time window allowed to amplify this contrast. All different time windows detected the corner defect. However, when including later frames (e.g., frame 100 to 3000) defect A was more perceptible. The second eigenvector was used to produce the final inspection images shown in Figure E.55-3.

Figure E.55-3. UTC 0.5-inch pillow defect Flange 2 sample.

Figure E.55-4. SSIR inspection of UTC 0.5-inch pillow defect Flange 2 sample's top section processed with PCA from frame 100 (1.66s) to 3000 (50s).

Figure E.55-5. SSIR inspection of UTC 0.5-inch pillow defect Flange 2 sample's knee and flange section processed with PCA from frame 100 (1.66s) to 3000 (50s).

E.55.1.8 References

[1] Rajic, N.: "Principal Component Thermography for Flaw Contrast Enhancement and Flaw Depth Characterization in Composite Structures," *Composite Structures*, Vol. 58, pp. 521--528, 2002.

[2] Zalameda, J. N.; Bolduc S.; and Harman R.: "Thermal Inspection of a Composite Fuselage Section using a Fixed Eigenvector Principal Component Analysis Method," Proc. *SPIE* 10214, *Thermosense: Thermal Infrared Applications XXXIX*, 102140H, 5 May 2017.

[3] Cramer, K. E.; and Winfree, W. P.: "Fixed Eigenvector Analysis of Thermographic NDE Data", Proceedings of *SPIE*, *Thermosense XXXIII*, edited by Morteza Safai and Jeff Brown, Vol. 8013, 2011.

E.55.2　Method: Through-Transmission Infrared Thermography (TTIR)

E.55.2.1　Partner: NASA

E.55.2.2　Technique Applicability: ★☆☆

TT thermography is capable of imaging the corner defect.

E.55.2.3　Laboratory Setup

The TT thermal inspection system setup is shown in Figure E.55-6. The test specimen is placed between the heat source and the IR camera. The lamp used to induce the heat was a commercially available photographic flash lamp powered by a 6,400-Joule power supply (manufactured by Balcar). The camera used was a Forward-looking Infrared (FLIR) SC6000 with a 640×512 Indium Antimonide (InSb) array operating in the 3- to 5-µm IR band. The image data frame rate was 60-image frames per second. The computer records the IR image of the specimen immediately prior to the firing of the flash lamp (for emissivity correction), and then the thermal response of the specimen at a user defined sampling rate and for a user defined duration is acquired.
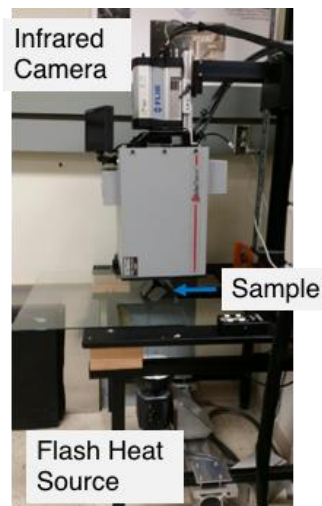
Figure E.55-6. TTIR setup.

E.55.2.4　Equipment List and Specifications:

- TWI System
- TWI System flash heat source using Balcar power supply externally triggered by TWI system.
- SC6000 FLIR camera, 640×512 InSb array, NEDT < 20 mK
- 25 mm and 50 mm Germanium Optics

E.55.2.5　Settings:

- 60Hz Frame Rate
- Flash on frame #10
- Total number of Frames 3500
- Total data acquisition time of 58.33 sec
- IR camera was positioned to view the entire sample

E.55.2.6 Principal Component Analysis

PCA is common for processing of thermal data [1−3]. This algorithm is based on decomposition of the thermal data into its principal components or eigenvectors. Singular value decomposition is a routine used to find the singular values and corresponding eigenvectors of a matrix. Since thermal NDE signals are slowly decaying waveforms, the predominant variations of the entire data set are usually contained in the first or second eigenvectors, and thus account for most of the data variance of interest. The principle components are computed by defining a data matrix A, for each data set, where the time variations are along the columns and the spatial image pixel points are row-wise. The matrix A is adjusted by dividing the maximum value (normalization) and subtracting the mean along the time dimension. The covariance matrix is defined as the A^T*A. The covariance matrix is now a square matrix of number of images used for processing. The covariance matrix can then be decomposed using singular value decomposition as:

$$covariance\ matrix = \ A^T A = V*S*V^T$$

Where S is a diagonal matrix containing the square of the singular values and V is an orthogonal matrix, which contains the basis functions or eigenvectors describing the time variations. The eigenvectors can be obtained from the columns of V. The PCA inspection image is calculated by dot product multiplication of the selected eigenvector times the temperature response (data matrix A), pixel by pixel.

E.55.2.7 Inspection Results

The 3500 frames of data (58.33 sec) were processed using iterations of different time windows. The processing of frames 50 to 500 corresponding to a time window of 0.83−8.33 sec yielded the best results. The top section has many contrasting patterns that appear. These are most likely due to the weave pattern of the fabric. The corner defect detected in Figure E.55-9 is clearest with the thermography inspection of the knee.
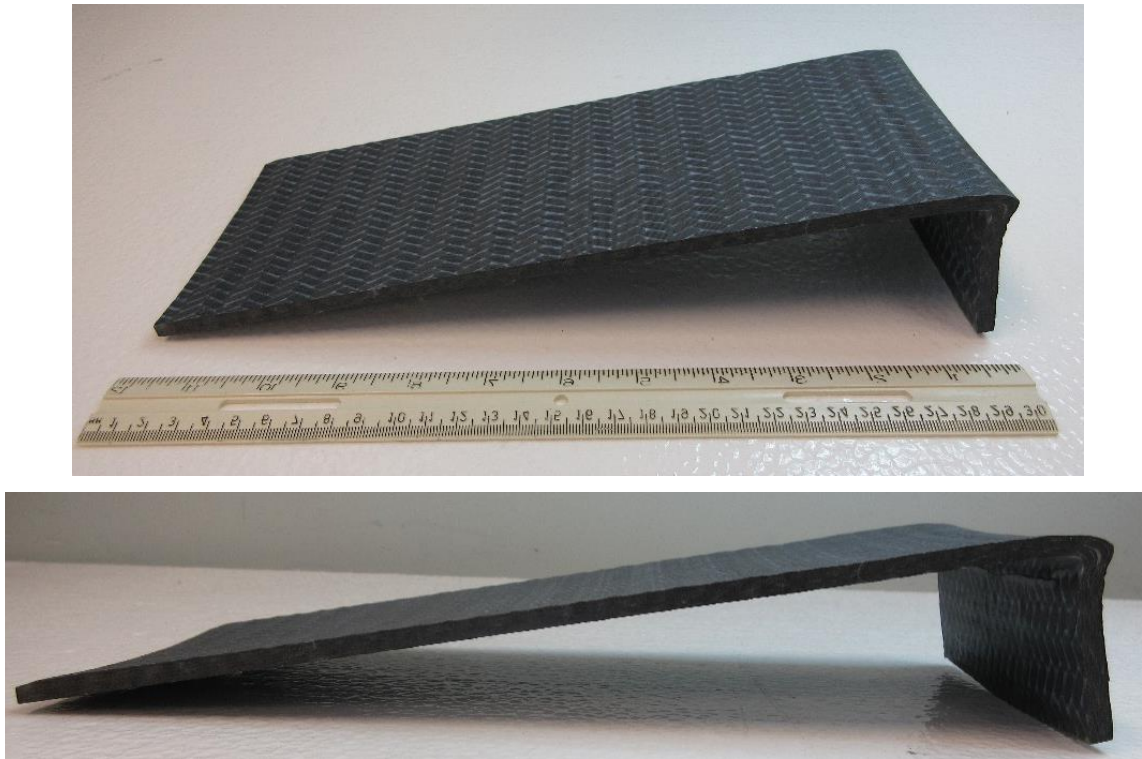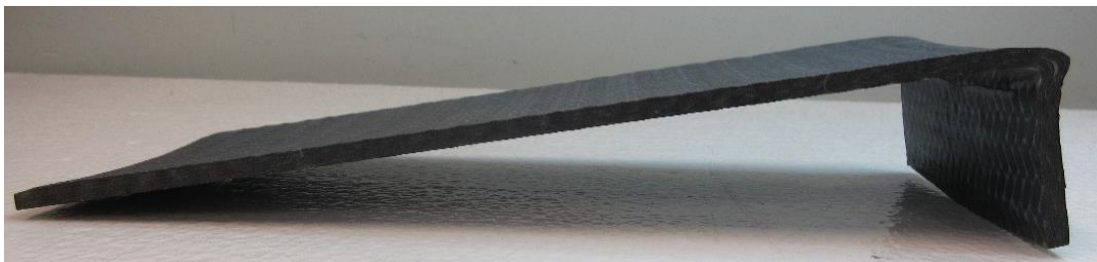

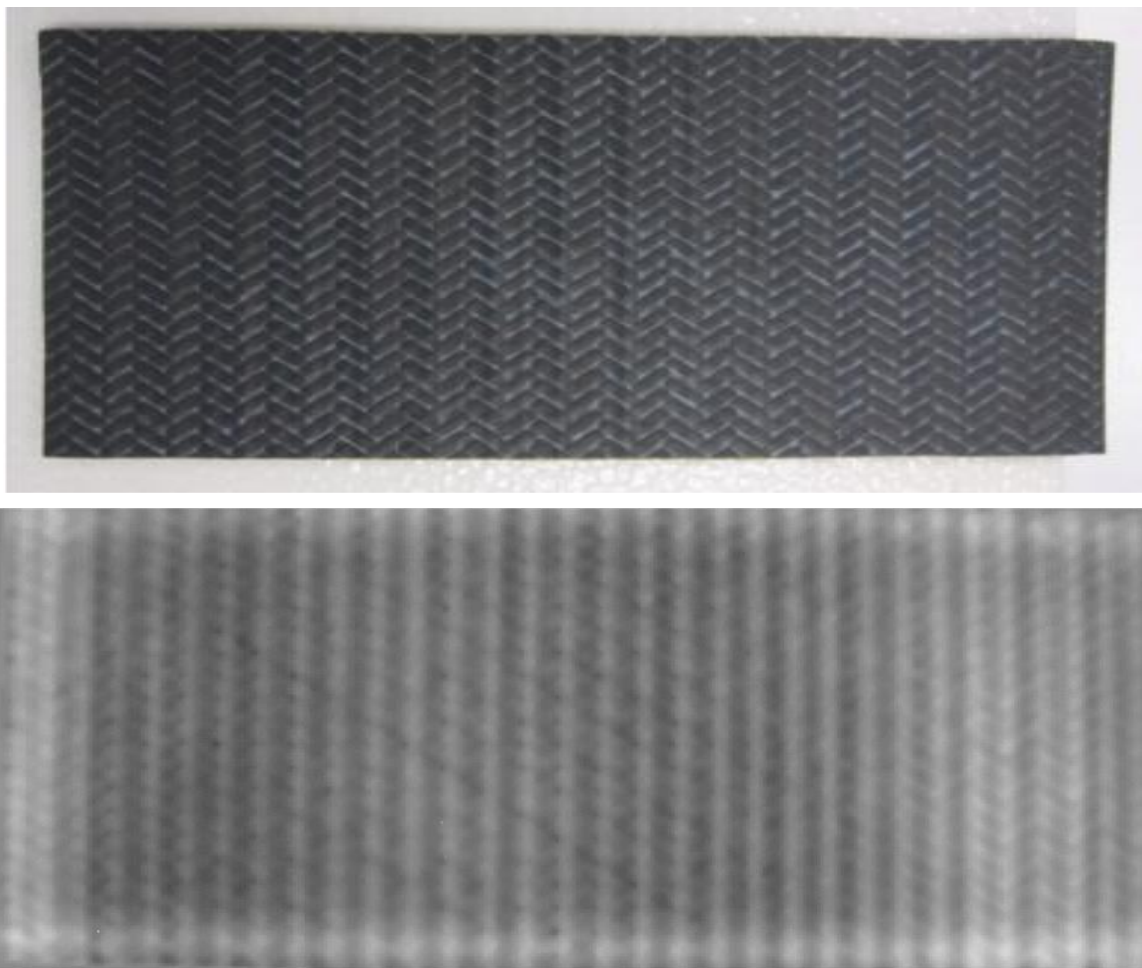***Figure E.55-7. UTC 0.5-inch pillow defect Flange 2 sample.***

51
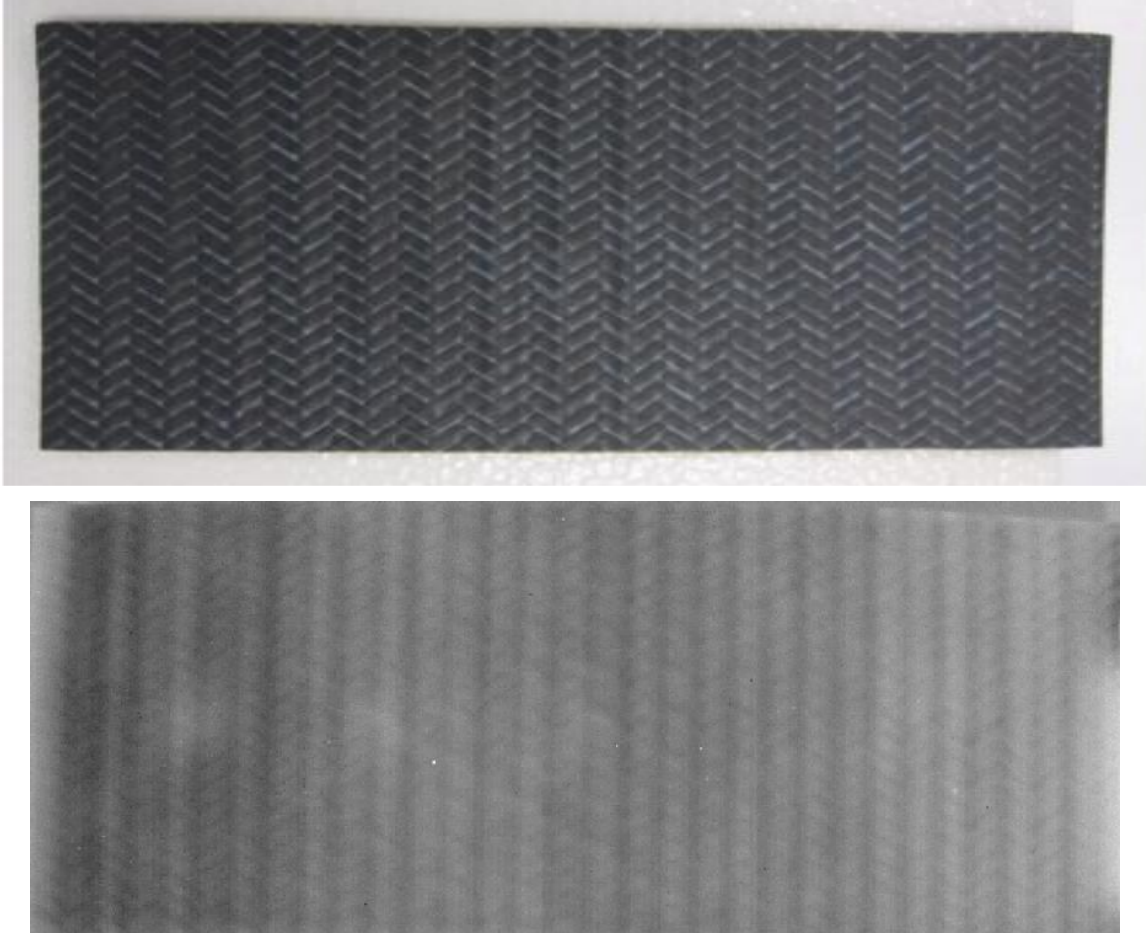
Figure E.55-8. TTIR inspection of UTC 0.5-inch pillow defect Flange 2 sample's top section processed with PCA from frame 50 (0.83s) to 500 (8.33s).
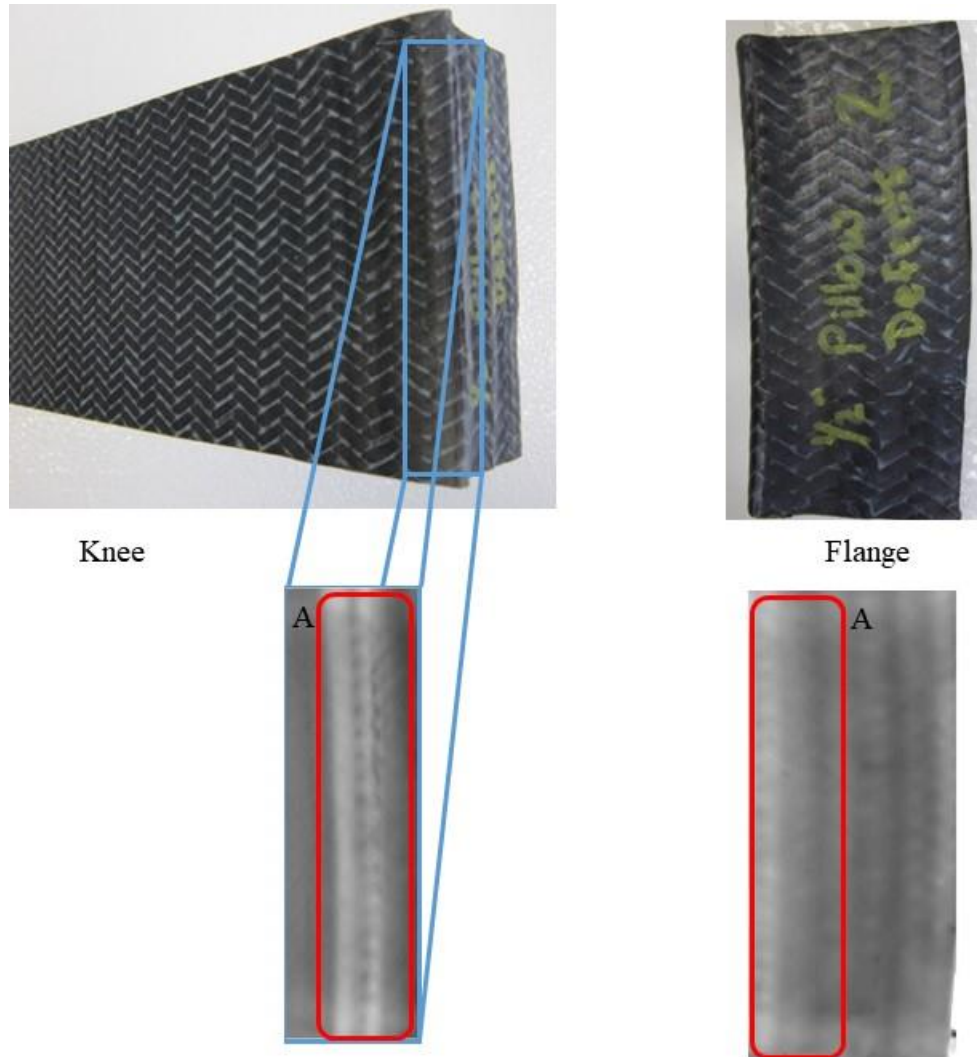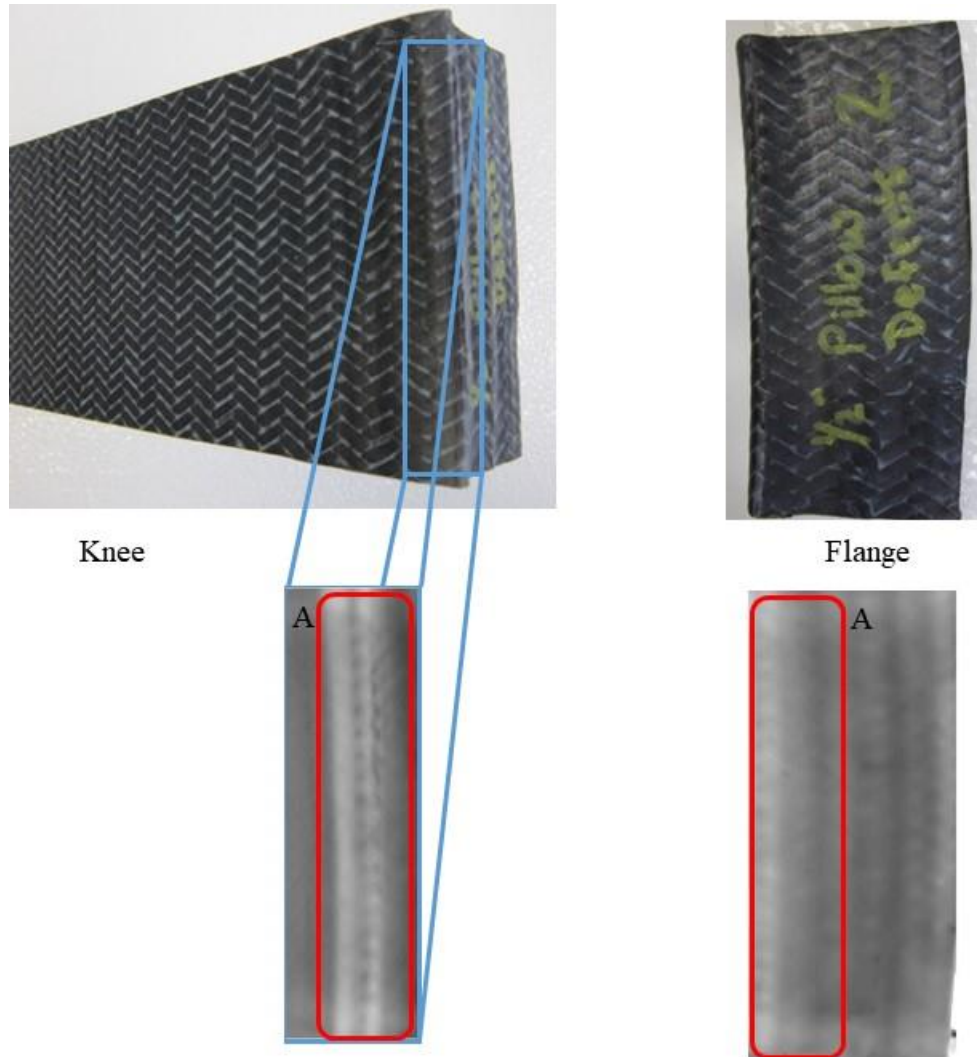
Figure E.55-9. TTIR inspection of UTC 0.5-inch pillow defect Flange 2 sample's knee and flange section processed with PCA from frame 50 (0.83s) to 500 (8.33s).

E.55.2.8   References

[1]   Rajic, N.: "Principal Component Thermography for Flaw Contrast Enhancement and Flaw Depth Characterization in Composite Structures," *Composite Structures*, Vol. 58, pp. 521--528, 2002.

[2]   Zalameda, J. N.; Bolduc S.; and Harman R.: "Thermal Inspection of a Composite Fuselage Section using a Fixed Eigenvector Principal Component Analysis Method," Proc. *SPIE* 10214, *Thermosense: Thermal Infrared Applications XXXIX*, 102140H, 5 May 2017.

[3]   Cramer, K. E.; and Winfree, W. P.: "Fixed Eigenvector Analysis of Thermographic NDE Data", Proceedings of *SPIE*, *Thermosense XXXIII*, edited by Morteza Safai and Jeff Brown, Vol. 8013, 2011.

E.55.3 Method: Single-Side Flash Thermography- Thermographic Signal Reconstruction (SSFT-TSR)

E.55.3.1 Partner: Thermal Wave Imaging, Inc.*

*TWI was not part of the ACC but reviewed specimens.

E.55.3.2 Technique Applicability: ★★★

SSFT-TSR is capable of detecting subsurface anomalies in this specimen that could be the result of delamination, voids or porosity. All indications appear in the head-on image, but more accurate sizing is achieved by inspecting the flat surfaces separately.

E.55.3.3 Laboratory Setup:

The sample was inspected with a commercially available flash thermography system (EchoTherm®, Thermal Wave Imaging, Inc.), equipped with 2 linear xenon flash/reflector assemblies mounted in a reflective hood optimized to provide uniform output at the 10-inch × 14-inch exit aperture. Each lamp is powered by a 6 kJ power supply that allows truncation of the flash to a rectangular pulse with duration <1 msec d. A cryogenically cooled IR camera is mounted to view the plane of the hood exit aperture, with the camera lens positioned at the plane of the flashlamps. Excitation, data capture and processing and analysis using TSR are controlled at the system console using Virtuoso software.

E.55.3.4 Equipment List and Specifications:

- EchoTherm® Flash Thermography System
- 2 linear xenon flash lamps and power supplies (6 kJ each)
- TWI Precision Flash Control (truncation to 4 msec rectangular pulse)
- A6751sc FLIR camera, 640 × 512 InSb array, NEDT < 20 mK
- 25 mm Germanium Lens
- TWI Virtuoso® software

E.55.3.5 Settings:

- 30 Hz Frame Rate
- 10 Preflash Frames
- 1800 total frames
- 7 Polynomial order
- 60-sec data acquisition time
- Field of View (FOV): 10-inch × 14-inch

Settings were determined following the recommendations in ASTM E2582-14. Acquisition duration was set according to the time of the break from linearity (t* ~20 sec) due to the back wall for typical points in the log time history. The acquisition period was then set to 60 sec (3 × t*), per ASTM E2582-14.
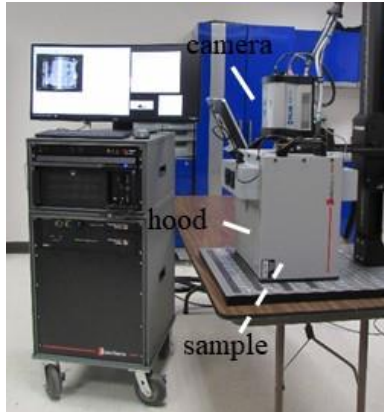
Figure E.55-10. SSFT system with TSR.

E.55.3.6 Thermographic Signal Reconstruction (TSR)

After acquisition, captured data are processed using TSR to reduce temporal noise, enhance deviation from normal cooling behavior and allow segmentation of the data based on signal attributes. For each pixel, the average of 10 frames immediately preceding the flash pulse is subtracted from the pixel time history, and a 7th order polynomial is fit to the logarithmically scaled result using least squares. First and 2nd derivatives of the result are calculated and the derivative images are displayed in the Virtuoso software. Derivative signals associated normal areas of the sample exhibit minimal activity over the duration of the acquisition. Signals associated with subsurface anomalies typically behave identically to the normal signals until a particular time (dependent on host material characteristics and the depth of the feature) after which their behavior deviates from normal (the degree of the deviation depends on the relative difference in the thermal properties of the anomaly and the surrounding normal matrix).

E.55.3.7 Inspection Results

No subsurface indications were observed.
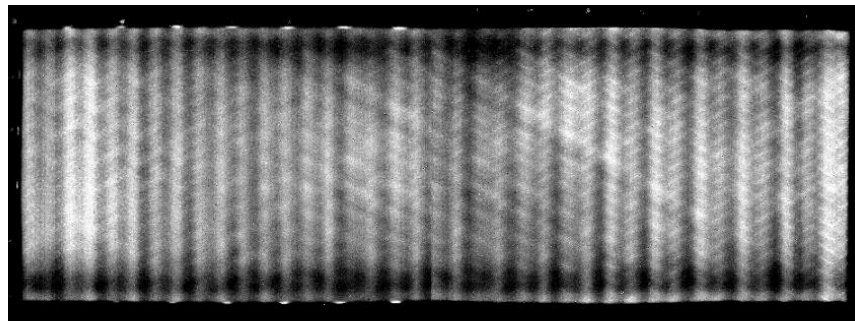
Long Flange
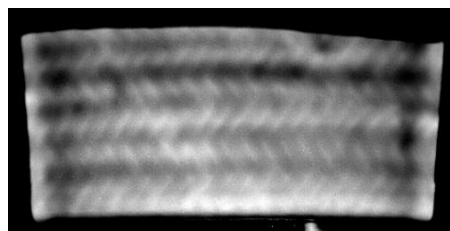
Short Flange

Figure E.55-11. TSR 1st derivative at 7.93 sec of UTC Pillow DF2.

55

References

[1] ASNT: *ASNT Aerospace NDT Industry Handbook*, Chapter 11, "Thermography," Nov 2014.

[2] ASTM International: "Standard Practice for Infrared Flash Thermography of Composite Panels and Repair Patches," *ASTM E2582–07*, 2007.

[3] Shepard, S.; and Frendberg, M.: "Thermographic Detection and Characterization of Flaws in Composite Materials," *Materials Evaluation*, ASNT, July 2014.

[4] Hou, Y.; Lhota, J. R.; and Golden, T. J. M.: "Automated processing of thermographic derivatives for quality assurance," *Opt. Eng.*, Vol. 46, 051008, 2007.

[5] *Temporal noise reduction, compression and analysis of data sequences*, U.S. Patent 6,516,084.

E.56   Specimen #56: UTC-Snag-1

Structure	Material	Details	Dimensions (inches)	Partner	Methods
Triaxial Braid, 0/+60/-60	T-800SC with 3M AMD-825	Flange with fabric Snag	$9 \times 12 \times 2$	NASA	E.56.1 XCT
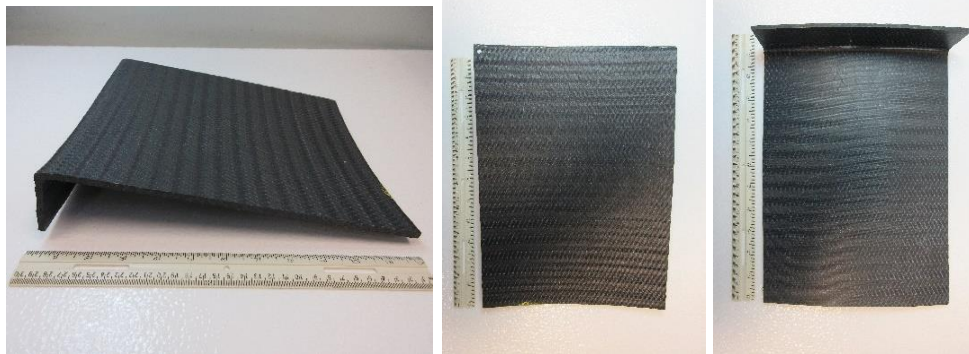
Figure E.56-1. Photographs of Specimen #56: UTC-Snag-1.

E.56.1   Method: X-ray Computed Tomography (XCT)

E.56.1.1   Partner: NASA

E.56.1.2   Technique Applicability: ☆☆☆

XCT is not capable of imaging the fiber snags in this specimen.

E.56.1.3   Laboratory Setup

The microfocus XCT system at NASA LaRC is a commercially available Avonix (Nikon C2) Metrology System designed for high-resolution NDE inspections. The system is an advanced microfocus X-ray system, capable of resolving details down to 5 μm, and with magnifications up to 60X. Supplied as complete, the system is a large-dimension radiation enclosure with X-ray source, specimen manipulator, and an amorphous silica detector, as shown in Figure E.56-2 The imaging controls are housed in a separate control console. The detector is a Perkin-Elmer, 16-bit, amorphous-silicon digital detector with a 2000×2000-pixel array.

A consistent Cartesian coordinate system is used to define slice direction as illustrated in Figure E.56-2 and Figure E.56-3. Slices normal to the X-, Y-, and Z-directions are shown in Figures E.56-3a, b, and c, respectively.
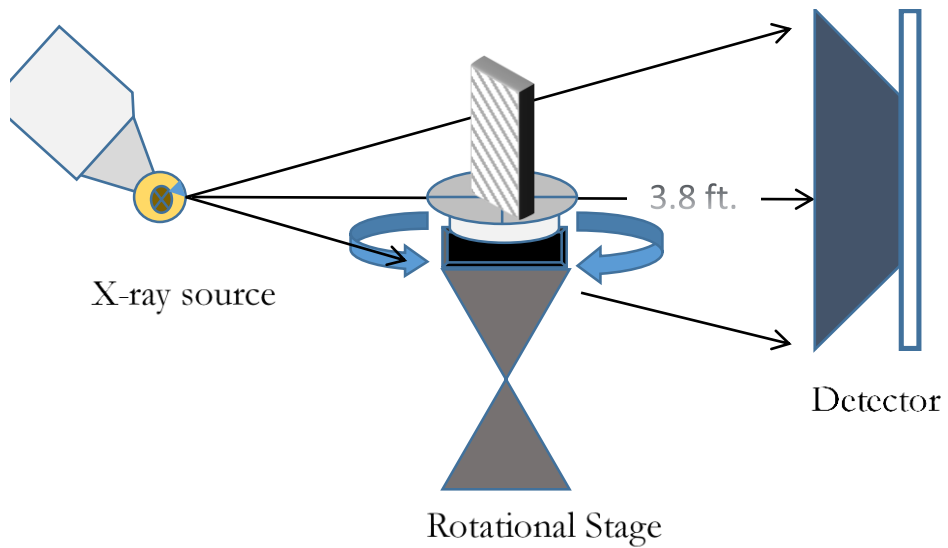
Figure E.56-2. XCT system components.

Slices Normal to X Direction	Slices Normal to Y Direction	Slices Normal to Z Direction
a)	*b)*	*c)*
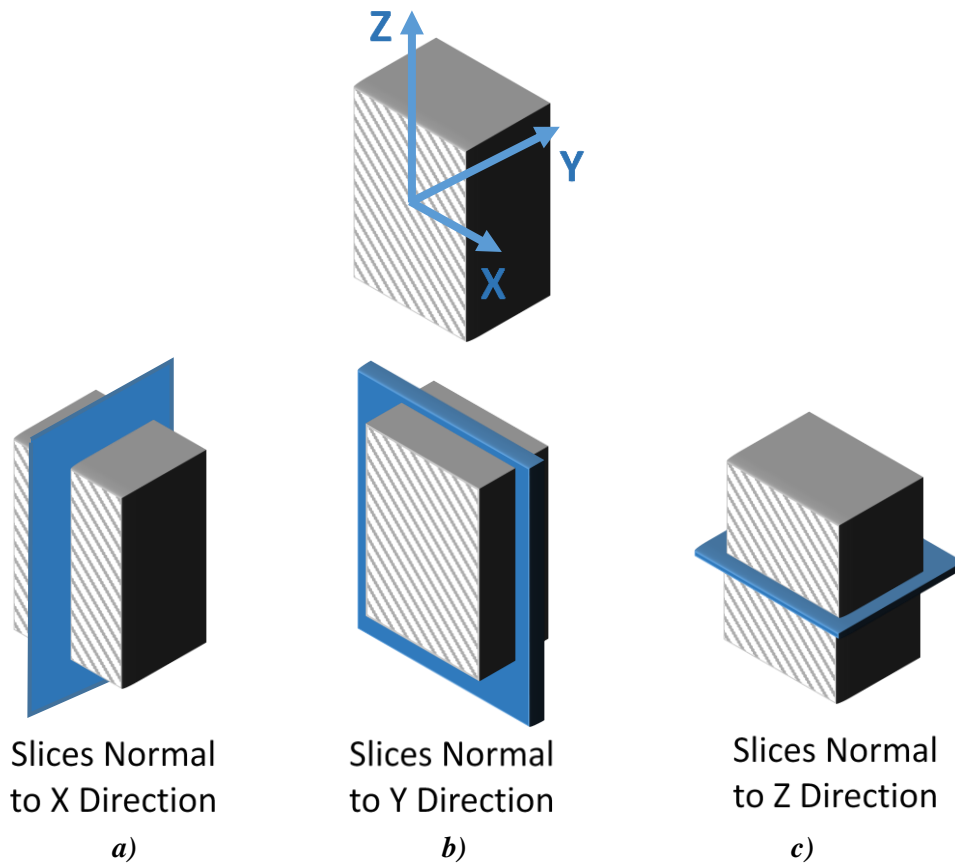
Figure E.56-3. Slice direction nomenclature.
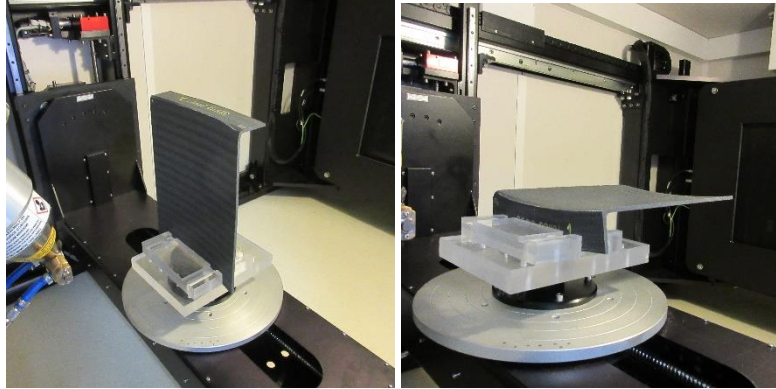
Figure E.56-4. Test setup showing specimen orientation.

E.56.1.4 Equipment List and Specifications:

- Avonix 225 CT System
- 225 kV microfocus X-ray source with 5 µm focal spot size
- 15 or 30 kg Capacity, 5-axis, fully programmable manipulator
- Detector: Perkin Elmer XRD 1621 − 2000 × 2000 pixels with 200 µm pitch
- 10 µm spatial resolution for specimens 1.5 cm wide
- Thin panels 10 × 10 inches – full volume 200 µm spatial resolution

E.56.1.5 Settings

Table E.56-1. Data collection settings.

Source Energy	150 kV
Current	50 µA
Magnification	1.65 X
Filter	NF
# Rotational angles	3142
Exposure time / frame	1.0 sec.
Max Histogram Grey Level	30 K
# Averages	8
Resolution (µm)	120.947 µm
Array Dimensions (pixels)	Set 1: 1999 × 362 × 1998 Set 2: 1998 × 686 × 1997

The specimen is placed vertically (rotated about the smallest dimension) on the rotational stage located between the radiation source and the detector. The rotational stage is computer-controlled and correlated to the position of the sample. As the sample is rotated the full 360° (~0.11° increments), the detector collects radiographs at each rotated angle as the X-ray path intersects the sample. 3D reconstruction of the collection of radiographs produces a volume of data that can then be viewed along any plane in the volume. The closer the sample can be placed to the X-ray source, the higher the spatial resolution that can be obtained.

E.56.1.6 Inspection Results

Specimen #56, UTC-Snag-1, is a flange panel fabricated from T-800SC with 3M AMD-825, with an objective of achieving snags in the fabric layup. XCT was performed on this specimen in NASA LaRC's CT system with the settings defined in Section E.56.1.6. There are several points of porosity and surface flaws in the specimen, as highlighted in Figure E.56-5.
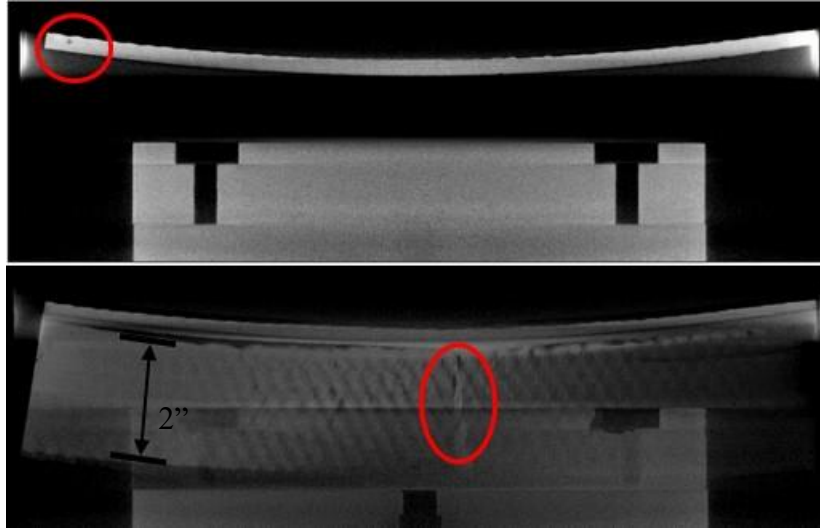
Figure E.56-5. CT slices from the y-direction showing porosity and surface flaws within the sample.

From XCT analysis, there were some instances of porosity and surface defects within the specimen. The bottom block seen in both images in Figure E.56-5 is the plexiglass clamp used to hold the specimin in place. The z direction shows the flat curved region of the specimen where the snag defects were introduced (Figure E.56-6) . XCT showed no evidence of defects in the region. This is most likely due to the nature of the defect type. Snags will cause a distortion in the fiber; however, the density does not change from the bulk material.
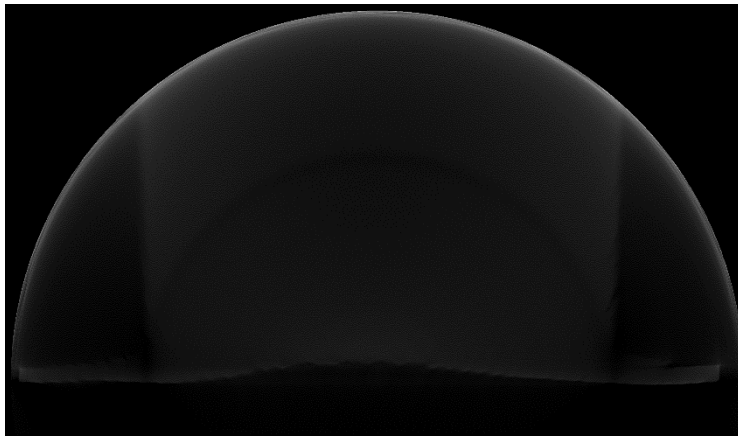
Figure E.56-6. CT slices from the z-direction showing no obvious defects within the bulk of the specimen.

E.57   Specimen #57: NASA-03-Twisted-Tow-001

Structure	Material	Details	Dimensions (inches)	Partner	Methods
Fiber placed panel	IM7/8552-1 Slit Tape	Flat panel Twisted Tow – 1ply	$16 \times 16 \times 0.15$	NASA	E.57.1 PEUT E.57.2 SSIR E.57.3 TTIR
				TWI	E.57.3 SSFT
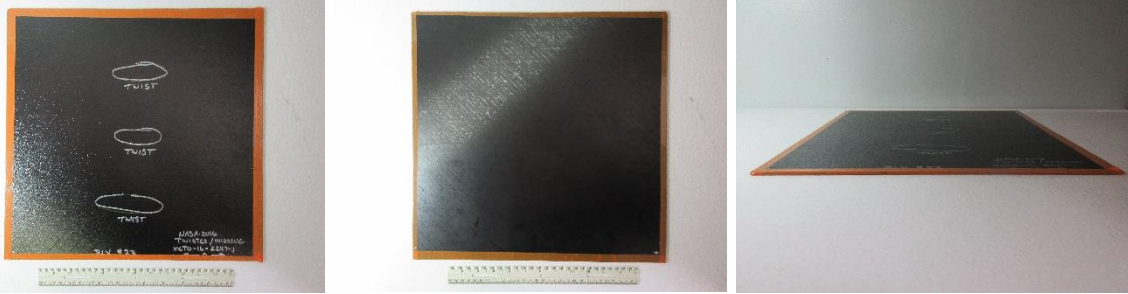
Figure E.57-1. Photographs of Specimen #57: NASA 03 Twisted Tow 001.

E.57.1   Method: Pulse-Echo Ultrasound Testing (PEUT)

E.57.1.1   Partner: NASA

E.57.1.2   Technique Applicability: ★★☆

PEUT is capable of detecting the twisted tows with some interference.

E.57.1.3   Laboratory Setup

Immersion Ultrasonic Testing: NASA LaRC uses a custom-designed single-probe ultrasonic scanning system. The system has an 8-axis motion controller, a multi-axis gantry robot mounted above a medium-size water tank, a dual-channel, 16-bit, high-speed digitizer, and an off-the-shelf ultrasonic pulser receiver. The system can perform TT and PEUT inspections. TT inspection employs two aligned ultrasonic probes, one transmitter and one receiver, placed on either side of a test specimen. Pulse-echo inspection is a single-sided method where a single ultrasonic probe is both transmitter and receiver. In each method, data are acquired while raster scanning the ultrasonic probe(s) in relation to a part. Figure E.57-2 shows a simplified block diagram of a scanning Pulse-echo inspection.
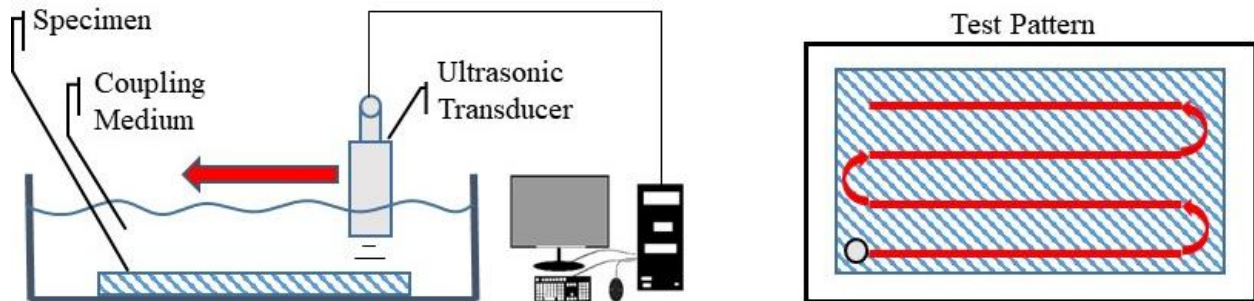
Figure E.57-2. Ultrasonic system components.

Figure E.57-3. Specimen orientation within testing apparatus.

E.57.1.4 Equipment List and Specifications:

- Pulser/Receiver: Olympus 5073PR
- Digitizer: AlazarTech ATS9462, dual channel, 16 bit, 180 MS/s
- Sensor: Olympus 2-inch spherical focus immersion ultrasonic transducer
- Motion system: open looped stepper motor based X-YY-Z gantry robot
- Motion Controller: Galil DMC-4183
- Acquisition Software: FastScan, custom developed at NASA LaRC
- Signal Processing Software: DataViewer, custom developed at NASA LaRC

E.57.1.5 Settings

Table E.57-1. Data collection settings.

Resolution horizontal [in/pixel]	0.02
Resolution vertical [in/pixel]	0.02
Probe frequency [MHz]	5
Focal Length [in]	1.9
Array Dimensions [pixels]	726×711

The specimen is placed flat against the zero position of the tank raised above the glass bottom by several metal washers. The test probe is computer-controlled and correlated to the position on the sample. It is also focused to a point 1 mm below the surface of the test material. The specimen remains in place while the transducer follows a preprogrammed test grid across the surface as indicated in Figure E.57-2. At each point, ultrasonic data are collected from individual pulses. Larger step sizes between data collection result in lower image resolution. These data points are reconstructed into a data cube displaying spatial coordinates as time progresses. 2D reconstruction of the collection of ultrasonic responses create flattened slices at varying depths within the material.

E.57.1.6 Inspection Results

Specimen #57 is a fiber placed flat panel fabricated from IM7/8552-1 Slit Tape with the objective of achieving twisted tows beneath the first ply of the sample. PEUT was performed on this specimen in NASA's immersion tank specified above.

In Figure E.57-4 evidence of three twisted tows in the material appear in the middle of the specimen. The fiber twists reflect and cause perturbations in the acoustic waves that differ from the pattern representing the bulk of the material. This difference, while small, makes visual detection of the twisted tows possible. These defects were detected at a depth of 0.02 inch.
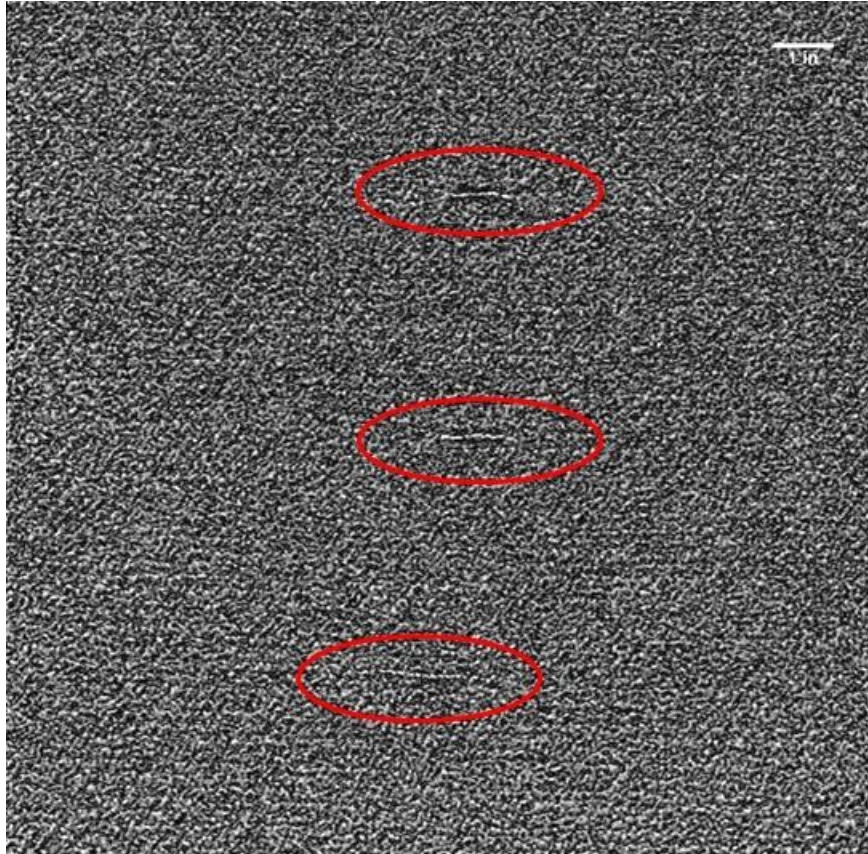
Figure E.57-4. UT image showing surface flaws and a near-surface delamination.

E.57.2   Method: Single-Sided Infrared Thermography (SSIR)

E.57.2.1   Partner: NASA

E.57.2.2   Technique Applicability: ★★☆

SSIR thermography is incapable of detecting the twisted tows.

E.57.2.3   Laboratory Setup

A commercially available flash thermography system was used for the inspection. The flash thermography system consisted of two linear flash tubes mounted within a hood. An IR camera was mounted at the back of the hood viewing through a circular hole between the flash tubes and were positioned to view the hood opening. In this configuration, the flash lamps heated an area equal to the hood opening and the IR camera captured the thermal response. The IR camera operates in the mid-wave IR band (3 to 5 μm) and is configured with a 25-mm germanium lens. The focal plane array size for the camera is 640×512 with a detector pitch size of 14×14 μm.

Figure E.57-5. SSIR setup.

E.57.2.4   Equipment List and Specifications:

- TWI System
- System flash heat source using Speedotron power supplies.
- SC6000 FLIR camera, 640×512 InSb array, NEDT < 20 mK
- 25 mm Germanium Optics

E.57.2.5   Settings:

- 60Hz Frame Rate
- Flash on frame #10
- Total number of Frames 1499
- Total data acquisition time of 24.98 sec
- The camera/hood was positioned to view the entire sample

E.57.2.6   Principal Component Analysis

PCA is common for processing of thermal data [1–3]. This algorithm is based on decomposition of the thermal data into its principal components or eigenvectors. Singular value decomposition is a routine used to find the singular values and corresponding eigenvectors of a matrix. Since thermal NDE signals are slowly decaying waveforms, the predominant variations of the entire data set are usually contained in the first or second eigenvectors, and thus account for most of the data variance of interest. The principle components are computed by defining a data matrix A, for each data set, where the time variations are along the columns and the spatial image pixel points are row-wise. The matrix A is adjusted by dividing the maximum value (normalization) and subtracting the mean along the time dimension. The covariance matrix is defined as the $A^T * A$. The covariance matrix is now a square matrix of number of images used for processing. The covariance matrix can then be decomposed using singular value decomposition as:

$$covariance\ matrix = \ A^T A = V * S * V^T$$

Where S is a diagonal matrix containing the square of the singular values and V is an orthogonal matrix, which contains the basis functions or eigenvectors describing the time variations. The eigenvectors can be obtained from the columns of V. The PCA inspection image is calculated by dot product multiplication of the selected eigenvector times the temperature response (data matrix A), pixel by pixel.

E.57.2.7   Inspection Results

The 1499 frames of data (24.98 sec) were processed using iterations of different time windows. No apparent defect was detected. An example of a PCA image processed using the second eigenvector from the 50th (0.83s) to 1249th (20.82s) frame is shown in Figure E.57-7.

Figure E.57-6. NASA-03-Twisted-Tow-001 sample.

Figure E.57-7. SSIR inspection of NASA-03-Twisted-Tow-001 sample processed with PCA from frame 50 (0.83s) to 1249 (20.82s).

E.57.2.8 References

[1]   Rajic, N.: "Principal Component Thermography for Flaw Contrast Enhancement and Flaw Depth Characterization in Composite Structures," *Composite Structures*, Vol. 58, pp. 521--528, 2002.

[2]   Zalameda, J. N.; Bolduc S.; and Harman R.: "Thermal Inspection of a Composite Fuselage Section using a Fixed Eigenvector Principal Component Analysis Method," Proc. *SPIE* 10214, *Thermosense: Thermal Infrared Applications XXXIX*, 102140H, 5 May 2017.

[3]   Cramer, K. E.; and Winfree, W. P.: "Fixed Eigenvector Analysis of Thermographic NDE Data", Proceedings of *SPIE*, *Thermosense XXXIII*, edited by Morteza Safai and Jeff Brown, Vol. 8013, 2011.

[4]   Shephard, S. M.: "Flash Thermography of Aerospace Composites," *IV Conferencia Panamerica de END*, Buenos Aires – October (2007).

E.57.3   Method: Through-Transmission Infrared Thermography (TTIR)

E.57.3.1   Partner: NASA

E.57.3.2   Technique Applicability: ★☆☆

TT thermography can detect the twisted tows.

E.57.3.3   Laboratory Setup

The TT thermal inspection system setup is shown in Figure E.57-8. The test specimen is placed between the heat source and the IR camera. The lamp used to induce the heat was a commercially available photographic flash lamp powered by a 6,400-Joule power supply (manufactured by Balcar). The camera used was a FLIR SC6000 with a 640×512 InSb array operating in the 3- to 5-µm IR band. The image data frame rate was 60 image frames per second. The computer records the IR image of the specimen immediately prior to the firing of the flash lamp (for emissivity correction), and then the thermal response of the specimen at a user defined sampling rate and for a user defined duration is acquired.
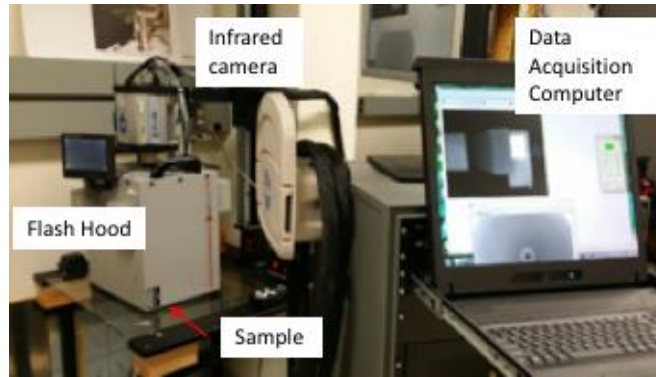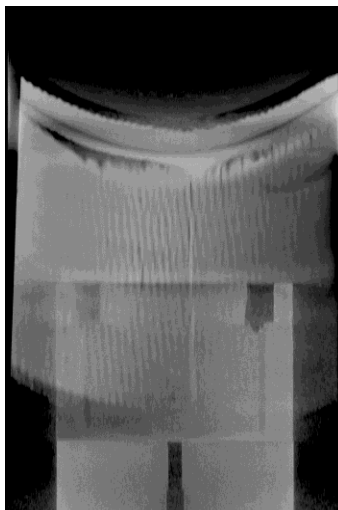

Figure E.57-8. TTIR setup.

E.57.3.4   Equipment List and Specifications:

- TWI System
- TWI System flash heat source using Balcar power supply externally triggered by TWI system.
- SC6000 FLIR camera, 640×512 InSb array, NEDT < 20 mK
- 25 mm Germanium Optics

E.57.3.5   Settings:

- 60 Hz Frame Rate
- Flash on frame #10
- Total number of Frames 2000
- Total data acquisition time of 33.33 sec
- IR camera was positioned to view the entire sample

E.57.3.6   Principal Component Analysis

PCA is common for processing of thermal data [1–3]. This algorithm is based on decomposition of the thermal data into its principal components or eigenvectors. Singular value decomposition is a routine used to find the singular values and corresponding eigenvectors of a matrix. Since thermal NDE signals are slowly decaying waveforms, the predominant variations of the entire data set are usually contained in the first or second eigenvectors, and thus account for most of the data variance of interest. The principle components are computed by defining a data matrix A, for each data set, where the time variations are along the columns and the spatial image pixel points are row-wise. The matrix A is adjusted by dividing the maximum value (normalization) and subtracting the mean along the time dimension. The covariance matrix is defined as the $A^T\!*\!A$. The covariance matrix is now a square matrix of number of images used for processing. The covariance matrix can then be decomposed using singular value decomposition as:

$$covariance\ matrix = A^T A = V * S * V^T$$

where S is a diagonal matrix containing the square of the singular values and V is an orthogonal matrix, which contains the basis functions or eigenvectors describing the time variations. The eigenvectors can be obtained from the columns of V. The PCA inspection image is calculated by dot product multiplication of the selected eigenvector times the temperature response (data matrix A), pixel by pixel.

E.57.3.7   Inspection Results

The 2000 frames of data (33.33 sec) were processed using iterations of different time windows. The processing of frames 50 to 250 corresponding to a time window of 0.83–4.17 sec yielded the best result, as shown in Figure E.57-10. Possible defects, labeled A through C were detected. They exhibit features consistent with those of twisted tows. The contrast is very faint and the defects easily overlooked.
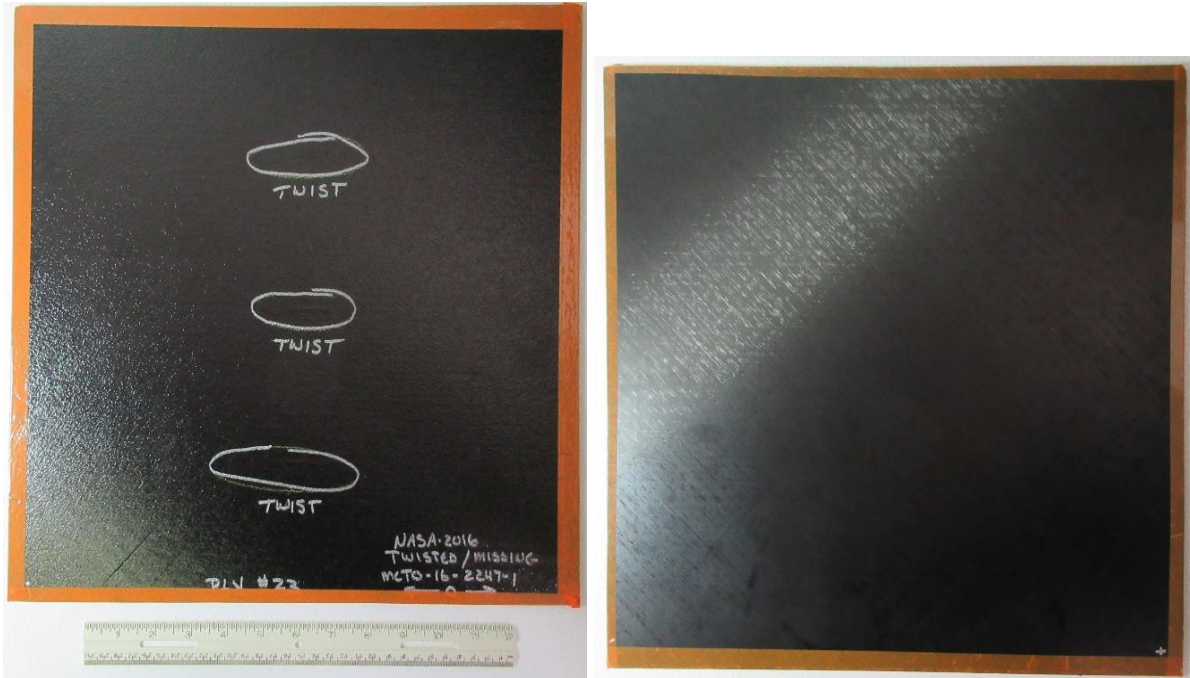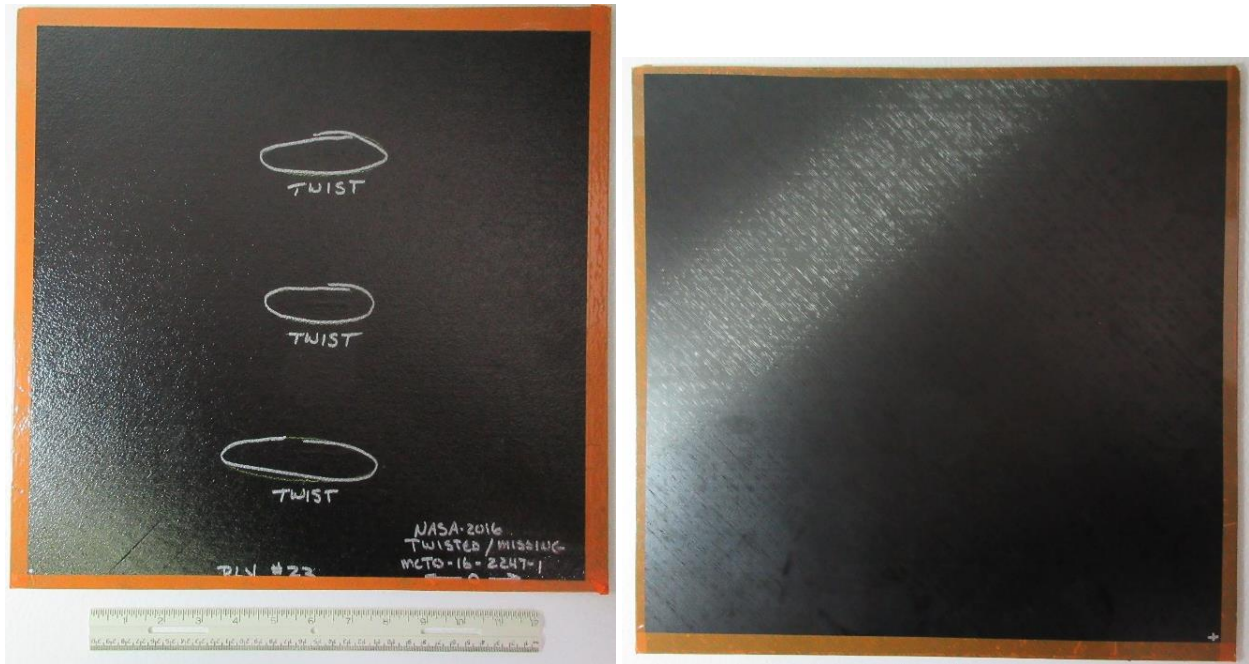
Figure E.57-9. NASA-03-Twisted-Tow-001 sample.
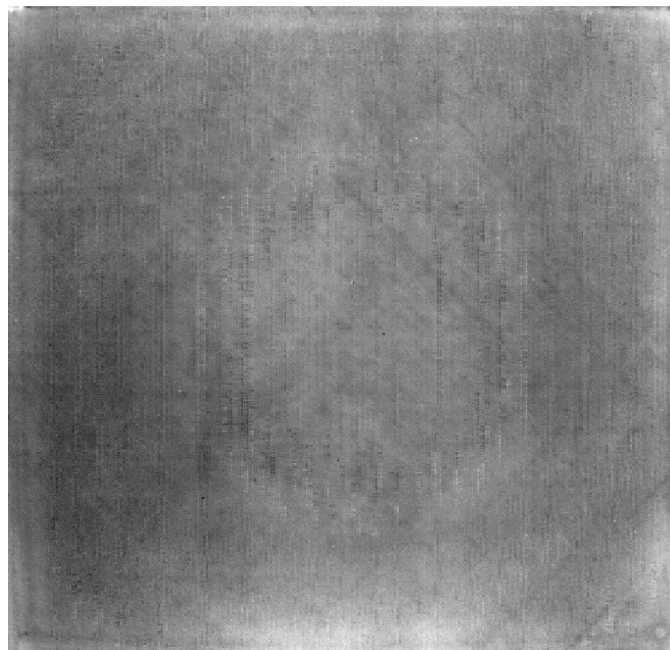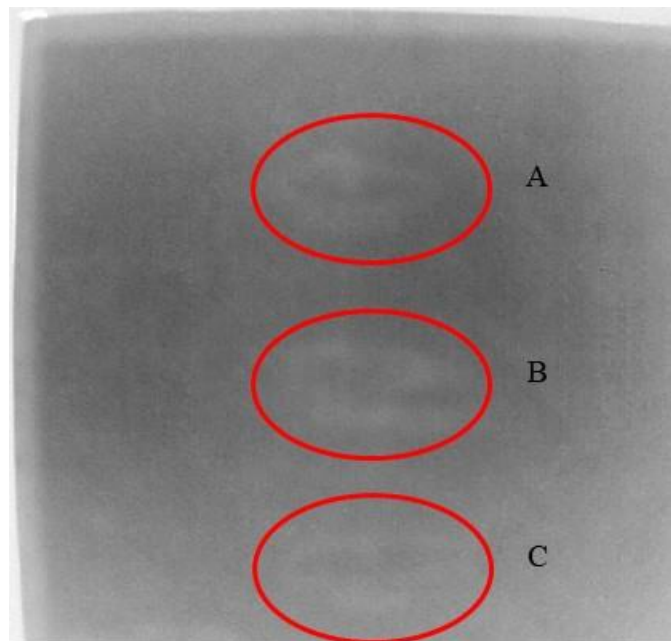

Figure E.57-10. TTIR inspection of NASA-03-Twisted-Tow-001 sample processed with PCA from frame 50 (0.83s) to 250 (4.17s).

E.57.3.8   References

[1]   Rajic, N.: "Principal Component Thermography for Flaw Contrast Enhancement and Flaw Depth Characterization in Composite Structures," *Composite Structures*, Vol. 58, pp. 521-528, 2002.

[2]   Zalameda, J. N.; Bolduc S.; and Harman R.: "Thermal Inspection of a Composite Fuselage Section using a Fixed Eigenvector Principal Component Analysis

Method," Proc. *SPIE* 10214, *Thermosense: Thermal Infrared Applications XXXIX*, 102140H, 5 May 2017.

[3]   Cramer, K. E.; and Winfree, W. P.: "Fixed Eigenvector Analysis of Thermographic NDE Data", Proceedings of *SPIE*, *Thermosense XXXIII*, edited by Morteza Safai and Jeff Brown, Vol. 8013, 2011.

E.57.4   Method: Single-Side Flash Thermography (SSFT-TSR)

E.57.4.1   Partner: Thermal Wave Imaging, Inc.*

*TWI was not part of the ACC but reviewed specimens.

E.57.4.2   Technique Applicability: ★★★

SSFT-TSR is capable of detecting subsurface anomalies in this specimen that could be the result of delamination, voids or porosity. All indications appear in the head-on image, but more accurate sizing is achieved by inspecting the flat surfaces separately.

E.57.4.3   Laboratory Setup:

The sample was inspected with a commercially available flash thermography system (EchoTherm®, Thermal Wave Imaging, Inc.), equipped with 2 linear xenon flash/reflector assemblies mounted in a reflective hood optimized to provide uniform output at the 10-inch × 14-inch exit aperture. Each lamp is powered by a 6 kJ power supply that allows truncation of the flash to a rectangular pulse with duration <1 msec d. A cryogenically cooled IR camera is mounted to view the plane of the hood exit aperture, with the camera lens positioned at the plane of the flashlamps. Excitation, data capture and processing and analysis using TSR are controlled at the system console using Virtuoso software.

E.57.4.4   Equipment List and Specifications:

- EchoTherm® Flash Thermography System
- 2 linear xenon flash lamps and power supplies (6 kJ each)
- TWI Precision Flash Control (truncation to 4 msec rectangular pulse)
- A6100sc FLIR camera, 640 × 512 InSb array, NEDT < 20 mK
- 13 mm Germanium Lens
- TWI Virtuoso® software

E.57.4.5   Settings:

- 30 Hz Frame Rate
- 10 Preflash Frames
- 1800 total frames
- 7 Polynomial order
- 60-sec data acquisition time
- FOV: 10-inch × 14-inch

Settings were determined following the recommendations in ASTM E2582-14. Acquisition duration was set according to the time of the break from linearity (t* ~8 sec) due to the back wall for typical points in the log time history. The acquisition period was then set to 30 sec (3 × t*), per ASTM E2582-14.

Figure E.57-11. SSFT system with TSR.

E.57.4.6   Thermographic Signal Reconstruction (TSR)

After acquisition, captured data are processed using TSR to reduce temporal noise, enhance deviation from normal cooling behavior and allow segmentation of the data based on signal attributes. For each pixel, the average of 10 frames immediately preceding the flash pulse is subtracted from the pixel time history, and a 7th order polynomial is fit to the logarithmically scaled result using least squares. First and 2nd derivatives of the result are calculated and the derivative images are displayed in the Virtuoso software. Derivative signals associated normal areas of the sample exhibit minimal activity over the duration of the acquisition. Signals associated with subsurface anomalies typically behave identically to the normal signals until a particular time (dependent on host material characteristics and the depth of the feature) after which their behavior deviates from normal (the degree of the deviation depends on the relative difference in the thermal properties of the anomaly and the surrounding normal matrix).

E.57.4.7   Inspection Results

No subsurface indications were observed.
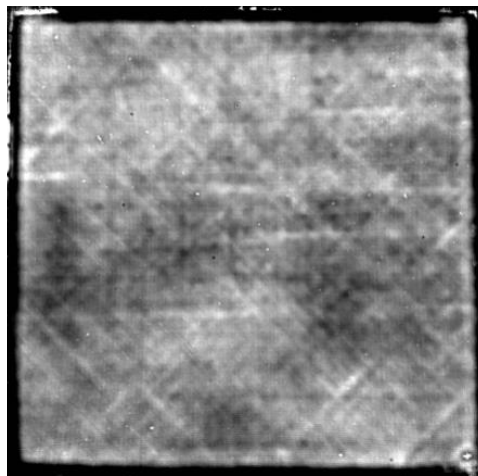
Figure E.57-12. TSR 2nd derivative at 9.20 sec of #57-Twist Ply #23.

E.57.4.8   References

[1]   ASNT: *ASNT Aerospace NDT Industry Handbook*, Chapter 11, "Thermography," Nov 2014.

[2]   ASTM International: "Standard Practice for Infrared Flash Thermography of Composite Panels and Repair Patches," *ASTM E2582*–07, 2007.

[3]   Shepard, S.; and Frendberg, M.: "Thermographic Detection and Characterization of Flaws in Composite Materials," *Materials Evaluation*, ASNT, July 2014.

[4]   Hou, Y.; Lhota, J. R.; and Golden, T. J. M.: "Automated processing of thermographic derivatives for quality assurance," *Opt. Eng.*, Vol. 46, 051008, 2007.

[5]   *Temporal noise reduction, compression and analysis of data sequences*, U.S. Patent 6,516,084.

E.58   Specimen #58: NASA-03-Twisted-Tow-002

Structure	Material	Details	Dimensions (inches)	Partner	Methods
Fiber placed panel	IM7/8552-1 Slit Tape	Flat panel Twisted Tow – mid	$16 \times 16 \times 0.15$	NASA	E.58.1 PEUT
					E.58.2 SSIR
					E.58.3 TTIR
				TWI	E.58.4 SSFT
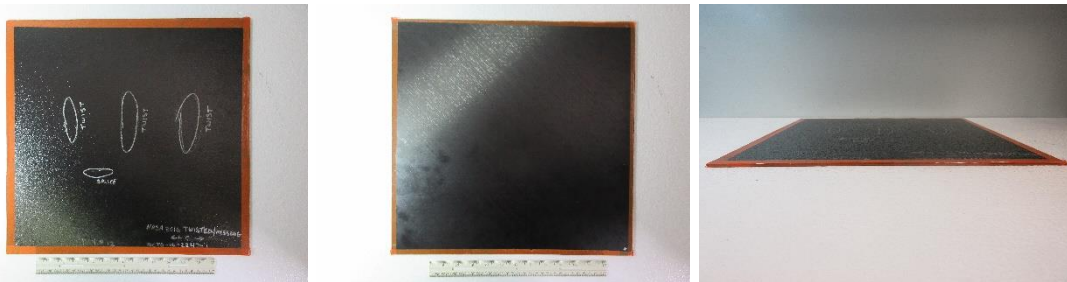
Figure E.58-1. Photographs of Specimen #58: NASA 03 Twisted Tow 002.

E.58.1   Method: Pulse-Echo Ultrasound Testing (PEUT)

E.58.1.1   Partner: NASA

E.58.1.2   Technique Applicability: ★★☆

PEUT is capable of detecting the twisted tows in this specimen with some interference.

E.58.1.3   Laboratory Setup

Immersion Ultrasonic Testing: NASA LaRC uses a custom-designed single-probe ultrasonic scanning system. The system has an 8-axis motion controller, a multi-axis gantry robot mounted above a medium-size water tank, a dual-channel, 16-bit, high-speed digitizer, and an off-the-shelf ultrasonic pulser receiver. The system can perform TT and PEUT inspections. TT inspection employs two aligned ultrasonic probes, one transmitter and one receiver, placed on either side of a test specimen. Pulse-echo inspection is a single-sided method where a single ultrasonic probe is both transmitter and receiver. In each method, data are acquired while raster scanning the ultrasonic probe(s) in relation to a part. Figure E.58-2 shows a simplified block diagram of a scanning Pulse-echo inspection.
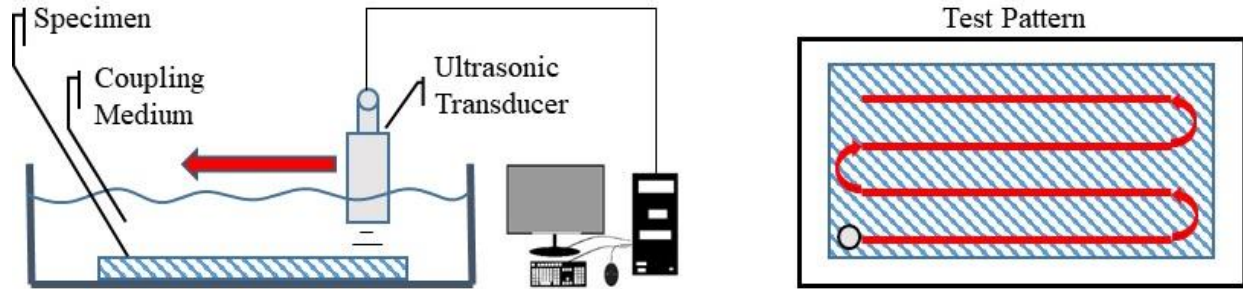
Figure E.58-2. Ultrasonic system components.
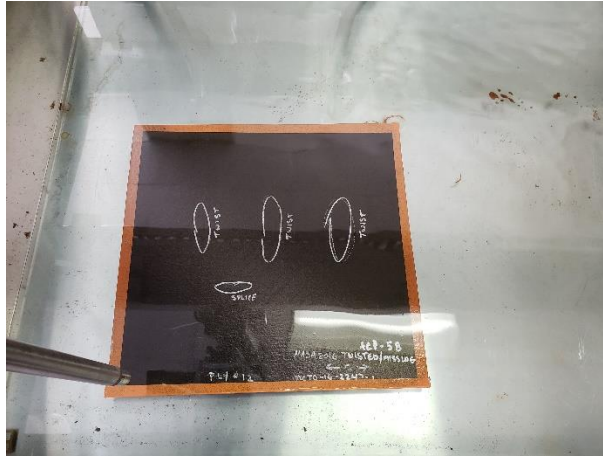
Figure E.58-3. Specimen orientation within testing apparatus.

E.58.1.4   Equipment List and Specifications:

- Pulser/Receiver: Olympus 5073PR
- Digitizer: AlazarTech ATS9462, dual channel, 16 bit, 180 MS/s
- Sensor: Olympus 2-inch spherical focus immersion ultrasonic transducer
- Motion system: open looped stepper motor based X-YY-Z gantry robot
- Motion Controller: Galil DMC-4183
- Acquisition Software: FastScan, custom developed at NASA LaRC
- Signal Processing Software: DataViewer, custom developed at NASA LaRC

E.58.1.5   Settings

Table E.58-1. Data collection settings.

Resolution horizontal [in/pixel]	0.02
Resolution vertical [in/pixel]	0.02
Probe frequency [MHz]	5
Focal Length [in]	1.9
Array Dimensions [pixels]	751×726

The specimen is placed flat against the zero position of the tank raised above the glass bottom by several metal washers. The test probe is computer-controlled and correlated to the position on the sample. It is also focused to a point one mm below the surface of the test material. The specimen remains in place while the transducer follows a preprogrammed test grid across the surface as indicated in Figure E.58-2. At each point, ultrasonic data are collected from individual pulses. Larger step sizes between data collection result in lower image resolution. These data points are

71

reconstructed into a data cube displaying spatial coordinates as time progresses. 2D reconstruction of the collection of ultrasonic responses create flattened slices at varying depths within the material.

E.58.1.6 Inspection Results

Specimen #58 is a fiber placed flat panel fabricated from IM7/8552-1 Slit Tape with the objective of achieving twisted tows midway through the sample. PEUT was performed on this specimen in NASA's immersion tank specified above.

In Figure E.58-4, evidence of three twisted tows in the material appear in the middle of the specimen. The fiber twists reflect and cause perturbations in the acoustic waves that differ from the pattern representing the bulk of the material. This difference, while small, makes visual detection of the twisted tows possible. These defects were detected at a depth of 0.056 inch. The twisted tows can be seen further in the specimen in Figure E.58-5. A tow splice was also detected in the specimen as seen in Figure E.58-6.
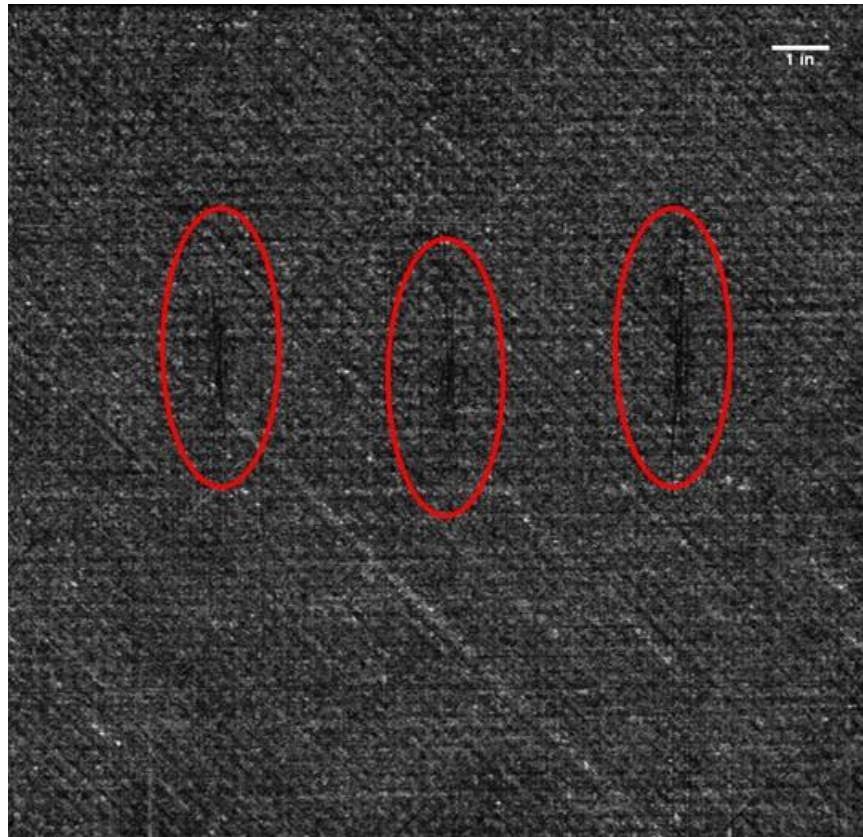
Figure E.58-4. UT image showing surface flaws and a near surface delamination.
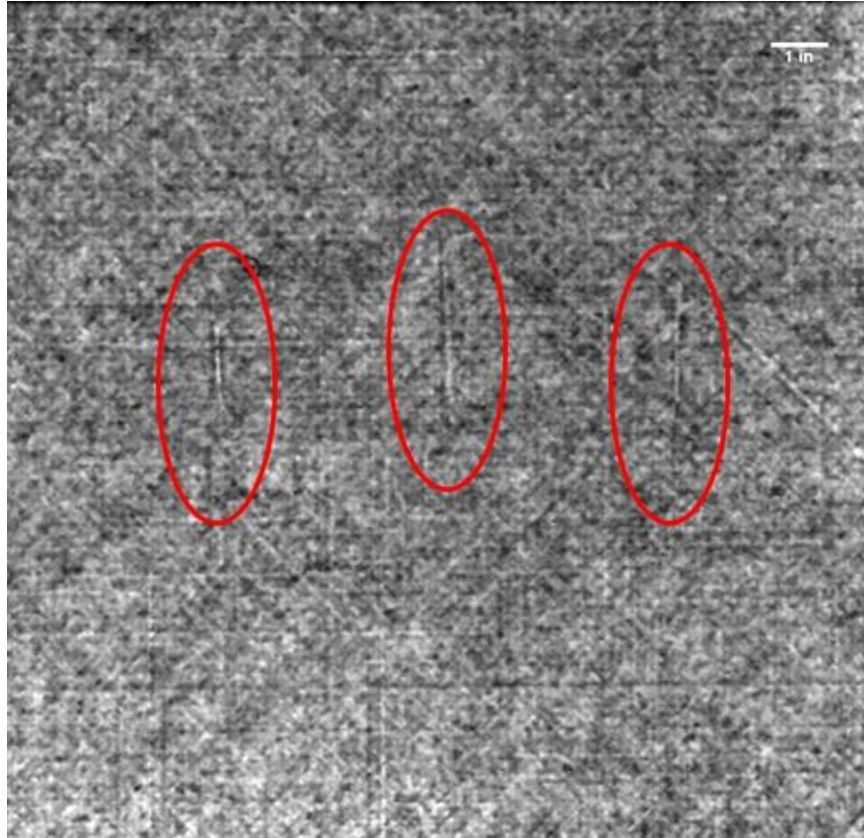
Figure E.58-5. UT image showing twisted tows in the bulk of the specimen.
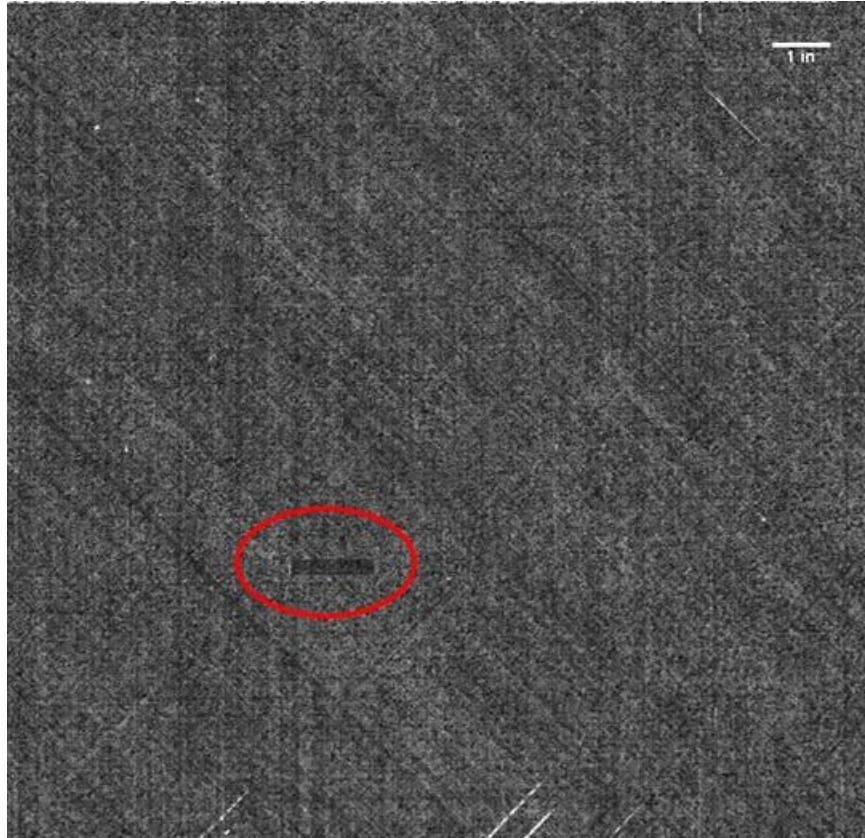
Figure E.58-6. UT image showing tow splice within the specimen.

E.58.2 Method: Single-Sided Infrared Thermography (SSIR)

E.58.2.1 Partner: NASA

E.58.2.2 Technique Applicability: ★★☆

SSIR thermography is incapable of detecting the twisted tows.

E.58.2.3 Laboratory Setup

A commercially available flash thermography system was used for the inspection. The flash thermography system consisted of two linear flash tubes mounted within a hood. An IR camera was mounted at the back of the hood viewing through a circular hole between the flash tubes and were positioned to view the hood opening. In this configuration, the flash lamps heated an area equal to the hood opening and the IR camera captured the thermal response. The IR camera operates in the mid-wave IR band (3–5 µm) and is configured with a 25-mm germanium lens. The focal plane array size for the camera is 640×512 with a detector pitch size of 14×14 µm.

Figure E.58-7. SSIR setup.

E.58.2.4   Equipment List and Specifications:

- TWI System
- TWI System flash heat source using Speedotron power supplies.
- SC6000 FLIR camera, 640×512 InSb array, NEDT < 20 mK
- 25 mm Germanium Optics

E.58.2.5   Settings:

- 60 Hz Frame Rate
- Flash on frame #10
- Total number of Frames 1499
- Total data acquisition time of 24.98 sec
- The camera/hood was positioned to view the entire sample

E.58.2.6   Principal Component Analysis

PCA is common for processing of thermal data [1–3]. This algorithm is based on decomposition of the thermal data into its principal components or eigenvectors. Singular value decomposition is a routine used to find the singular values and corresponding eigenvectors of a matrix. Since thermal NDE signals are slowly decaying waveforms, the predominant variations of the entire data set are usually contained in the first or second eigenvectors, and thus account for most of the data variance of interest. The principle components are computed by defining a data matrix A, for each data set, where the time variations are along the columns and the spatial image pixel points are row-wise. The matrix A is adjusted by dividing the maximum value (normalization) and subtracting the mean along the time dimension. The covariance matrix is defined as the $A^{T}*A$. The covariance matrix is now a square matrix of number of images used for processing. The covariance matrix can then be decomposed using singular value decomposition as:

$$covariance\ matrix = \ A^{T}A = V * S * V^{T}$$

Where S is a diagonal matrix containing the square of the singular values and V is an orthogonal matrix, which contains the basis functions or eigenvectors describing the time variations. The eigenvectors can be obtained from the columns of V. The PCA inspection image is calculated by dot product multiplication of the selected eigenvector times the temperature response (data matrix A), pixel by pixel.

E.58.2.7   Inspection Results

The 1499 frames of data (24.98 sec) were processed using iterations of different time windows. No apparent defect was detected. An example of a PCA image processed using the second eigenvector from the 50th (0.83s) to 1499th (24.98s) frame is shown in Figure E.58-9.

Figure E.58-8. NASA-03-Twisted-Tow-002 sample.

Figure E.58-9. SSIR inspection of NASA-03-Twisted-Tow-002 sample processed with PCA from frame 50 (0.83s) to 1499 (24.98s).

E.58.2.8   References

[1]   Rajic, N.: "Principal Component Thermography for Flaw Contrast Enhancement and Flaw Depth Characterization in Composite Structures," *Composite Structures*, Vol. 58, pp. 521-528, 2002.

[2]   Zalameda, J. N.; Bolduc S.; and Harman R.: "Thermal Inspection of a Composite Fuselage Section using a Fixed Eigenvector Principal Component Analysis Method," Proc. *SPIE* 10214, *Thermosense: Thermal Infrared Applications XXXIX*, 102140H, 5 May 2017.

[3]   Cramer, K. E.; and Winfree, W. P.: "Fixed Eigenvector Analysis of Thermographic NDE Data", Proceedings of *SPIE*, *Thermosense XXXIII*, edited by Morteza Safai and Jeff Brown, Vol. 8013, 2011.

E.58.3   Method: Through-Transmission Infrared Thermography (TTIR)

E.58.3.1   Partner: NASA

E.58.3.2   Technique Applicability: ★★☆

TT thermography can detect the twisted tows. The signal is very faint.

E.58.3.3   Laboratory Setup

The TT thermal inspection system setup is shown in Figure E.58-10. The test specimen is placed between the heat source and the IR camera. The lamp used to induce the heat was a commercially available photographic flash lamp powered by a 6,400-Joule power supply (manufactured by Balcar). The camera used was a FLIR SC6000 with a 640 × 512 InSb array operating in the 3- to 5-μm IR band. The image data frame rate was 60 Hz image. The computer records the IR image of the specimen immediately prior to the firing of the flash lamp (for emissivity correction), and then the thermal response of the specimen at a user defined sampling rate and for a user defined duration is acquired.
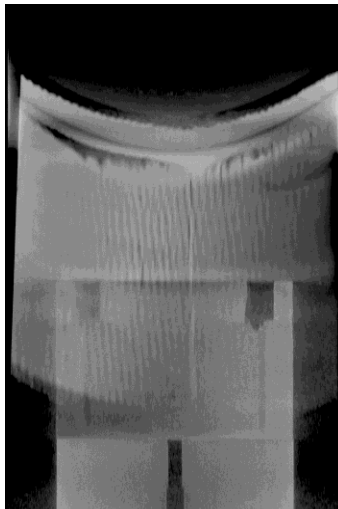
Figure E.58-10. TTIR setup.

E.58.3.4   Equipment List and Specifications:

- TWI System
- TWI System flash heat source using Balcar power supply externally triggered by TWI system.
- SC6000 FLIR camera, 640 × 512 InSb array, NEDT < 20 mK
- 25 mm Germanium Optics

E.58.3.5   Settings:

- 60 Hz Frame Rate
- Flash on frame #10
- Total number of Frames 2000
- Total data acquisition time of 33.33 sec
- IR camera was positioned to view the entire sample

E.58.3.6   Principal Component Analysis

PCA is common for processing of thermal data [1–3]. This algorithm is based on decomposition of the thermal data into its principal components or eigenvectors. Singular value decomposition is a routine used to find the singular values and corresponding eigenvectors of a matrix. Since thermal NDE signals are slowly decaying waveforms, the predominant variations of the entire data set are usually contained in the first or second eigenvectors, and thus account for most of the data variance of interest. The principle components are computed by defining a data matrix A, for each data set, where the time variations are along the columns and the spatial image pixel points are row-wise. The matrix A is adjusted by dividing the maximum value (normalization) and subtracting the mean along the time dimension. The covariance matrix is defined as the A^T*A. The covariance matrix is now a square matrix of number of images used for processing. The covariance matrix can then be decomposed using singular value decomposition as:

$$covariance\ matrix = A^T A = V * S * V^T$$

Where S is a diagonal matrix containing the square of the singular values and V is an orthogonal matrix, which contains the basis functions or eigenvectors describing the time variations. The eigenvectors can be obtained from the columns of V. The PCA inspection image is calculated by dot product multiplication of the selected eigenvector times the temperature response (data matrix A), pixel by pixel.

E.58.3.7   Inspection Results

The 2000 frames of data (33.33 sec) were processed using iterations of different time windows. The processing of frames 50 to 250 corresponding to a time window of 0.83–4.17 sec yielded the best result, shown in Figure E.58-11. Possible defects, labeled A through D, were detected. The contrast is very faint and the defects easily overlooked.
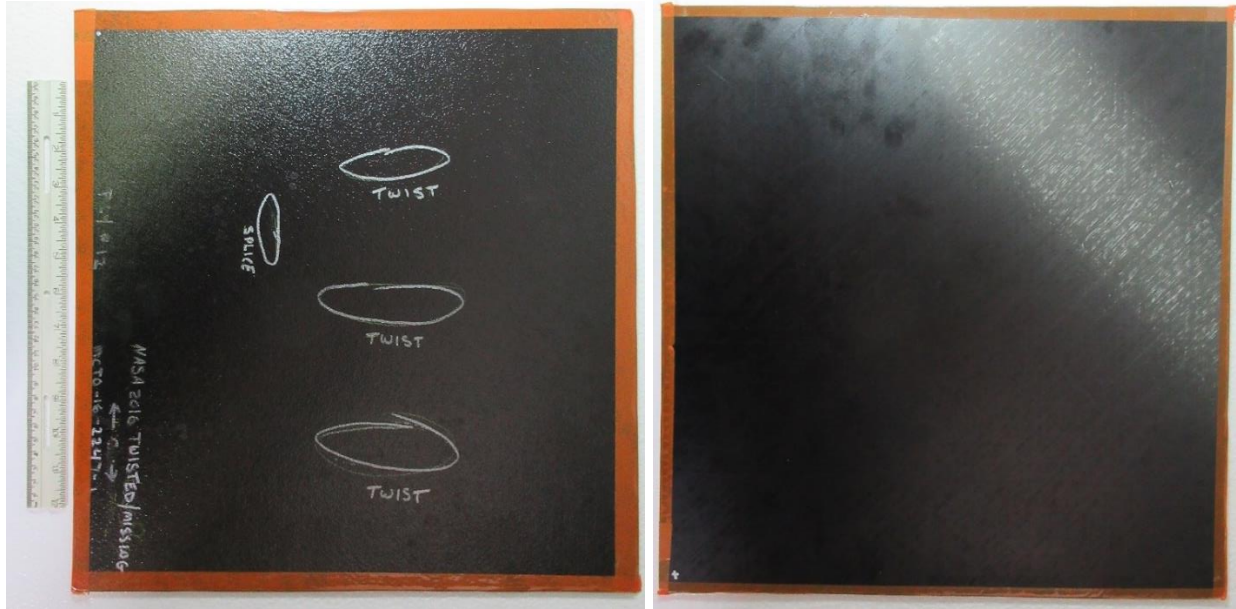
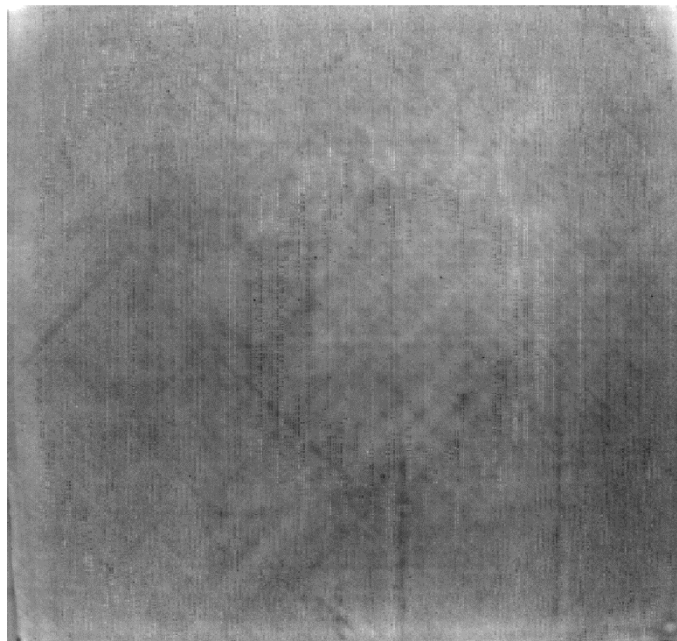*Figure E.58-11. NASA-03-Twisted-Tow-002 sample.*
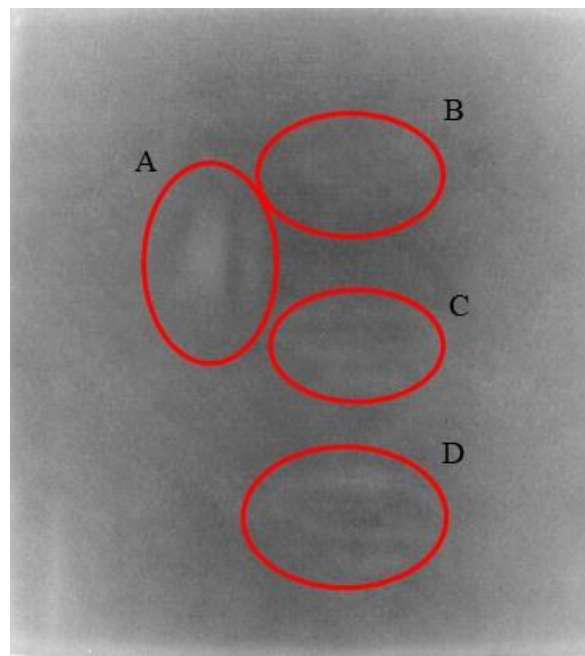
Figure E.58-12. TTIR inspection of NASA-03-Twisted-Tow-002 sample processed with PCA from frame 50 (0.83s) to 250 (4.17s).

E.58.3.8 References

[1]   Rajic, N.: "Principal Component Thermography for Flaw Contrast Enhancement and Flaw Depth Characterization in Composite Structures," *Composite Structures*, Vol. 58, pp. 521-528, 2002.

[2]   Zalameda, J. N.; Bolduc S.; and Harman R.: "Thermal Inspection of a Composite Fuselage Section using a Fixed Eigenvector Principal Component Analysis Method," Proc. *SPIE* 10214, *Thermosense: Thermal Infrared Applications XXXIX*, 102140H, 5 May 2017.

[3]   Cramer, K. E.; and Winfree, W. P.: "Fixed Eigenvector Analysis of Thermographic NDE Data", Proceedings of *SPIE*, *Thermosense XXXIII*, edited by Morteza Safai and Jeff Brown, Vol. 8013, 2011.

E.58.4   Method: Single-Side Flash Thermography (SSFT-TSR)

E.58.4.1   Partner: Thermal Wave Imaging, Inc.*

*TWI was not part of the ACC but reviewed specimens.

E.58.4.2   Technique Applicability: ★★★

SSFT-TSR is capable of detecting subsurface anomalies in this specimen that could be the result of delamination, voids or porosity. All indications appear in the head-on image, but more accurate sizing is achieved by inspecting the flat surfaces separately.

E.58.4.3   Laboratory Setup:

The sample was inspected with a commercially available flash thermography system (EchoTherm®, Thermal Wave Imaging, Inc.), equipped with 2 linear xenon flash/reflector assemblies mounted in a reflective hood optimized to provide uniform output at the 10-inch × 14-inch exit aperture. Each lamp is powered by a 6 kJ power supply that allows truncation of the flash to a rectangular pulse with duration <1 msec d. A cryogenically cooled IR camera is mounted to view the plane of the hood exit aperture, with the camera lens positioned at the plane of the flashlamps. Excitation, data capture and processing and analysis using TSR are controlled at the system console using Virtuoso software.

E.58.4.4   Equipment List and Specifications:

- EchoTherm® Flash Thermography System
- 2 linear xenon flash lamps and power supplies (6 kJ each)
- TWI Precision Flash Control (truncation to 4 msec rectangular pulse)
- A6100sc FLIR camera, 640 × 512 InSb array, NEDT < 20 mK
- 13 mm Germanium Lens
- TWI Virtuoso® software

E.58.4.5   Settings:

- 30 Hz Frame Rate
- 10 Preflash Frames
- 1800 total frames
- 7 Polynomial order
- 60-sec data acquisition time
- FOV: 10-inch × 14-inch

Settings were determined following the recommendations in ASTM E2582-14. Acquisition duration was set according to the time of the break from linearity (t* ~8 sec) due to the back wall for typical points in the log time history. The acquisition period was then set to 30 sec (3 × t*), per ASTM E2582-14.
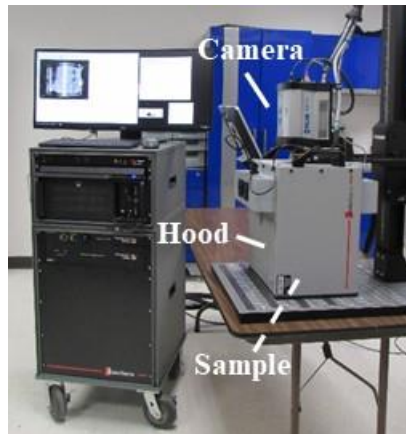
Figure E.58-13. SSFT system with TSR.

E.58.4.6 Thermographic Signal Reconstruction (TSR)

After acquisition, captured data are processed using TSR to reduce temporal noise, enhance deviation from normal cooling behavior and allow segmentation of the data based on signal attributes. For each pixel, the average of 10 frames immediately preceding the flash pulse is subtracted from the pixel time history, and a 7th order polynomial is fit to the logarithmically scaled result using least squares. First and 2nd derivatives of the result are calculated and the derivative images are displayed in the Virtuoso software. Derivative signals associated normal areas of the sample exhibit minimal activity over the duration of the acquisition. Signals associated with subsurface anomalies typically behave identically to the normal signals until a particular time (dependent on host material characteristics and the depth of the feature) after which their behavior deviates from normal (the degree of the deviation depends on the relative difference in the thermal properties of the anomaly and the surrounding normal matrix).

E.58.4.7 Inspection Results

Two possible indications were observed and confirmed to be subsurface by their late divergence in the logarithmic temperature time plot. The 1st derivative at 20.41 sec was used to produce the final inspection images shown in Figure E.58-14.

Figure E.58-14. TSR 1st derivative at 20.41 sec of #58-Twist/Splice Ply #12.

E.58.4.8   References

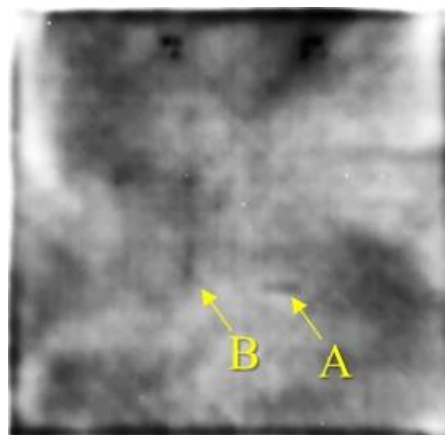[1]   ASNT: *ASNT Aerospace NDT Industry Handbook*, Chapter 11, "Thermography," Nov 2014.

[2]   ASTM International: "Standard Practice for Infrared Flash Thermography of Composite Panels and Repair Patches," *ASTM E2582*–07, 2007.

[3]   Shepard, S.; and Frendberg, M.: "Thermographic Detection and Characterization of Flaws in Composite Materials," *Materials Evaluation*, ASNT, July 2014.

[4]   Hou, Y.; Lhota, J. R.; and Golden, T. J. M.: "Automated processing of thermographic derivatives for quality assurance," *Opt. Eng.*, Vol. 46, 051008, 2007.

[5]   *Temporal noise reduction, compression and analysis of data sequences*, U.S. Patent 6,516,084.

E.59   Specimen #59 – NASA-03-Steered-Two-003 – Not Tested

Structure	Material	Details	Dimensions (inches)	Partner Methods
AFP Fiber Placed panel	IM7/8552-1 Slit Tape	Flange with air pillow delaminations	$46.5 \times 46.5 \times 0.15$	Not Tested

E.60   Specimen #60: NASA-03-Folded-Tow-001

Structure	Material	Details	Dimensions (inches)	Partner	Methods
Fiber placed panel	IM7/8552-1 Slit Tape	Flat panel Twisted Tow – mid	$16 \times 16 \times 0.15$	NASA	E.60.1 PEUT
					E.60.2 SSIR
					E.60.3 TTIR
				TWI	E.60.4 SSFT
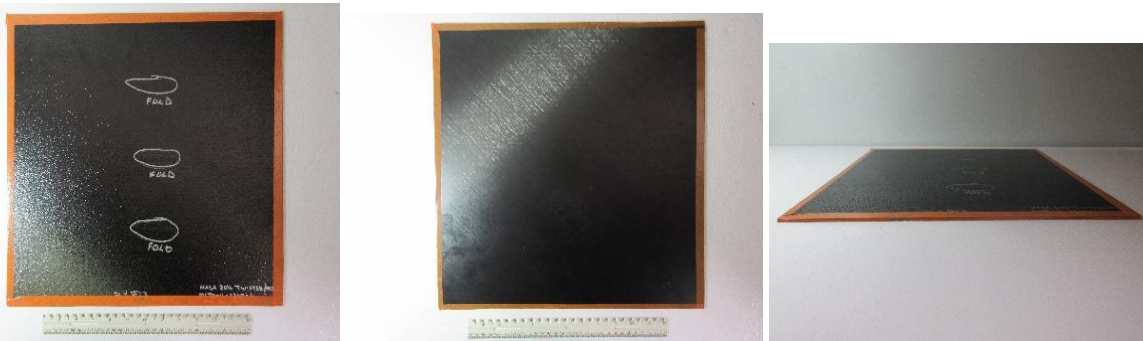
Figure E.60-1. Photographs of specimen #60: NASA 03 Folded Tow 001.

E.60.1   Method: Pulse-Echo Ultrasound Testing (PEUT)

E.60.1.1   Partner: NASA

E.60.1.2   Technique Applicability: ★★★

PEUT is capable of detecting the folded tows in this sample.

E.60.1.3   Laboratory Setup

Immersion Ultrasonic Testing: NASA LaRC uses a custom-designed single-probe ultrasonic scanning system. The system has an 8-axis motion controller, a multi-axis gantry robot mounted above a medium-size water tank, a dual-channel, 16-bit, high-speed digitizer, and an off the shelf ultrasonic pulser receiver. The system can perform TT and PEUT inspections. TT inspection employs two aligned ultrasonic probes, one transmitter and one receiver, placed on either side of

a test specimen. Pulse-echo inspection is a single-sided method where a single ultrasonic probe is both transmitter and receiver. In each method, data are acquired while raster scanning the ultrasonic probe(s) in relation to a part. Figure E.60-2 shows a simplified block diagram of a scanning Pulse-echo inspection.
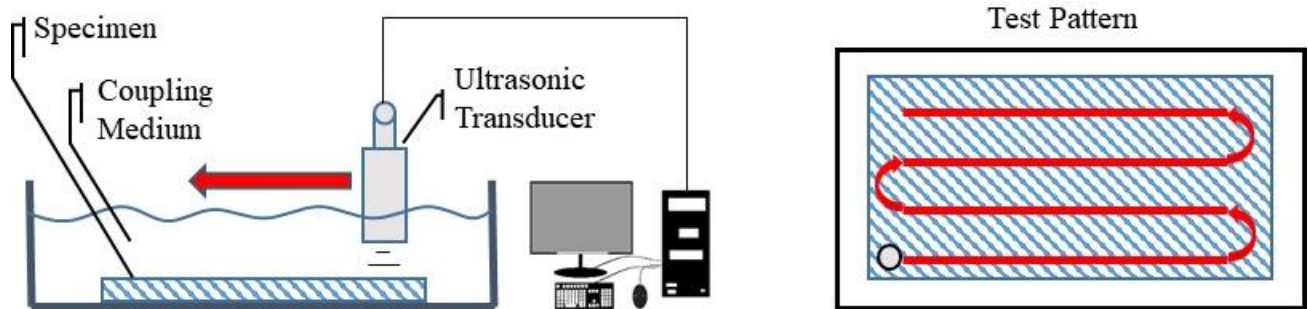
Figure E.60-2. Ultrasonic system components.
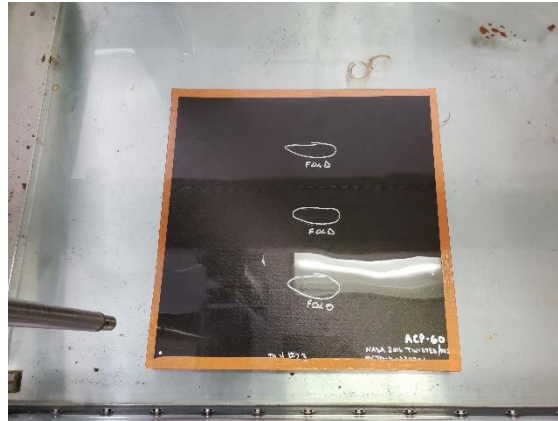
Figure E.60-3. Specimen orientation within testing apparatus.

E.60.1.4   Equipment List and Specifications:

- Pulser/Receiver: Olympus 5073PR
- Digitizer: AlazarTech ATS9462, dual channel, 16 bit, 180 MS/s
- Sensor: Olympus 2-inch spherical focus immersion ultrasonic transducer
- Motion system: open looped stepper motor based X-YY-Z gantry robot
- Motion Controller: Galil DMC-4183
- Acquisition Software: FastScan, custom developed at NASA LaRC
- Signal Processing Software: DataViewer, custom developed at NASA LaRC

E.60.1.5   Settings

Table E.60-1. Data collection settings.

Resolution horizontal [in/pixel]	0.02
Resolution vertical [in/pixel]	0.02
Probe frequency [MHz]	5
Focal Length [in]	1.9
Array Dimensions [pixels]	751×736

The specimen is placed flat against the zero position of the tank raised above the glass bottom by several metal washers. The test probe is computer-controlled and correlated to the position on the

sample. It is also focused to a point one mm below the surface of the test material. The specimen remains in place while the transducer follows a preprogrammed test grid across the surface as indicated in Figure E.60-2. At each point, ultrasonic data are collected from individual pulses. Larger step sizes between data collection result in lower image resolution. These data points are reconstructed into a data cube displaying spatial coordinates as time progresses. 2D reconstruction of the collection of ultrasonic responses create flattened slices at varying depths within the material.

E.60.1.6 Inspection Results

Specimen #60 is a fiber placed flat panel fabricated from IM7/8552-1 Slit Tape with the objective of achieving folded tows beneath the first ply of the sample. PEUT was performed on this specimen in NASA's immersion tank specified above.

In Figure E.60-4 evidence of three folded tows in the material appear in the middle of the specimen. The fiber folds reflect and cause peterbations in the acoustic waves that differ from the pattern representing the bulk of the material. This difference, while small, makes visual detection of the folded tows possible. These defects were detected at a depth of 0.006 inch just below the first ply of the composite.
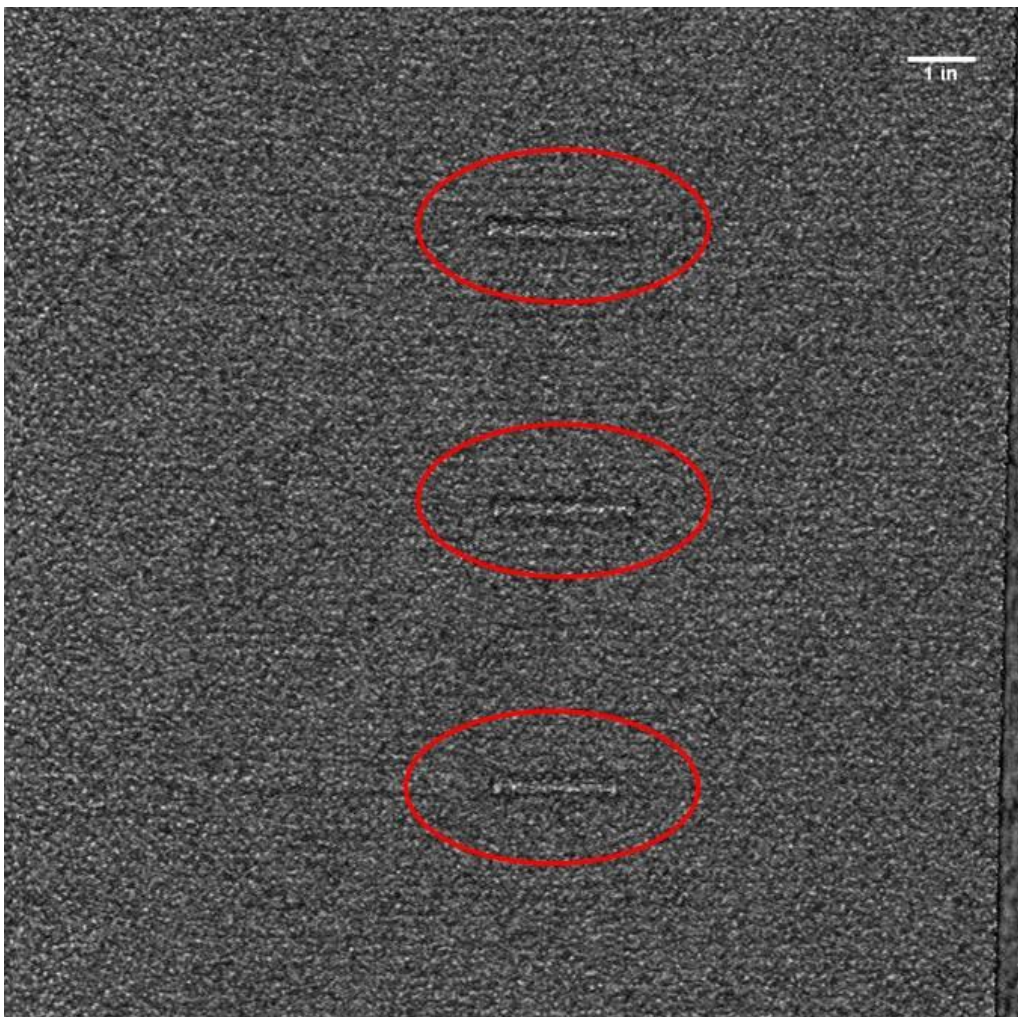

Figure E.60-4. UT image showing folded tows near the surface of the specimen.

84

E.60.2 Method: Single-Sided Infrared Thermography (SSIR)

E.60.2.1 Partner: NASA

E.60.2.2 Technique Applicability: ★★☆

SSIR thermography was capable of detecting the folded tows.

E.60.2.3 Laboratory Setup:

A commercially available flash thermography system was used for the inspection. The flash thermography system consisted of two linear flash tubes mounted within a hood. An IR camera was mounted at the back of the hood viewing through a circular hole between the flash tubes and were positioned to view the hood opening. In this configuration, the flash lamps heated an area equal to the hood opening and the IR camera captured the thermal response. The IR camera operates in the mid-wave IR band (3–5 µm) and is configured with a 25-mm germanium lens. The focal plane array size for the camera is 640×512 with a detector pitch size of 14×14 µm.

Figure E.60-5. SSIR setup.

E.60.2.4 Equipment List and Specifications:

- TWI System
- TWI System flash heat source using Speedotron power supplies.
- SC6000 FLIR camera, 640×512 InSb array, NEDT < 20 mK
- 25 mm Germanium Optics

E.60.2.5 Settings:

- 60Hz Frame Rate
- Flash on frame #10
- Total number of Frames 1499
- Total data acquisition time of 24.98 sec
- The camera/hood was positioned to view the entire sample

E.60.2.6 Principal Component Analysis

PCA is common for processing of thermal data [1–3]. This algorithm is based on decomposition of the thermal data into its principal components or eigenvectors. Singular value decomposition is a routine used to find the singular values and corresponding eigenvectors of a matrix. Since thermal NDE signals are slowly decaying waveforms, the predominant variations of the entire data set are usually contained in the first or second eigenvectors, and thus account for most of the data variance

of interest. The principle components are computed by defining a data matrix A, for each data set, where the time variations are along the columns and the spatial image pixel points are row-wise. The matrix A is adjusted by dividing the maximum value (normalization) and subtracting the mean along the time dimension. The covariance matrix is defined as the A^T*A. The covariance matrix is now a square matrix of number of images used for processing. The covariance matrix can then be decomposed using singular value decomposition as:

$$covariance\ matrix = \ A^T A = V * S * V^T$$

Where *S* is a diagonal matrix containing the square of the singular values and *V* is an orthogonal matrix, which contains the basis functions or eigenvectors describing the time variations. The eigenvectors can be obtained from the columns of *V*. The PCA inspection image is calculated by dot product multiplication of the selected eigenvector times the temperature response (data matrix A), pixel by pixel.

E.60.2.7   Inspection Results

The 1499 frames of data (24.98 sec) were processed using iterations of different time windows. The processing of frames 100 to 1249 corresponding to a time window of 1.67-20.82 sec yielded the best results. The three folded tows named A, B, and C were detected and are shown in Figure E.60-6. A time delay of 1.67 sec allowed enough time after the flash for the heat to flow into the sample and 20.82 sec was sufficient to provide good contrast of the defects. The second eigenvector was used to produce the final inspection images shown in Figure E.60-7. Without prior knowledge of the existence of defect C, it is unclear that it would have been categorized as a flaw as its signal is very faint.

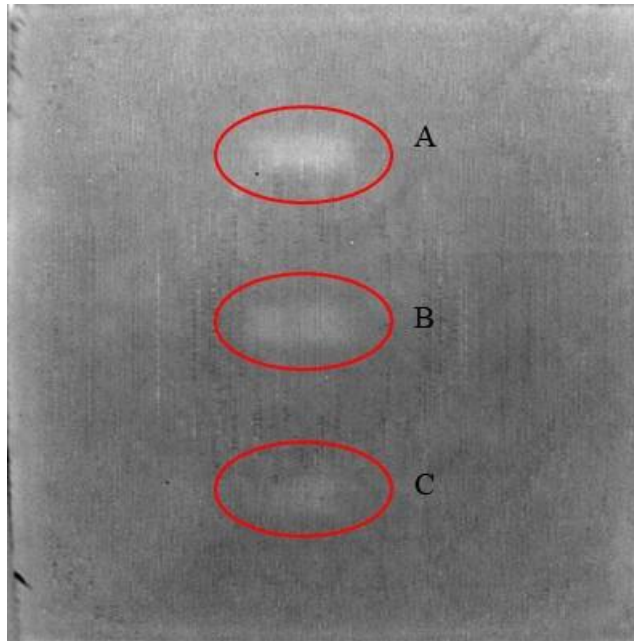***Figure E.60-6. NASA-03-Folded-Tow-001 sample.***

Figure E.60-7. SSIR inspection of NASA-03-Folded-Tow-001 sample processed with PCA from frame 100 (1.66s) to 1249 (20.82s).

E.60.2.8   References

[1]   Rajic, N.: "Principal Component Thermography for Flaw Contrast Enhancement and Flaw Depth Characterization in Composite Structures," *Composite Structures*, Vol. 58, pp. 521-528, 2002.

[2]   Zalameda, J. N.; Bolduc S.; and Harman R.: "Thermal Inspection of a Composite Fuselage Section using a Fixed Eigenvector Principal Component Analysis Method," Proc. *SPIE* 10214, *Thermosense: Thermal Infrared Applications XXXIX*, 102140H, 5 May 2017.

[3]   Cramer, K. E.; and Winfree, W. P.: "Fixed Eigenvector Analysis of Thermographic NDE Data", Proceedings of *SPIE*, *Thermosense XXXIII*, edited by Morteza Safai and Jeff Brown, Vol. 8013, 2011.

E.60.3   Method: Through-Transmission Infrared Thermography (TTIR)

E.60.3.1   Partner: NASA

E.60.3.2   Technique Applicability: ★☆☆

TT thermography was capable of detecting the folded tows.

E.60.3.3   Laboratory Setup

The TT thermal inspection system setup is shown in Figure E.60-8. The test specimen is placed between the heat source and the IR camera. The lamp used to induce the heat was a commercially available photographic flash lamp powered by a 6,400-Joule power supply (manufactured by Balcar). The camera used was a FLIR SC6000 with a 640×512 InSb array operating in the 3- to 5-μm IR band. The image data frame rate was 60 image frames per second. The computer records the IR image of the specimen immediately prior to the firing of the flash lamp (for emissivity

correction), and then the thermal response of the specimen at a user defined sampling rate and for a user defined duration is acquired.
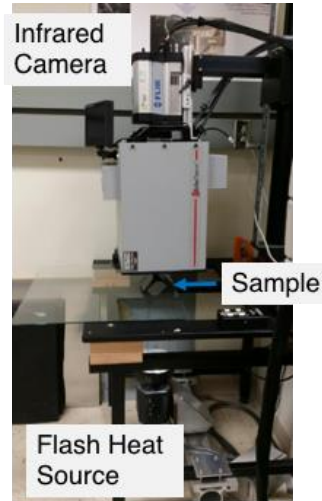

Figure E.60-8. TTIR setup.

E.60.3.4 Equipment List and Specifications:

- TWI System
- TWI System flash heat source using Balcar power supply externally triggered by TWI system.
- SC6000 FLIR camera, 640×512 InSb array, NEDT < 20 mK
- 25 mm Germanium Optics

E.60.3.5 Settings:

- 60 Hz Frame Rate
- Flash on frame #10
- Total number of Frames 2000
- Total data acquisition time of 33.33 sec
- IR camera was positioned to view the entire sample

E.60.3.6 Principal Component Analysis

PCA is common for processing of thermal data [1−3]. This algorithm is based on decomposition of the thermal data into its principal components or eigenvectors. Singular value decomposition is a routine used to find the singular values and corresponding eigenvectors of a matrix. Since thermal NDE signals are slowly decaying waveforms, the predominant variations of the entire data set are usually contained in the first or second eigenvectors, and thus account for most of the data variance of interest. The principle components are computed by defining a data matrix A, for each data set, where the time variations are along the columns and the spatial image pixel points are row-wise. The matrix A is adjusted by dividing the maximum value (normalization) and subtracting the mean along the time dimension. The covariance matrix is defined as the $A^T\!*\!A$. The covariance matrix is now a square matrix of number of images used for processing. The covariance matrix can then be decomposed using singular value decomposition as:

$$covariance\ matrix = \ A^T A = V * S * V^T$$

Where S is a diagonal matrix containing the square of the singular values and V is an orthogonal matrix, which contains the basis functions or eigenvectors describing the time variations. The eigenvectors can be obtained from the columns of V. The PCA inspection image is calculated by dot product multiplication of the selected eigenvector times the temperature response (data matrix A), pixel by pixel.

E.60.3.7   Inspection Results

The 2000 frames of data (33.33 sec) were processed using iterations of different time windows. The processing of frames 50 to 250 corresponding to a time window of 0.83–4.17 sec yielded the best result, and is shown in Figure E.60-10. Possible defects, labeled A through D, were detected. However, the contrast is faint and the defects easily overlooked.
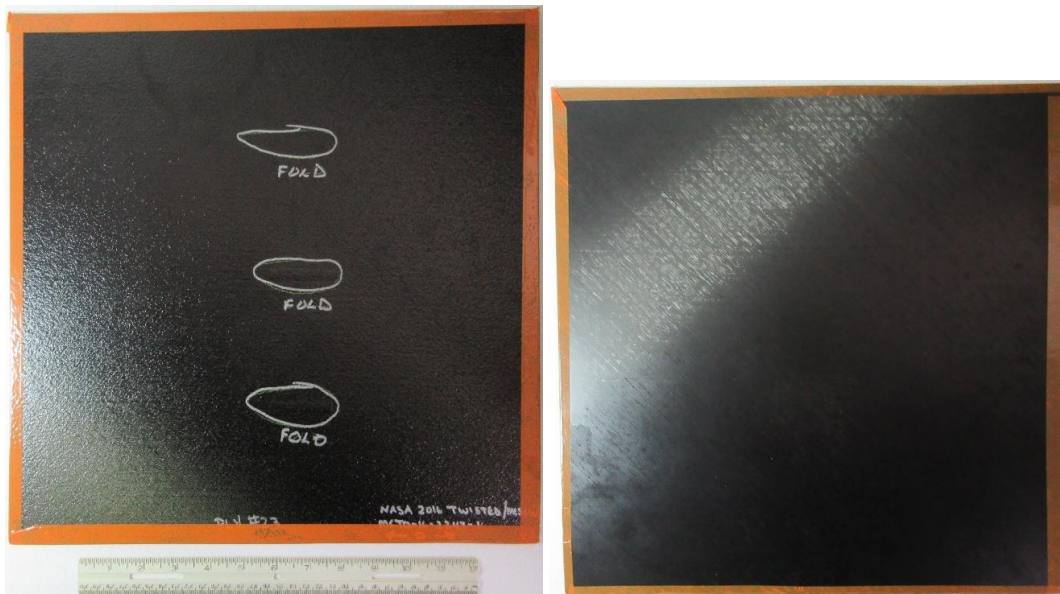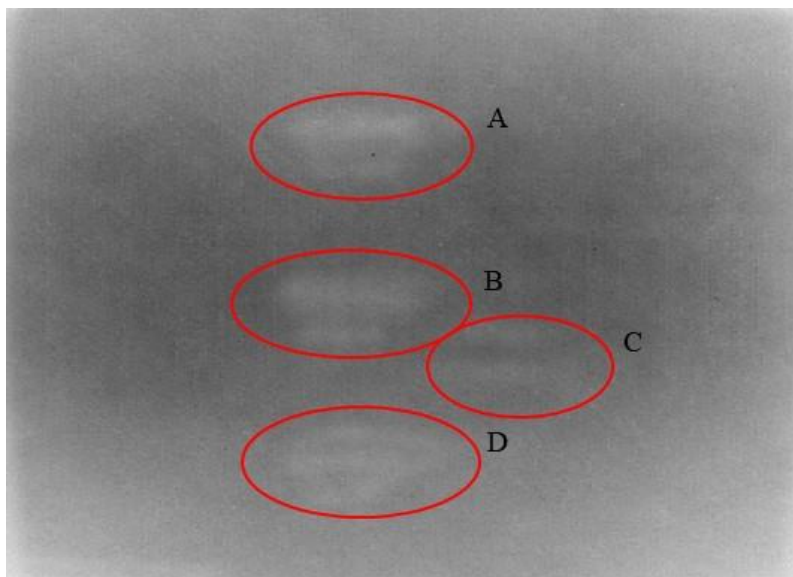

Figure E.60-9. NASA-03-Folded-Tow-001 sample.

Figure E.60-10. TTIR inspection of NASA-03-Folded-Tow-001 sample processed with PCA from frame 50 (0.83s) to 250 (4.17s).

E.60.3.8 References

[1]   Rajic, N.: "Principal Component Thermography for Flaw Contrast Enhancement and Flaw Depth Characterization in Composite Structures," *Composite Structures*, Vol. 58, pp. 521-528, 2002.

[2]   Zalameda, J. N.; Bolduc S.; and Harman R.: "Thermal Inspection of a Composite Fuselage Section using a Fixed Eigenvector Principal Component Analysis Method," Proc. *SPIE* 10214, *Thermosense: Thermal Infrared Applications XXXIX*, 102140H, 5 May 2017.

[3]   Cramer, K. E.; and Winfree, W. P.: "Fixed Eigenvector Analysis of Thermographic NDE Data", Proceedings of *SPIE*, *Thermosense XXXIII*, edited by Morteza Safai and Jeff Brown, Vol. 8013, 2011.

E.60.4   Method: Single Side Flash Thermography (SSFT-TSR)

E.60.4.1   Partner: Thermal Wave Imaging, Inc.*

*TWI was not part of the ACC but reviewed specimens.

E.60.4.2   Technique Applicability: ★★★

SSFT-TSR is capable of detecting subsurface anomalies in this specimen that could be the result of delamination, voids or porosity. All indications appear in the head-on image, but more accurate sizing is achieved by inspecting the flat surfaces separately.

E.60.4.3   Laboratory Setup:

The sample was inspected with a commercially available flash thermography system (EchoTherm®, Thermal Wave Imaging, Inc.), equipped with 2 linear xenon flash/reflector assemblies mounted in a reflective hood optimized to provide uniform output at the 10-inch × 14-inch exit aperture. Each lamp is powered by a 6 kJ power supply that allows truncation of the flash to a rectangular pulse with duration <1 msec d. A cryogenically cooled IR camera is mounted to view the plane of the hood exit aperture, with the camera lens positioned at the plane of the flashlamps. Excitation, data capture and processing and analysis using TSR are controlled at the system console using Virtuoso software.

E.60.4.4   Equipment List and Specifications:
- EchoTherm® Flash Thermography System
- 2 linear xenon flash lamps and power supplies (6 kJ each)
- TWI Precision Flash Control (truncation to 4 msec rectangular pulse)
- A6100sc FLIR camera, 640 × 512 InSb array, NEDT < 20 mK
- 13 mm Germanium Lens
- TWI Virtuoso® software

E.60.4.5   Settings:
- 30 Hz Frame Rate
- 10 Preflash Frames
- 1800 total frames
- 7 Polynomial order
- 60-sec data acquisition time
- FOV: 10-inch × 14-inch

Settings were determined following the recommendations in ASTM E2582-14. Acquisition duration was set according to the time of the break from linearity (t* ~8 sec) due to the back wall for typical points in the log time history. The acquisition period was then set to 30 sec (3 × t*), per ASTM E2582-14.
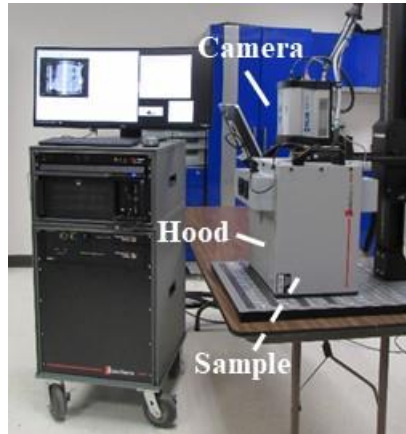

Figure E.60-11. SSFT system with TSR.

E.60.4.6   Thermographic Signal Reconstruction (TSR)

After acquisition, captured data are processed using TSR to reduce temporal noise, enhance deviation from normal cooling behavior and allow segmentation of the data based on signal attributes. For each pixel, the average of 10 frames immediately preceding the flash pulse is subtracted from the pixel time history, and a 7th order polynomial is fit to the logarithmically scaled result using least squares. First and 2nd derivatives of the result are calculated and the derivative images are displayed in the Virtuoso software. Derivative signals associated normal areas of the sample exhibit minimal activity over the duration of the acquisition. Signals associated with subsurface anomalies typically behave identically to the normal signals until a particular time (dependent on host material characteristics and the depth of the feature) after which their behavior deviates from normal (the degree of the deviation depends on the relative difference in the thermal properties of the anomaly and the surrounding normal matrix).

E.60.4.7   Inspection Results

Three subsurface indications were observed and confirmed to be subsurface by their late divergence in the logarithmic temperature time plot. The 1st derivative at 21.36 sec was used to produce the final inspection images shown in Figure E.60-12.
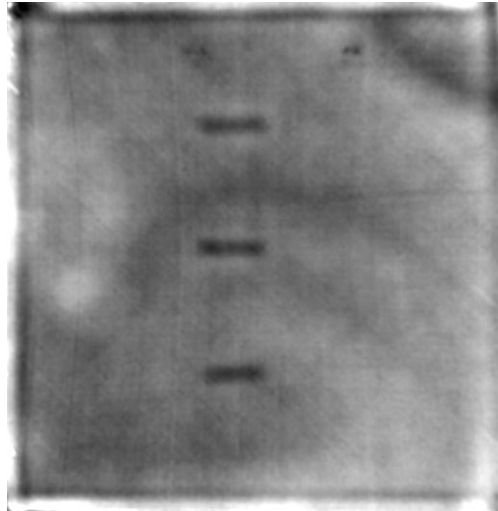
Figure E.60-12. TSR 1st derivative at 21.36 sec of #60-Fold Ply #23.

E.60.4.8   References

[1]   ASNT: *ASNT Aerospace NDT Industry Handbook*, Chapter 11, "Thermography," Nov 2014.

[2]   ASTM International: "Standard Practice for Infrared Flash Thermography of Composite Panels and Repair Patches," *ASTM E2582–07*, 2007.

[3]   Shepard, S.; and Frendberg, M.: "Thermographic Detection and Characterization of Flaws in Composite Materials," *Materials Evaluation*, ASNT, July 2014.

[4]   Hou, Y.; Lhota, J. R.; and Golden, T. J. M.: "Automated processing of thermographic derivatives for quality assurance," *Opt. Eng.*, Vol. 46, 051008, 2007.

[5]   *Temporal noise reduction, compression and analysis of data sequences*, U.S. Patent 6,516,084.